European Spatial Data Research

March 2013

Radiometric Aspects of Digital Photogrammetric Images

Eija Honkavaara, Lauri Markelin,
Roman Arbiol, Lucas Martínez

Mobile Mapping - Road Environment Mapping using Mobile Laser Scanning

Harri Kaartinen, Juha Hyyppä, Antero Kukko,
Matti Lehtomäki, Anttoni Jaakkola, George Vosselman,
Sander Oude Elberink, Martin Rutzinger, Shi Pu, Matti Vaaja

Official Publication Nº 62

Published by EuroSDR

Printed by Gopher, Amsterdam, The Netherlands

EUROPEAN SPATIAL DATA RESEARCH

PRESIDENT 2012 – 2014:
Thorben Brigsted Hansen, Denmark

VICE-PRESIDENT 2009 – 2013:
Dieter Fritsch, Germany

SECRETARY-GENERAL:
Joep Crompvoets, Belgium

DELEGATES BY MEMBER COUNTRY:

Austria: Michael Franzen
Belgium: Ingrid Vanden Berghe; Jean Theatre
Croatia: Željko Hećimović; Ivan Landek
Cyprus: Andreas Sokratous, Georgia Papathoma
Denmark: Thorben Brigsted Hansen; Lars Bodum
Finland: Juha Hyyppä, Jurkka Tuokko
France: Jean-Philippe Lagrange; Xavier Briottet
Germany: Hansjörg Kutterer; Klement Aringer; Dieter Fritsch
Ireland: Colin Bray; Ned Dwyer
Italy: Fabio Crosilla
Netherlands: Jantien Stoter; Aart-jan Klijnjan
Norway: Jon Arne Trollvik; Ivar Maalen-Johansen
Spain: Antonio Arozarena
Sweden: Anders Olsson; Anders Östman
Switzerland: Francois Golay; André Streilein-Hurni
United Kingdom: Malcolm Havercroft; Jeremy Morley

COMMISSION CHAIRPERSONS:

Sensors, Primary Data Acquisition and Georeferencing: Michael Cramer, Germany
Image Analysis and Information Extraction: Norbert Pfeifer, Austria
Production Systems and Processes: André Streilein-Hurni, Switzerland
Data Specifications: Jantien Stoter, The Netherlands
Network Services: Lars Bernard, Germany

OFFICE OF PUBLICATIONS:

Bundesamt für Kartographie und Geodäsie (BKG)
Publications Officer: Andreas Busch
Richard-Strauss-Allee 11
60598 Frankfurt
Germany
Tel.: + 49 69 6333 312
Fax: + 49 69 6333 441

CONTACT DETAILS:

Web: www.eurosdr.net
President: president@eurosdr.net
Secretary-General: secretary@eurosdr.net
Secretariat: admin@eurosdr.net

EuroSDR Secretariat
Public Management Institute
K.U. Leuven
Faculty of Social Sciences
Parkstraat 45 Bus 3609
3000 Leuven
Belgium
Tel.: +32 16 323180

The official publications of EuroSDR are peer-reviewed.

APPENDIXES (available on attached CD-ROM only)

1. Bovet, S., 2010. Phase2 empirical evaluation of ADS data Product generation with the Hyytiälä dataset at Swisstopo. Project report.
2. Brédif, M., Lelégard, L., 2010. Study of DMC panchro images resolution. Project report.
3. Chandelier, L., 2010. Performance test of IGN radiometric aerial triangulation. Project report.
4. Comerón, A., Muñoz, C., Md Reba, N., Rocadenbosch, F., Sicard, M., Tomás, S., 2008. Banyoles 2008 Campaign, UPC Lidar Measurements.
5. Cunilera, J., L.Martinez, 2010. Banyoles 2008 Campaign, SMC Report,
6. Markelin, L, 2012. Weather conditions during the 23rd Aug, 1st Sep and 25th Sep 2008 Campaigns in Finland.
7. Markelin, L, 2012. Supplementary results for the article XI: „Assessment of Radiometric Correc-tion Methods for ADS40 Imagery“.
8. Schläpfer, D., 2010. The Potential of Atmospheric and Topo-graphic Correction for ADS40/80. EuroSDR project report.
9. Sola, Y., Lorente, J., Campmany, E., 2008. Banyoles 2008 Campaign, UB Report.
10. Phase I: Questionnaire

EuroSDR-Project
Commission 1 “Radiometric aspects of digital photogrammetric images”

Final Report

Report by

Eija Honkavaara and Lauri Markelin
Remote Sensing and Photogrammetry – Finnish Geodetic Institute, Masala

Roman Arbiol and Lucas Martínez
Institut Cartogràfic de Catalunya, Catalonia

Abstract

This report presents the results and conclusions of the EuroSDR project "Radiometric aspects of digital photogrammetric images" that was carried out during 2008-2011. The project was a European-wide multi-site research project, where the participants represented stakeholders of photogrammetric data in National Mapping Agencies, software development and research. The project began with a review phase, which consisted of a literature review and a questionnaire to the stakeholders of photogrammetric data. The review indicated excellent radiometric potential of the novel imaging systems, but also revealed many shortcomings in the radiometric processing lines. The second phase was an empirical investigation, for which radiometrically controlled flight campaigns were carried out in Finland and in Spain using the Leica Geosystems ADS40 and Intergraph DMC large-format photogrammetric cameras. The investigations considered vicarious radiometric calibration and validation of sensors, spatial resolution assessment, radiometric processing of photogrammetric image blocks and practical applications. The results proved the stability and quality of evaluated imaging systems with respect to radiometry and optical system. The first new-generation methods for reflectance image production and equalization of photogrammetric image blocks provided promising results and were also functional from the productivity and usability points of view. For reflectance images, an accuracy of up to 5% was obtained without need of ground reference measurements. Application oriented results indicated that automatic interpretation methods will benefit from the optimal use of radiometrically accurate stereoscopic photogrammetric imagery. Many improvements are still needed for the processing chains in order to obtain full advantage of the radiometric potential of photogrammetric sensors.

During the project, the quantitative radiometric processing in photogrammetric processing lines was not mature technology at all. Operational applications used qualitative and statistical methods in assessing and processing the radiometry, and the output image products were mainly used in visual interpretation. The major emphasis in this investigation was to consider the radiometry from the quantitative point of view. This report summarizes many points of view to the radiometric processing and all the evaluated methods can be further developed and implemented as automated tools in modern photogrammetric processes of National Mapping Agencies in the future.

1 Introduction

A special advantage of the new digital large-format photogrammetric imagery is a high-quality multi-spectral radiometry. The high-quality radiometry opens up new prospects for the utilization of the photogrammetric imagery, but also requires new approaches for the data processing. The rigorous treatment of image radiometry is a new issue in photogrammetric processing chains. To investigate these issues, the European Spatial Data Research organization (EuroSDR) launched a project called "Radiometric aspects of digital photogrammetric images" in May 2008.

1.1 Objectives of the Project

The fundamental objectives of this EuroSDR project were as follows:

1. Improve knowledge on radiometric aspects of digital photogrammetric cameras.

2. Review existing methods and procedures for radiometric image processing

3. Compare and share operative solutions through a comparison of these techniques on a same test data set.

4. Analyse the benefit of radiometric calibration and correction in different applications (classification, quantitative remote sensing, change detection etc.).

1.2 Phases of the project

The project was realized in two phases. In the first phase, a review was made on radiometric aspects of digital photogrammetric images based on literature and a questionnaire to stakeholders of photogrammetric processes. In the second phase, a comparative, multi-site, empirical investigation was conducted.

1.3 Participants

In total, six National Mapping Agencies (NMA), one company and seven research participants participated the project (Table 1).

Participant	Organization	Role	Phases
Institut Cartogràfic de Catalunya (ICC)	NMA	Software developer, Data provider, Data user, Research	1,2
Institut Géographique National, France (IGN), Ecole Nationale des Sciences Géographiques (IGN/ENSG) and Laboratoire MATIS (IGN/MATIS)	NMA	Sensor manufacturer, Software developer, Data provider, Data user, Research	1, 2
National Survey and Cadastre, Denmark (KMS)	NMA	Data user	1
National Land Survey, Finland (NLS)	NMA	Data provider, Data user	1
Ordnance Survey, Great Britain (OS)	NMA	Data provider, Data user	1
Swiss Federal Office of Topography (Swisstopo)	NMA	Data provider, Data user	1, 2
ReSe Applications Schläpfer, Switzerland (ReSe)	Company	Software, Consultant, Research	1, 2
Finnish Geodetic Institute, Finland (FGI)	Research	Research	1, 2
Institut für Geoinformatik und Fernerkundung, Universität Osnabrück (IGF)	University	Research	1
University of Helsinki (UH)	University	Research	2
University of Eastern Finland (UEF)	University	Research	2
Instituto de Desarrollo Regional – Universidad de Castilla La Mancha (IDR-UCLM)	University	Research	2
Centre de Recerca Ecològica i Aplicacions Forestals – Universitat Autònoma de Barcelona (CREAF-UAB)	University	Research	2

Universitat de Barcelona (UB)	University	Research	2
Universitat Politècnica de Catalunya (UPC)	University	Research	2
Servei Meteorològic de Catalunya (SMC)	Meteorological Institute	Research	2

Table 1. Participants of the project

1.4 Publications

Results of the project have been presented in several scientific articles and reports. This final report will present some of the highlights of the results, and the summary and conclusions of the project; detailed results are given in the detailed publications. In this report, these publications will be referred using bold Roman numbers.

General descriptions of the project

I. Arbiol, R., Martinez, L., 2009. ICC-Banyoles 2008 Campaign in the framework of EUROSDR Radiometry Project. Project description and preliminary results. Proceedings of XI Geomatic Week, Barcelona. 3 - 5 March.

http://www.icc.cat/cat/content/download/48926/340513/file/banyoles_2008.pdf

II. Arbiol, R., Martínez, L., 2010. ICC EuroSDR Banyoles08 research activities. International Calibration and Orientation Workshop EuroCOW 2010. Castelldefels (Barcelona), 10–12 Feb.

http://www.ideg.es/page.php?id=1360

http://www.icc.cat/cat/content/download/20086/64380/file/11_ICC%20EUROSDR%20BANYOLES08%20RESEARCH%20ACTIVITIES.pdf

III. Honkavaara, E., Arbiol, R., Markelin, L., Martinez L., Cramer, M., Korpela, I., Bovet, S., Thom, C., Chandelier, L., Ilves, R., Klonus, S., Reulke, R., Marshall, P., Tabor, M., Schläpfer, D., and N. Veje, 2009. Status report of the EuroSDR project "Radiometric aspects of digital photogrammetric airborne images". Proceedings of the ISPRS Hannover Workshop 2009, Hannover, Germany, June 2-5, 2009.

http://www.isprs.org/proceedings/XXXVIII/1_4_7-W5/paper/Honkavaara-154.pdf

IV. Honkavaara, E., Arbiol, R., Markelin, L., Martinez, L., Bovet, S., Bredif, M., Chandelier, L., Heikkinen, V., Korpela, I., Lelegard, L., Pérez, F., Schläpfer, D., Tokola, T., 2011. The EuroSDR project "Radiometric aspects of digital photogrammetric images" – Results of the empirical phase. In Proceedings of the ISPRS Hannover Workshop 2011, June 14-17, 2011, Hannover, 8 pages.

http://www.isprs.org/proceedings/XXXVIII/4-W19/paper/Contribution172.pdf

Theory of image radiometry and results of Phase I

V. Honkavaara, E., Arbiol, R., Markelin, L., Martinez, L., Cramer, M., Bovet, S., Chandelier, L., Ilves, R., Klonus, S., Marshall, P., Schläpfer, D., Tabor, M., Thom, C., and N. Veje, 2009.

Digital airborne photogrammetry – A new tool for quantitative remote sensing? – A state-of-the-art review on radiometric aspects of digital photogrammetric images. Remote Sensing, Vol. 1, 577-605.

http://dx.doi.org/10.3390/rs1030577

Calibration

VI. Honkavaara, E., Nurminen, K., Markelin, L., Suomalainen, J., Ilves, R., 2011. Calibrating and validating multispectral photogrammetric 3D imaging system at a permanent test site – Case study with an Intergraph DMC. Photogrammetric Record, 26 (134), 229-249.

http://dx.doi.org/10.1111/j.1477-9730.2011.00634.x

VII. Markelin, L., Honkavaara, E., Hakala, T., Suomalainen and J., Peltoniemi, J., 2010. Radiometric stability assessment of an airborne photogrammetric sensor in a test field. ISPRS Journal of Photogrammetry and Remote Sensing, 65(4): 409-421.

http://dx.doi.org/doi:10.1016/j.isprsjprs.2010.05.003

VIII. Martínez, L., Arbiol, R., Pérez, F., 2010. Casi characterization and atmospheric correction for EuroSDR Banyoles08 dataset. International Calibration and Orientation Workshop EuroCOW 2010. Castelldefels (Barcelona).

http://www.ideg.es/page.php?id=1360

IX. Martinez, L., Soler, M.E., Pérez, F., Arbiol, R., 2011. Efecto de la atmósfera en la resolución óptica de la Z/I Digital Mapping Camera. Revista de Teledetección, nº 35, p. 32-40.

http://www.aet.org.es/revistas/revista35/Numero35_04.pdf

http://www.icc.cat/cat/content/download/48052/330277/file/2011_RET_35_Martinez.pdf

Atmospheric correction of images

X. Markelin, L., Honkavaara, E., Beisl, U. and Korpela, I., 2010. Validation of the radiometric processing chain of the Leica ADS40 airborne photogrammetric sensor. International Archives of Photogrammetry, Remote Sensing and Spatial Information Sciences, 38(7A): 145-150.

http://www.isprs.org/proceedings/XXXVIII/part7/a/pdf/145_XXXVIII-part7A.pdf

XI. Markelin, L., Honkavaara, E., Schläpfer, D., Bovet, S. and Korpela, I., 2012. Assessment of radiometric correction methods for ADS40 imagery. PFG 3/2012: 251-266

http://dx.doi.org/10.1127/1432-8364/2012/0115

Results of applications using reflectance signatures

XII. Heikkinen, V., Korpela, I., Tokola, T., Honkavaara, E. and Parkkinen, J., 2011. An SVM classification of tree species radiometric signatures based on the Leica ADS40 sensor. IEEE

Transactions on Geoscience and Remote Sensing. IEEE Transactions on Geoscience and Remote Sensing, 49(11): 4539-4551.

http://dx.doi.org/10.1109/TGRS.2011.2141143

XIII. Korpela, I., Heikkinen, V., Honkavaara, E., Rohrbach, F. and Tokola, T., 2011. Variation and directional anisotropy of reflectance at the crown scale - Implications for tree species classification in digital aerial images. Remote Sensing of Environment 115 (8), 2062-2074.

http://dx.doi.org/10.1016/j.rse.2011.04.008

XIV. Martínez, L., Pérez, F., Arbiol, R., and Magariños, A., 2012. Development of NDVI WMS geoservice from reflectance DMC imagery at ICC. International Calibration and Orientation Workshop EuroCOW 2012. Castelldefels (Barcelona), 8–10 Feb.

http://www.ideg.es/page.php?id=1360

Reports of individual participants

XV. Bovet, S., 2010. Phase2 empirical evaluation of ADS data Product generation with the Hyytiälä dataset at Swisstopo. Project report.

XVI. Brédif, M., Lelégard, L., 2010. Study of DMC panchro images resolution. Project report.

XVII. Chandelier, L., 2010. Performance test of IGN radiometric aerial triangulation. Project report.

XVIII. A. Comerón, A., Muñoz, C., Md Reba, N., Rocadenbosch, F., Sicard, M., Tomás, S., 2008. Banyoles 2008 Campaign, UPC Lidar Measurements.

XIX. Cunilera , J., Martinez, L., 2010. Banyoles 2008 Campaign, SMC Report.

XX. Markelin, L., 2012. Weather conditions during the 23rd Aug, 1st Sep and 25th Sep 2008 Campaigns in Finland.

XXI. Markelin, L., 2012. Supplementary results for the article XI: "Assessment of Radiometric Correction Methods for ADS40 Imagery".

XXII. Schläpfer, D., 2010. The Potential of Atmospheric and Topographic Correction for ADS40/80. EuroSDR project report.

XXIII. Sola, Y., Lorente, J., Campmany, E., 2008. Banyoles 2008 Campaign, UB Report.

XXIV. Phase I questionnaire.

2 Phase I – Review

2.1 Objectives

The objective of the review phase was to provide the necessary background information on the radiometric aspects of photogrammetric images, and it consisted of a literature review and a questionnaire to various stakeholders. The questionnaire was considered crucial, because existing literature covered only partially the modern photogrammetric process and it did not give information about radiometric processing in operational processes. Detailed results of the review are given in **V**.

Objectives of the questionnaire were to:

1. obtain a picture of the actual situation;
2. detect main weaknesses of existing digital camera radiometric processing;
3. look for main trends on existing and future development in this field;
4. learn what the advantages of better radiometric processing are and find which applications ask for better radiometric processing.

The questions were classified into five themes: sensor, calibration, image collection, post-processing and utilization of the images. For each theme, the questions were further divided into questions related to the current situation and to the desired situation. The questionnaire is given in **XXIV**.

2.2 Outcome of questionnaire

The questionnaire was delivered to several large and medium format photogrammetric sensor manufacturers, photogrammetric software providers, NMAs and Universities in October 2008.

The organizations that replied to the query are shown in Table 1. The widest response was obtained from NMAs, most of which are both data providers and users; some also have their own software development (IGN, ICC), and IGN is manufacturing its own sensor. ReSe is a software company behind the atmospheric correction software ATCOR for spaceborne and airborne scanner images, and is specialized in processing and utilization of imaging spectroscopy data in particular. In total, five responses were obtained from data providers, six from data users, one from a sensor manufacturer, three from radiometric software developers, and two from research organizations.

The major conclusions of the questionnaire were that improvements were requested for the entire process: sensors, calibration, data collection, data post-processing and data utilization. The fundamental problems could be listed as follows:

1. there was insufficient information on the radiometric processing chain,
2. radiometric processing chains were inadequate and
3. standards were missing, including methods, calibration, reference targets, and terminology.

The basic radiometric end products requested by image users were true color images and reflectance images. The expected benefit of a more accurate radiometric processing includes a more automatic and efficient image post-processing, better visual image quality, more accurate and automatic interpretation, and the quantitative use of data.

The results indicated that it is necessary to identify the interest groups related to the photogrammetric process. The fundamental processes are the sensor manufacturing, software development, photo-

grammetric image acquisition, photogrammetric image product generation (orthophotos, stereomodels), applications and research. The main interest groups are data users, data providers, sensor manufacturers, software developers and research organizations. Each interest group can be further divided into different subclasses based on the tasks they undertake. For example, the data user can undertake all phases of the process (sensor manufacturing, image collection, software development, image product generation, applications) or he can concentrate on only the application. Each of these groups has a different possibility to manage, influence or discover the details of the radiometric processing chain. Important interest groups are presented in Table 2; the interest groups of the participants of the questionnaire are shaded.

Type	Sensor manufacturing	Software development	Data collection	Image products	Applications	Research
U1	x	x	x	x	x	(x)
U2		x	x	x	x	(x)
U3			x	x	x	(x)
U4				x	x	(x)
U5					x	(x)
P1	x	x	x			(x)
P2	x	x	x	x		(x)
P3			x			(x)
P4			x	x		(x)
R1						x
SW1		x				(x)
M1	x	x				(x)

Table 2. Various interest groups dealing with image radiometry. The groups that are covered in the questionnaire are shaded. U1-U5: different classes of users, P1-P4: different classes of image producers. R1: research; SW1: software developer; M1: sensor manufacturer.

All data users expressed concern about the traceability of the radiometry. An important comment comes from the organization that purchases all the imagery: “We lack information on the entire data processing and also lack technical information on the integrated sensor system (e.g. position of GNSS/IMU related to the image sensor) and how the resulting image frame is computed”. The traceability and comparability of data collected with various sensors is especially a problem for users that order images. For the IGN, who is manufacturing its own sensor, all relevant information is available when needed.

2.3 Fundamental equations of image radiometry

As a part of the review, the fundamental equations related to the radiometric processing of photogrammetric images were identified. These are summarized below and more details are given in **V** and referenced literature.

Fundamental output products of the radiometric correction process are reflectance images and true color images:

- Reflectance images contain information about the reflection characteristics of objects in scene and they have a lot of potential in automatic and quantitative interpretation applications. Fundamental steps in the reflectance image generation are the compensation of sensor

artefacts (based on sensor calibration), atmospheric effects as well as object bidirectional reflection behavior.

- In true color images, colors are presented in a way which is attractive for the human visual system. In this case, the standard way to proceed is to transform the images to a standard color space, such as the CIE-XYZ color space. Colorimetric calibration is useful for applications where images are interpreted visually, but only applicable for images collected in blue, green and red wavelengths. For color infrared images this approach is not functional.

In this study we emphasize the reflectance image generation. The rigorous color image production requires the same steps and an additional colorimetric calibration; Martínez et al. (2007) gives more details about this process.

In high resolution photogrammetric imaging, the elementary components of radiance entering the sensor (L_{at_sensor}) are the radiance components from the object of interest, that is to say, the surface-reflected solar radiance (L_s), the reflected skylight (L_{sky}), the reflected background radiance (L_{bg}) and the radiance reflected first by the background objects and then by the atmosphere (L_{bg_multi}); the adjacency effect (L_{adj}) and atmospheric path radiance (L_{atm}) are radiance components that do not carry any information of the object of interest (Schott, 2007):

$$L_{at\_sensor} = L_s + L_{sky} + L_{bg} + L_{bg\_multi} + L_{adj} + L_{atm}. \quad (1)$$

The digital grey value (DN) at a given pixel, after dark pixel subtraction is applied, can be given as follows:

$$DN = GA_d \Omega \tau \int_0^{\infty} L_{at-sensor}(\lambda) S(\lambda) d\lambda \,, \quad (2)$$

where G is system gain, A_d is the area of the detector, Ω is the lens solid angle (aperture), τ is the integration or exposure time, $S(\lambda)$ is the system level spectral response, and λ is the wavelength. The sensor model in Equation 2 is given for the Intergraph DMC (Ryan and Pagnutti, 2009). This equation is referred as a sensor model in this report.

In practice, the band averaged values are used. For each band the relationship between the DN and band averaged at-sensor radiance ($\overline{L}$) can be given as follows:

$$\overline{L} = K' \frac{\tau}{f_{number}^{\,2}} DN \,, \quad (3)$$

where K' is the calibration coefficient needed for each band and f_{number} is f-number (aperture). Ideally, K' is needed for each band, but for example in the case of DMC, K' is determined for various apertures due to the insuffient stability (Ryan and Pagnutti, 2009).

In practice, the most significant components that are taken into account by atmospheric correction methods are L_s, L_{sky} and L_{atm}. The reflectance where atmospheric influences are corrected can be given as:

$$\rho = \pi (L_{at-sensor} - L_{atm})(1 - s\rho') / (S \tau_s \tau_v) \,, \quad (4)$$

where ρ is the surface reflectance, s is the spherical albedo of atmosphere (the fraction of the upward radiance that is backscattered by the atmosphere), ρ' is the average reflectance of the surrounding area, $(1-s\rho')$ is the term to take into account the multiple scattering, S is the mean solar irradiance in surface ($S=E_\lambda^0 \cos\theta_s$) and τ_s and τ_v are the transmittance in solar and viewing paths, respectively. (**V**; Richter and Schläpfer, 2002; Besil et al., 2008)

One of the important aspects related to the radiometry of photogrammetric images is the anisotropy of object reflectance. This phenomenon means that the reflection of object is a function of the viewing and illumination geometries. This can be modelled by the bidirectional reflectance distribution fubction (BRDF):

$$\rho(\theta_i,\varphi_i,\theta_r,\varphi_r) = \frac{L(\theta_i,\varphi_i,\theta_r,\varphi_r)}{E(\theta_i,\varphi_i)}\,, \tag{5}$$

where $L(\theta_i,\varphi_i,\theta_r,\varphi_r)$ is the radiance reflected by the object, $E(\theta_i,\varphi_i)$ is the irradiance at object, θ_i,φ_i are the zenith and azimuth angles of incident light and θ_r,φ_r are the zenith and azimuth angles of reflected light (Schaepman-Strub et al., 2005; von Schönermark et al., 2004).

2.4 Objectives of the empirical phase

Based on the results of the questionnaire and the potential of the available image materials, the following topics were selected as the general objectives of the empirical phase:

1. Radiometric calibration and characterization
2. Spatial resolution assessment
3. Reflectance image calculation and image block equalization
4. Color enhancement of the calibrated data
5. Application oriented studies

These topics cover the fundamental processes of the radiometric processing chain.

Objectives 1 and 2 are related to validation and calibration of the imaging sensor and system, which should be carried out on a regular basis (e.g. yearly) to ensure the quality of the imaging system. These aspects should be considered also in the acceptance testing of a purchased new sensor system. The use of a test field for calibration purpose, instead of using either laboratory calibration or calibration on the actual mapping task itself (on-the-job calibration), is known as vicarious calibration in the remote sensing community, and used also in this report.

Objectives 3 and 4 are related to the producing of output images that are used in various applications, such as stereo mapping and automatic change detection. The methods used by NMAs have to be suitable for processing of huge amounts of image data (tens to hundreds of thousands of km^2 every year). Radiometric correction is crucial in order to produce accurate, high-quality image data products. The key requirements for these processes include efficiency (fast processing, no ground reference targets), usability aspects (simplicity of use, automatic selection of parameters), reliability and accuracy. In this project, the color enhancement part was not covered.

The last objective is related to the fact that the radiometric processing level and quality of image data has influences in applications. In this project the application oriented studies concerned the NDVI data layer generation and tree species classification.

3 Phase II: Empirical investigation – Set-up

3.1 Empirical image data

In summer and autumn 2008, radiometrically controlled test flights were conducted in Catalonia and in Finland. Details of the campaigns are described below.

3.1.1 Integrated DMC and CASI test flight in Banyoles

ICC executed extensive radiometric test flights with a DMC and the Compact Airborne Spectrographic Imager (CASI) in Banyoles in 15 July, 2008 (Figure 1) (**I, II**). The imagery was collected from 820, 1125, 2250 and 4500 m flying altitudes, providing GSDs of 7.5 cm, 10 cm, 20 cm and 30 cm. Various manmade reflectance targets as well as several artificial and natural stable covers were available around the test field, including a lake; two groups carried out the radiance and reflectance ground-truth data acquisition with spectroradiometers. In addition, a Siemens star was installed in the test field. Atmospheric state was directly measured by several groups, instruments and techniques: an atmospheric Lidar provided aerosol profiles and two automatic sun tracking photometers provided column integrated values of Aerosol Optical Thickness (AOT) for the optical spectrum. Atmospheric information simultaneous to the airborne sensors overflight was also available. The atmospheric conditions were excellent with an AOT at 500 nm of less than 0.1 (**XVIII**, **XIX, XXIII**).

Figure 1. Airborne imagery and ground truth data collected on 15 July, 2008 in Banyoles. ICC test field is deployed on a football field.

The scientific objectives of this campaign were:

1. Radiometric calibration of a DMC by the radiance and the reflectance methods. Validation with radiometric targets. Radiance method will be performed with the simultaneous acquisition of CASI.

2. Spectral characterization of CASI regarding bandwidth and smiling effect. Comparison with laboratory results.

3. Atmospheric correction of CASI imagery with aerosol distribution and load, and water vapor derivation by an inversion method. Validation with radiometric targets and atmospheric measurements.

4. Atmospheric correction of DMC images by using CASI derived atmosphere parameters. Validation with radiometric targets.

5. Colorimetric calibration of DMC towards CIE standard color space. Validation with radiometric targets.

6. Resolution studies by means of a Siemens star and edge targets. Study of the relationship between atmosphere state and resolution. Comparison with computer radiative transfer simulations.

7. Application of DMC radiance and reflectance images to remote sensing studies.

3.1.2 DMC test flights in Sjökulla

The National Land Survey of Finland (NLS) carried out an acceptance testing of their new DMC on 1 and 25 September 2008 at the Sjökulla test field of the FGI (Figure 2) (Honkavaara et al., 2008; Honkavaara, 2008; **VI**). The flying height was 500 m above the ground level, which provided a 5 cm GSD. The reflectance reference targets included six permanent bidirectional reflectance factor (BRF) targets of gravel available at the test field, three transportable BRF targets and several natural covers. By using the BRF-calibrated targets, it is possible to obtain accurate reference reflectance for different viewing/illumination geometry (Suomalainen et al., 2009). In-situ groundtruth measurements were carried out using an ASD (Analytical Spectral Devices) field spectrometer during the flights. A Siemens star, edge target and line bar targets were available for the spatial resolution evaluations. Visibility measurements were carried out at the Helsinki-Vantaa airport at 30 km distance from the test area; in both flights the visibility was good, approximately 30-50 km (**XX**).

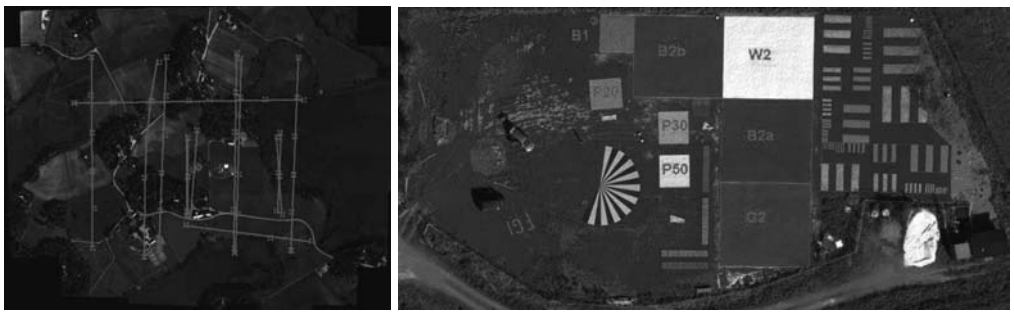

Figure 2. Left: Flight lines in Sjökulla on 1 September, 2008. Right: Radiometric and spatial resolution targets at Sjökulla test field. B1: Black gravel; R1: Red gravel; B2a: Black gravel, version a; B2b: Black gravel, version b; G: Grey gravel; W2: White gravel; P20, P30, P50: portable reference reflectance targets with nominal reflectance of 0.20m 0.30 and 0.50.

The scientific objectives of this campaign were:

1. Absolute radiometric calibration of the DMC by the reflectance method.

2. Spatial resolution studies of the DMC using Siemens star, edge targets and resolution bar targets.

3. Evaluation of the influences of various exposure and aperture settings on the radiometric performance and spatial resolution of the DMC.

4. Evaluation of the BRF measurement potential of the DMC.

The many difficulties in this campaign show the typical challenges of radiometrically controlled imaging campaign. The acceptance testing was scheduled for the beginning of August. Unfortunately the weather conditions were too poor in August, so the campaign could not be executed before September; the field measurement team was ready for takeoff for more than one month and three field campaigns were carried out unnecessarily. In the first successful airborne campaign the sensor settings were not optimum, and the images were saturated in worst cases already with a reflectance value of 0.25. To obtain unsaturated images and to allow proper acceptance testing, a second campaign was carried out by the end of September. The field measurement team was not prepared for this campaign and the spectrometer was not available, so only reflectance targets were installed in the test field.

3.1.3 Integrated ADS40/ALS50 test flight in Hyytiälä

The test flight with ADS40 (SH 52) and ALS50 (Airborne Laser Scanner) was carried out at the Hyytiälä forestry test field in co-operation with Leica Geosystems, University of Helsinki, University of Eastern Finland, Estonian Land Board and FGI (Figure 3). The test site was 3300 m x 8500 m in size and it contains more than 200 forest plots and over 15000 trees that have been measured for position and basic variables, in different forest conditions (density, age, species mixture, silvicultural history) (Korpela et al. **XIII**). A state-of-the-art weather station for atmospheric research runs at the area of interest (SMEAR II, AERONET) (Holben et al., 1998; Hari and Kulmala, 2005). FGI's BRF calibrated reflectance targets and a Siemens star were installed at the test field. The reflectance/radiance of the targets as well as various homogeneous land covers (asphalt, sand, gravel, grass) were measured by FGI and Leica Geosystems using spectroradiometers. ADS40 data was collected with the uncompressed mode from 1000, 2000, 3000 and 4000 m flying altitudes providing GSDs of 10 cm, 20 cm, 30 cm and 40 cm. Atmospheric conditions were not as perfect as in Banyoels campaign, with an AOT at 500 nm of 0.14 - 0.18 (**XX**).

The scientific objectives of this campaign were:

1. Absolute radiometric calibration of the ADS40 by the reflectance method and comparisons to laboratory calibration.

2. Evaluation of the performance of radiometric correction methods.

3. Evaluation of the BRF measurement potential of the ADS40.

4. Spatial resolution studies of the ADS40 using Siemens star.

5. Evaluation of influence of radiometric correction level in forestry applications.

6. Further objectives of the entire campaign include the radiometric calibration of ALS50 and its utilization in forestry applications, which is out of scope of this project.

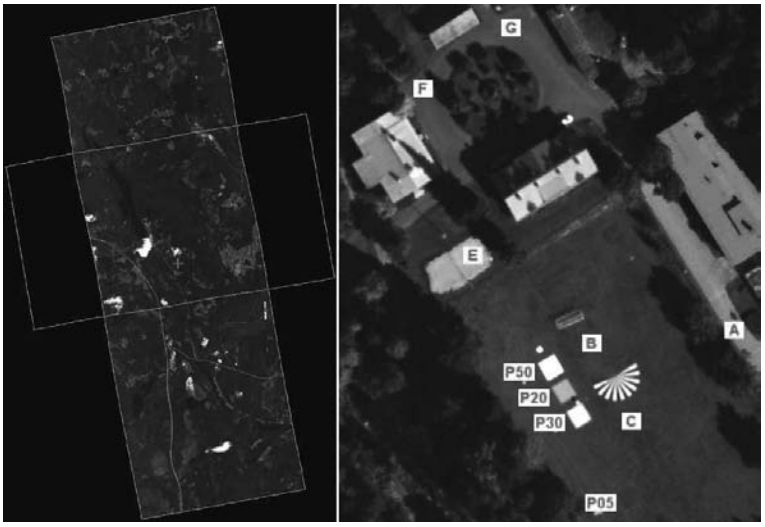

Figure 3. Left: 4 km flying height ADS40 image block from the Hyytiälä area on 23 August, 2008. Right: Reference measurements in Hyytiälä.

The varying weather conditions caused problems in this campaign as well. The field measurement team was ready for takeoff for one week; the campaign could be carried out in one Saturday morning. The positive feature of this campaign was that continuously operating sun photometer and weather station are permanent equipment at the test site, which helped greatly the field operations. After the airborne campaign clouds entered rapidly to the test site, thus complete BRF characterization of the natural targets at the test site could not be carried out.

Objective	DMC Banyoles	DMC-Sjökulla	ADS Hyytiälä	Participant, method
Radiometric calibration and characterization of the sensor/system	x			ICC: CASI+6S
		x	x	FGI: MODTRAN4
			x	FGI:ATCOR-4
			x	RESE: ATCOR-4
Spatial resolution assessment	x			IGN/MATIS: Siemens star
	x			IGN/MATIS: Image
	x			ICC: Siemens star
		x		FGI: Siemens star
		x		FGI: Resolving Power (RP) targets
Reflectance image generation, radiometric block adjustment	x			IGN: Pepita
		x		FGI: Empirical line method
			x	FGI: XPro
			x	FGI: ATCOR-4
			x	Rese: ATCOR-4
			x	Swisstopo: XPro
Applications	x			ICC: NDVI
			x	UH, UEF: tree species classification

Table 3. Summary of objectives, methods and participants in empirical study.

3.2 Processing of the data

The participants of the empirical phase included three National Mapping Agencies (NMAs), one company providing atmospheric correction software and eight research participants (Table 1). The data was delivered to some additional parties, but they did not return any results. Summary of the objectives of the empirical study and how these were covered by the project participants, data sets and approaches are given in Table 3. The methods are described in the following sections.

4 Phase II – Radiometric calibration and characterization of the sensor/system

Radiometric calibration determines the radiometric response of an imaging system. The central task is the determination of absolute and relative radiometric response (Beisl, 2006; Ryan and Pagnutti, 2009). The absolute radiometric calibration determines for each channel the calibration coefficients (Equation 3). The relative radiometric calibration normalizes the output of the sensor so that a uniform response is obtained in the entire image area; the corrections are determined at least for sensitivity differences of individual cells of a detector array, defect pixels, light falloff and dark signal. In addition, spectral and colorimetric models and PSF are necessary information in radiometric processing, and various non-uniformities are of interest to achieve high absolute calibration accuracies. The exact parameterization is always system dependent.

For airborne sensors, the laboratory calibration is the most accurate method to provide the full radiometric sensor calibration. The important tasks of vicarious calibration processes are to evaluate the validity of the laboratory calibration in flight conditions, to carry out the overall system validation and characterization and in general, to tune the image collection process (in particular the exposure settings); in some situations also to determine the absolute calibration. These are important steps to carry out especially after the sensor purchase and after updates and in beginning of the imaging season. As is the necessity in laboratory calibration, also in the vicarious radiometric calibration the fundamental prerequisite is to determine accurately the radiance entering the system. For this either radiative transfer calculations utilizing accurate information of atmospheric conditions and object reflectance (reflectance-based method), or simultaneous determination of the at-sensor radiance by a calibrated radiometer (radiance-based method) is used (see more details in **V**).

In the project, the empirical investigations were carried out using the photogrammetric systems DMC and ADS40 and a CASI hyperspectral scanner.

4.1 Characterization of the hyperspectral CASI system

The determination of the DMC radiometric calibration parameters was the main objective of the ICC's previous campaign in 2005 (Martinez and Arbiol, 2008). The obtained results were satisfactory enough, but the secondary objective concerning the results of atmospheric correction of DMC images was disappointing. Without field measurements the obtained values could not be applied. Even worse, the hypothesis that the CASI could be used as a calibration system was far from reality due to a poor knowledge on the detailed response of the hyperspectral sensor. With the 2008-campaign data it was possible to overcome the difficulties of the 2005-campaign (**I**, **II**).

The spectral shift characterization method of CASI is based on the hypothesis of global g-coefficients that need to be identically shifted for all the wavelengths for each look direction. The developed

methodology exploits the presence of the O2 atmospheric absorption band (about 760 nm) over a high reflectance cover in that wavelength. To determine the spectral shift, a non-orthorectified hyperspectral image over a vegetated area is aggregated in the along-track direction. This process generates a one-line image with 550 across-track spectral samples (look directions). Then, a subpixel Pearson correlation is computed for each one of the 550 spectra with a vegetation spectrum processed with the 6S code (Vermote et al., 1997) to take into account the effect of the O2 absorption band. The estimated spectral shift is then applied to the original image and the radiometric bands are spectrally resampled to fit the CASI channel nominal limits described by the g-coefficients. Details are given by Martínez et al. (**VIII**).

The first approximation of the spectral sensitivity of the bands was a rectangular response between the limits of each channel. This simple estimation works fine to correct the atmospheric scattering but is insufficient to solve the absorption regions. The manufacturer provided the accurate spectral sensitivities with a polynomial relationship between FWHM and wavelength, which showed values up to several times the nominal FWHM of the sensor (**VIII**).

Results by Martinez et al. (**VIII**) indicated that CASI smiling effect and accurate CASI spectral sensitivity had to be taken into account in order to obtain accurate atmospheric correction; in these circumstances correction yielded fewer artefacts on the atmospherically corrected spectra, even when only standard atmospheric parameters were used. The small artefacts still remaining around the absorption bands could be explained by a frequency dependence of the smiling effect, too week signal-to-noise ratio, etc.

4.2 Vicarious radiance based radiometric calibration of DMC in Banyoles

As an absolute radiometric calibration of the DMC was not available from the manufacturer during the empirical phase of the project, this relationship was obtained from simultaneous images from DMC and CASI sensors collected in the Banyoles campaign, by the radiance based calibration method. The CASI system is periodically recalibrated in the laboratory, and the idea was to transfer this calibration to the DMC. This is possible due to the fact that the acquisition geometry, atmospheric effects and illumination geometry are approximately equivalent for areas imaged simultaneously. Besides, the spectral resolution of CASI is high enough to reproduce DMC-like channels by integrating calibrated CASI hyper-spectral bands. In order to verify the previous hypothesis and because of the different FOV of DMC and CASI, only the central area of the DMC scenes were used. In addition, DMC pixels were aggregated to fit the coarse CASI spatial resolution. Then a median floating window filter was applied to both CASI and DMC imagery to avoid misregistration and other sources of noise. The radiometric calibration was performed through a linear regression between Digital Numbers (DN) from DMC and radiance values of a CASI image emulating DMC bands for each band and image (Martínez et al., 2007). Linear relationships with a zero intercept were found for all DMC used apertures and bands. All the R^2-values, characterizing the quality of least squares fit, were greater than 0.9. More results are given in **VIII**.

4.3 Vicarious reflectance based radiometric calibration of DMC in Sjökulla

The reflectance based vicarious calibration was applied to DMC using the Sjökulla images. The reflectance spectrums of several reference targets were measured during the campaign (Figure 2). The at-sensor radiances of the targets were calculated using the MODTRAN4 radiative transfer code. As in-situ measurements of atmospheric conditions were not available, the standard “Midlatitude summer” atmospheric settings and visibility information from the Helsinki airport in about 30 km

distance from the test field were used for the atmospheric radiative simulation. The images were collected using various exposure settings (aperture, exposure time), so the calibration was calculated using DNs that were normalized using the aperture and exposure time. Details of the approach are given by Markelin et al. in **VII**.

The results of the vicarious calibration showed that in general the sensor performance was linear; the R^2-values of linear regression were over 0.993 (Figure 4). The non-linear behavior with high at-sensor radiances is due to the saturation caused by failed exposure settings. In most cases the intercept and slope both were significant; absolute calibration parameters for different calculations are given in **VII**. Absolute radiometric laboratory calibration was not available for the DMC, so the vicarious and laboratory parameters could not be compared.

The vicarious calibration was calculated with nine different exposure settings (varying apertures and exposure times), and the radiometric stability of the system was assessed by evaluating the fit of the calibration parameters obtained for one setting with another setting, and for different days. The difference in R, G and B channels was on average 2.9–4.3% for the same day and the same aperture data, 3.5–4.5% for the same day and different aperture data and 3.1–5.2% for data collected on different days. The NIR channel showed weaker performance, and differences in corresponding cases were 5.7%, 9.2% and 10.9%, respectively. These differences appear in Figure 4 so that different lines are not accurately overlapping. Possible causes of these differences might be sensor instability, inaccuracy of the atmospheric modeling and inaccuracy of the reference values. The stability could be considered to be very good, as it derives from the instabilities of two independent sensors (PAN and MS). Detailed results are given in **VII**.

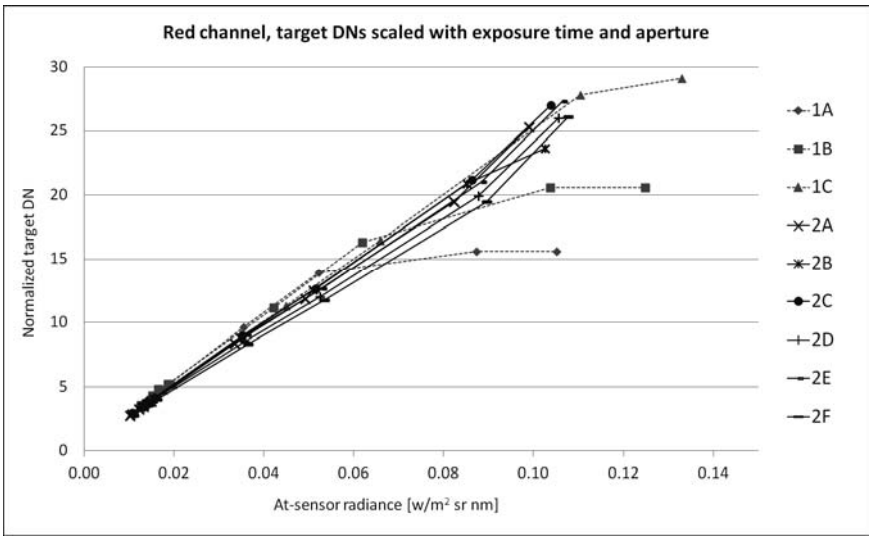

Figure 4. Normalized reference target average DNs as a function of simulated target at-sensor radiances. All settings, red channel. 1A-1C settings in 1 September, 2A-2F: settings in 25 September.

4.4 Vicarious reflectance based radiometric calibration of ADS40 in Hyytiälä

For the ADS40 campaigns in Hyytiälä the accurate in-situ measurements were available, including in-situ reflectance measurements of the reference targets and the atmospheric measurements of the

SMEAR-II and AERONET stations. An absolute radiometric calibration of the ADS40 was carried out using the reflectance based vicarious calibration method using ATCOR-4 (**XI**) and MODTRAN4 (**X**).

The main result from the reflectance based vicarious calibration was that both the gain and offset parameters were detected statistically significant (see detailed calibration parameters in **XXI**). Based on the laboratory calibration of the ADS40 (Beisl, 2006), only the gain parameter is needed. Differences in at-sensor radiances based on the MODTRAN4 based at-sensor radiance simulations by FGI and the ADS40 processing chain were larger than expected (10-20%) (Figure 5; **X**). Possible causes for the differences are on the one hand the inaccuracy of reference values and atmospheric modeling in the radiative transfer simulation, and on the other hand, possible inaccuracy of the ADS40 laboratory calibration. In this study it was not possible to find the exact reason for the differences. The assessment of accuracy of the reflectance images in Section 6.3 shows that using the vicarious calibration, the accuracy of ATCOR-4 based correction method improved significantly.

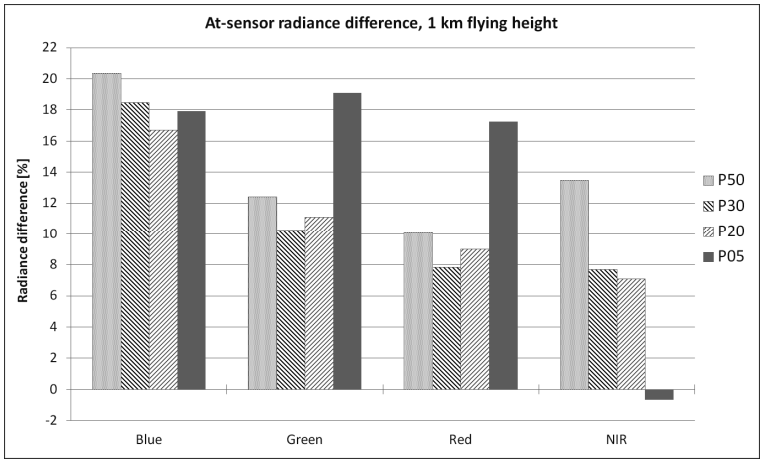

Figure 5. Relative differences of at-sensor radiances provided by MODTRAN4 and Leica XPro in different channels B, G, R and NIR on tarps on images from 1 km flying altitude. Difference = 100 * (MODTRAN4 – XPro) / XPro

5 Phase II – Spatial resolution assessment

The major factors influencing the image spatial resolution are the lens and detector properties. For high-quality photogrammetric sensors these are carefully designed and measured in laboratory. With multiple lens systems, such as DMC and UltraCam, the image stitching can cause additional deterioration of image quality. Important factors in dynamic applications influencing the image resolution are the forward image motion and the other motion components caused by the moving platform. Image quality is influenced also by the sensor exposure settings (Equation 2 and 3) and atmospheric conditions (Equation 1). The assessment of the system performance in flight conditions is important in two major situations: 1) to assess the performance of the entire imaging system and 2) to evaluate resolution of a specific campaign and individual images.

5.1 Methods for spatial resolution assessment

Spatial resolution measurements were performed for the Banyoles and Sjökulla DMC images. Different methods used in this study are described briefly below and summarized in Table 3 and 4.

Targets and participant	Method
ICC Siemens star, Banyoles, by ICC	The ICC method processes a region of interest that contains a single contour and makes a minimum square adjustment over the bi-dimensional function of the edge that is modelled as a sigmoid function. The five parameters are estimated in a least squares adjustment and the computed function is derived for obtaining the LSF (Line Spread Function). The FWHM (Full Width at Half Maximum) over the LSF is the measurement value (Talaya et al., 2008).
ICC Siemens star, Banyoles, IGN/MATIS	The IGN/MATIS used the Siemens star to determine the Modulation transfer functions (MTF) by evaluating contrasts of bright and dark sectors (**XVI)**.
Entire image, Banyoles, by IGN/MATIS	IGN/MATIS used a method that measured the local image sharpness over the entire image by using Haar Wavelets Transform (**XVI)**.
FGI RP targets, Sjökulla, by FGI	RP-values were automatically determined from line bar targets by finding the narrowest detectable lines (Honkavaara et al. 2006; Honkavaara, 2008).
FGI Siemens star, Sjökulla, by FGI	PSF-values were determined from Siemens star by first estimating the MTF based on contrasts of adjacent sectors and then calculating the PSF (Honkavaara et al., 2006; Honkavaara 2008)

Table 4. Methods for spatial resolution assessment.

The conventional, accurate method for spatial resolution measurement is to use artificial targets, such as line bar target, Siemens star or edge target:

- In the Banyoles campaign (Figure 1), there was a Siemens star made of canvas of size of 100 m^2 and with 5° sectors; the target appeared in different positions on 9 DMC images from the flying height of 820 m, with a GSD of about 8 cm.

- In the Sjökulla campaign (Figure 2), a Siemens star and resolving power (RP) line bar targets were available. The FGI's Siemens star is a semicircle with a size of 72 m^2 (radius of 6.8 m and 10° sectors). In the line bar targets, the widths of lines are 3-12 cm. In the image blocks, the resolution targets were located over the image area on 35 positions on first acquisition day and on 18 positions on second acquisition day. GSD was 5 cm and flying height was 500 m.

The methods that can evaluate image resolution automatically using the campaign image data and do not require artificial targets are very attractive. This type of a method has been developed by IGN/MATIS. The image sharpness map is determined by the Haar Wavelets (Brédif and Lelégard, **XVI**).

Influences of the following factors were studied in the resolution evaluations

1. Resolution in different positions in the image (all participants)

2. Resolution in radial and tangential directions (IGN/MATIS)

3. Resolution in flying direction and cross-flight direction (FGI)

4. Influence of exposure time and aperture (FGI)

5. Influence of atmosphere (ICC)

5.2 Results of spatial resolution assessment of the imaging system

The ICC used the Siemens star to determine the PSF. The averaged resolution obtained for each image did not show the expected correlation between the distance to the center of the image and the resolution. These unexpected results are probably due to variables of the acquisition process not taken into account during the study.

The analysis of MTF by IGN/MATIS from Siemens star showed that the optical system was isotropic and the lens was compatible with the CCD-array (no aliasing). The resolution was better in a centered band parallel to the flight direction. The sharpness map based on Haar wavelets derived from 156 images is shown in Figure 6. It shows some possible defects due to image formation process based on mosaicking four images and some additional minor defects. The method is a potential tool for detection of optical defects and the qualification of the mosaicking of multiple sensor images into a larger composite image. The conclusion of the IGN/MATIS evaluations was that the panchromatic photos provided by the DMC camera did not present major faults. Detailed results are given by Brédif and Lelégard (**XVI)**.

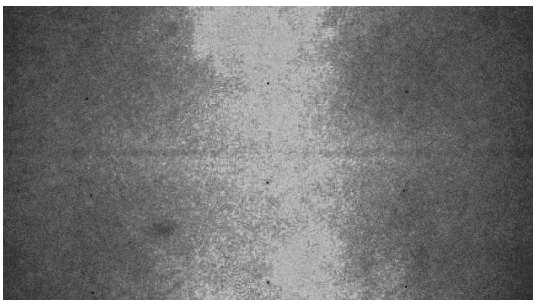

Figure 6. Image sharpness map obtained using 156 images of the Banyoles DMC campaign by IGN/MATIS (XVI). Yellow indicates better and green worse image sharpness.

The RP measured using the Sjökulla image data is shown as function of distance from image center in flight and cross-flight direction in Figure 7. Resolution was dependent on the distance from the image center: the farther the target was from the center, the worse the resolution was. By using linear regression, the resolution was worse by a factor of 1.5 in the furthest image corner compared with the image center. The same phenomenon had already been demonstrated both theoretically and empirically by Honkavaara et al. (2006). The theoretical expectation regarding the resolution of an image with a 12 µm pixel size is 84 lines/mm; with the tilted DMC images the theoretical expectation regarding the decrease of resolution is up to 1.6 in the image corner. The resolution was slightly better in the cross-flight than in the flight direction, which is most likely caused by the forward image motion. Any significant influences of the exposure settings (f-stop: 8, 11; exposure time 3.5–6.5 ms) on the resolution could not be detected. The evaluations of MTFs provided similar conclusions.

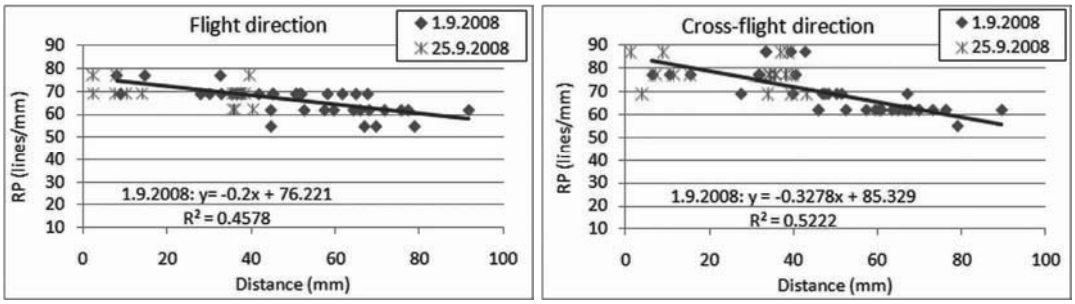

Figure 7. Resolving power as the function of the radial distance from the image center on flight (left) and cross-flight (right) directions.

5.3 Simulations on influences of atmosphere on spatial resolution

Imaging systems suffer from resolution degradation due to both the optical system and the atmosphere. Therefore, real resolution of the image is different from purely geometrical pixel size and the Ground Sampling Distance (GSD). The ICC analysed the image resolution as a function of the atmospheric radiative conditions. The 6S (Vermote et al., 1997) code was used to model the atmosphere. Atmosphere type, aerosol model and total load, illumination and observation geometries and spectral range were taken into account when computing simulations. The results were also compared with the resolution measures on the real images taken with the DMC images from Banyoles. See details in **IX.**

The histogram of the resolution (FWHM of LSF in pixel units) after implementing a step-like weather simulation for panchromatic channel showed a skewed distribution of resolution values with a large tail towards lower values of resolution (FWHM greater) (Figure 8). This distribution indicates that in the majority of cases the resolution is about the maximum frequency, but there are a lot of cases where the atmosphere will produce a large loss of resolution. Besides, there is a high dependence on wavelength, and the maximum effect appears at lower wavelengths. These simulation results and the resolution measured in the real DMC panchromatic images are compatible. A more detailed analysis shows that the type and amount of aerosols influence the loss of resolution (Figure 9). Details are given in **IX**.

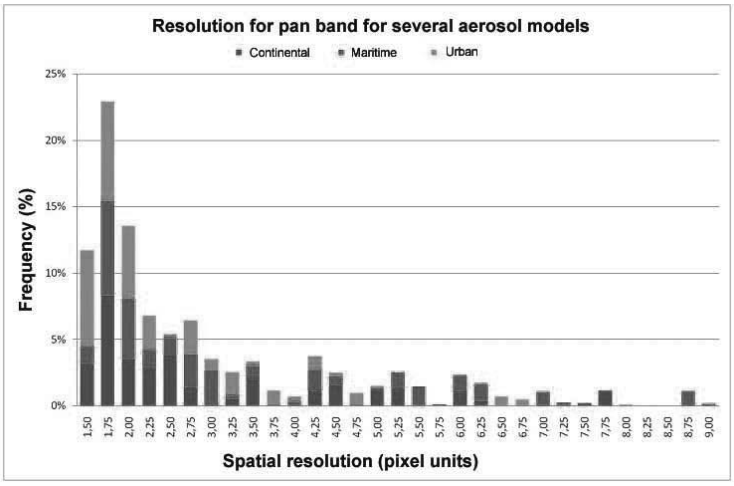

Figure 8. Resolution for DMC pan band with several aerosol models applied (FWHM of LSF in pixel units). (IX)

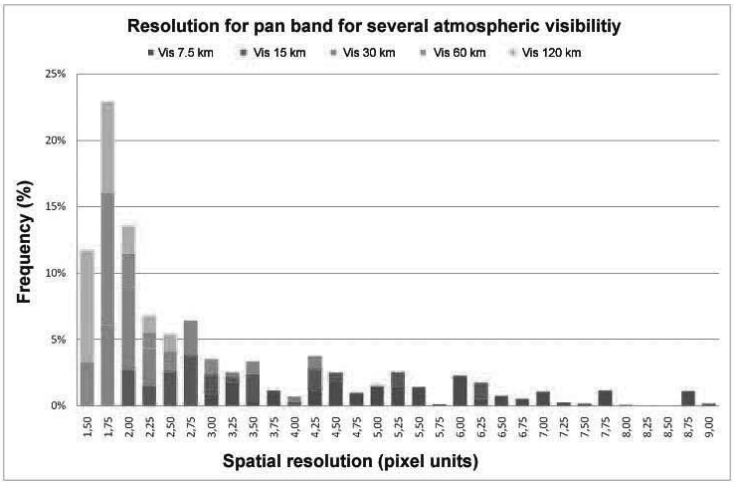

Figure 9. Resolution for DMC pan band with varying atmospheric visibility (FWHM of LSF in pixel units). (IX)

6 Phase II – Reflectance image production and image block equalization

The desired output products from the radiometric processing are reflectance images, true color images and in general, balanced image data. The radiometric processing method should take into account influences caused by the sensor, atmosphere and objects. The most significant sensor related influences are the sensor spectral and radiometric response, sensor instability and sensor settings during the data collection (Equation 2 and 3). The atmosphere has great influences on the image radiometry. The most significant factors to be compensated are the atmospheric path radiance and the influences of diffuse light (Equation 4). Finally with the large-format photogrammetric cameras the BRDF-effects have to be accounted for (Equation 5).

6.1 Methods for reflectance image production and image block equalization

Several relevant approaches for reflectance image calculation and image block equalization were evaluated in the project. These included the Pepita radiometric block adjustment method of IGN, two commercially available correction methods based on radiative transfer calculations (ReSe ATCOR-4 and Leica Geosystems XPro) and an empirical line based method (Table 3).

6.1.1 Pepita of IGN

The "radiometric aerial triangulation" Pepita software is a method for equalising a block of digital aerial images, which can be considered as relative radiometric calibration (Chandelier and Martinoty, 2009; **XVII**). It is based on a parametric, semi-empirical radiometric model taking into account BRDF, haze differences between blocks of images, solar elevation, sensor settings (exposure) and a optional radial component (mainly for chromatic aberration). The model parameters are computed through a global least-squares minimization process, using radiometric tie points in overlapping areas between the images. As a result, a relative equalization between the images is obtained. The method has been used in the IGN orthoimage workflow since 2005. At the beginning, Pepita has only been tested and used on IGN-v1 camera images, giving satisfying results. In 2008, some tests were carried out on DMC images, but the results did not meet the requirements of the IGN orthoimage database specifications. In 2009, IGN acquired its own UltraCam XP camera and Pepita is currently used both on UXP and IGN-v2 cameras.

6.1.2 ATCOR-4 of ReSe

The ATCOR-4 performs a physically based atmospheric and topographic correction for airborne scanner data in the solar (0.35-2.55 µm) and thermal (8-14 µm) spectral regions. The correction is based on pre-calculated MODTRAN® look-up tables of the atmospheric radiation field (Richter and Schläpfer, 2002; Richter and Schläpfer, 2011; **XXII**). The output in the solar region is the surface reflectance and in the thermal region it is the surface (brightness) temperature and emissivity. The capabilities of the software include determination of the aerosol map (requires bands in the near infrared and/or in the short wave infrared region) and the spatial water vapor map (requires bands in the 940/1130 nm region), haze and cirrus cloud removal (low altitude haze) and inflight sensor calibration using ground reference targets. ATCOR-4 is for wide FOV airborne scanner imagery and for all terrain types, and it includes the capability for radiometric correction in rugged terrain with cast shadow, topographic and BRDF corrections. The basic assumption of ATCOR-4 is a stable, accurately calibrated sensor.

6.1.3 XPro of Leica Geosystems

Leica Geosystems XPro software takes care of the entire post-processing workflow of the ADS-imagery from data download to the generation of stereo models and orthoimages. Main features from the radiometric point of view are the options to produce ground radiance and ground reflectance images. The default product of XPro is calibrated DN, which relates the pixel data to at-sensor radiances. There are two options to produce ground radiance data: the Dark Pixel Subtraction and the Modified Chavez methods. Ground radiances are still dependent on the illumination level and vary from flight line to flight line. Ground reflectances are calculated by dividing the reflected radiance by the incoming solar irradiance, which is estimated based on the radiative transfer equation by Fraser et al. (1992) and using a parameterization of the atmospheric parameters based on the method of Song et al. (2003). All three correction methods are based on an automatic dark object method to tune the corrections to the actual atmospheric conditions. Additionally, BRDF correction based on a modified Walthall model is implemented in XPro. All corrections rely entirely on a priori calibration information and parameters derived from the image data. The details of the correction methods are given by Beisl et al. (2008) and the method was analysed by Heikkinen et al. (**XII**).

6.1.4 Modified empirical line method

Empirical line method is widely used in reflectance calibration of remote sensing image data (Smith and Milton, 1999). In the method, a linear relationship of the DNs and ground reflectances is determined. In this study a modified version that takes into account the anisotropy of the reference target and uses DNs that are normalized with respect to size of aperture and exposure time was used. Details of the approach are given by Honkavaara et al. in **VI**.

6.1.5 Performance assessment of radiometric correction methods

The performance assessment of radiometric correction is dependent on the type of correction performed.

The validation of reflectance images can be carried out using reflectance reference measurements. In this investigation, artificial reference targets installed in the area and surfaces existing in the object were used as reference (see Section 3.1); in each reference target ground truth measurements were carried out using spectroradiometers. In most cases the nadir reflectances were measured, but in the case of FGI reference measurements also BRFs were measured in many cases. Repeatability of the reflectance image generation was evaluated by comparing images collected in repeated acquisitions of same targets from the same or different flying heights.

The difference of the reflectance in image and the reference reflectance is calculated for each target to obtain the reflectance error in reflectance units:

$$E_{refl} = \rho_{data} - \rho_{ref} \tag{6}$$

This difference is divided by the reference and multiplied by 100 to get the reflectance error in percents:

$$E_{refl\%} = 100(\rho_{data} - \rho_{ref}) / \rho_{ref} \tag{7}$$

From 6 and 7, root mean square error values ($RMSE_{refl}$ and $RMSE_{refl\%}$) are calculated for each image and sensor channel. The $RMSE_{refl\%}$ is:

$$RMSE_{refl\%} = \sqrt{(\sum E_{refl\%}{}^2)/n} \quad (8)$$

where n is the number of reference targets used.

Quantitative evaluation methods were not available for relative radiometric correction methods. The radiometric differences between images were visually estimated and the residuals at radiometric tie points were considered. Quantitative criteria for equalization methods could be based on radiometric differences between tie points before and after correction.

6.2 Results of radiometric block adjustment by Pepita software

The Pepita software was used to correct the DMC Banyoles image materials. The following conclusions were drawn by Chandelier (**XVII**) based on the results. The solar elevation, exposure time and aperture values were well corrected. The BRDF model worked well especially on forest and agricultural parcels. As expected, the BRDF model did not fit on the lake. In urban areas, the effect of the equalization was less visible: highest residuals are observed confirming that tie points are not really homogeneous (a DSM should be used). High residuals occurred also in the lake. The radial component didn't improve significantly the equalization: on the contrary, in urban areas, the radiometric model may not be convergent causing bad equalization for several images. As a conclusion, Pepita could be used as a tool for relative radiometric calibration for DMC images. To ensure that this result is correct, further testing should be done with additional datasets (more images, different dates…). Further improvement for the method would be a mode for absolute radiometric correction to calculate reflectance images. Performance of Pepita is fully automatic and it fulfills all the operational requirements of the IGN. Detailed evaluation is given by Chandelier in **XVII**.

6.3 Reflectance image generation using methods based on atmospheric radiative simulations

Reflectance calibration of the Hyytiälä data was carried out by several approaches (Table 5). FGI and Swisstopo used XPro to produce atmospherically corrected (ATM) images and ATM with BRDF correction. ReSe performed ATCOR-4 processing using Leica's calibration parameters and in-flight calibration parameters based on reference targets P05 and P50; cast shadow correction was tested in the latter case. The FGI carried out ATCOR-4 processing using Leica's laboratory calibration and in-flight calibration parameters derived separately for each image and also one set of calibration parameters derived from the 1 km flying height image and used for all images. Details of these evaluations are given in **XI** and **XXII**.

Different objects were evaluated separately:

- Artificial black tarp (P05 with reflectance 0.057 on ADS40 green channel)
- Artificial bright tarps (P20, P30 and P50 with reflectance 0.181, 0.261, 0.442)
- Uniform object surfaces (asphalt, gravel, sand)
- Grass surfaces

	XA1	XA2	XF1	XF2	AL1	AL2	AL3	AV1	AV2	AV3	AV4	AV5
Participant	FGI	ST	FGI	ST	FGI	FGI	ReSe	FGI	FGI	FGI	ReSe	ReSe
Cal.	lab	lab	lab	lab	lab	lab	lab	vic.	vic.	vic.	vic.	vic.
Atm.	imag.	imag.	imag.	imag.	in-situ	imag.	imag.	in-situ	imag.	imag.	imag.	imag.
Other			BRDF	BRDF						cal.1B		shd.

Table 5. Processing parameters of all evaluated image versions (X for XPro, A for ATCOR-4). Cal.: origin of the sensor radiometric calibration (lab: laboratory, vic: vicarious in-flight radiometric calibration with tarps P05 and P50); Atm.: origin of the atmospheric parameters used (imag.: derived from the imagery, in-situ: in-situ measurements). Other: BRDF = with empirical BRDF-correction, cal.1B = sensor calibration based on image line 1B and four tarps; shd. = with cast shadow correction.

Figure 10 gives the reflectance accuracy evaluation results of different methods for an image strip collected from 2 km flying height on good atmospheric conditions (difference to reference value in % of the reflectance) for bright tarps. On the bright tarps, when in-flight calibration parameters were used (ATCOR-4 processing, image versions AV1-AV5), the differences were well below 5% (with a minor exception). If laboratory calibration parameters were used (XPro image versions XA1 and XA2, ATCOR-4 image versions AL1-AL3), the differences were clearly higher in blue and NIR channels (7-13%). The accuracy was the best in the case where in-flight calibration parameters from 1 km flying height were used (dark target: better than 5%, bright targets: better than 1.5%). On the black tarp, when Leica's laboratory calibration was used, differences were 5-30%, depending on the channel; with in-flight calibration the differences were again lower than 5%. When cast shadow correction option of ATCOR-4 was used, large differences (60-120%) appeared on black target; obviously shadow correction has considered black target as a shadow.

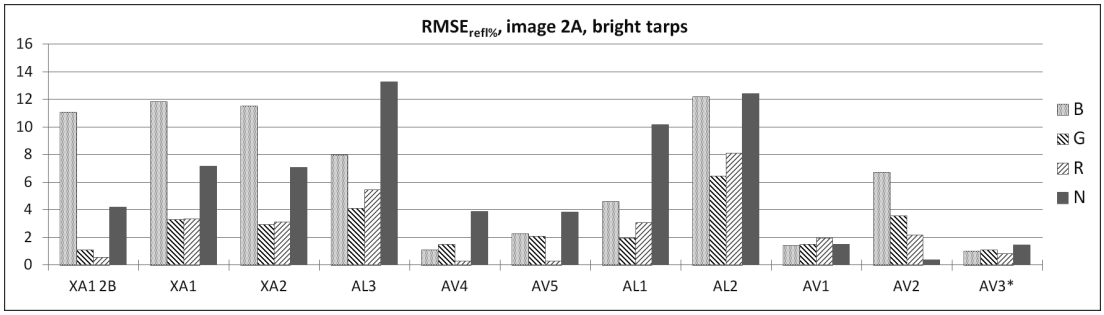

Figure 10. RMSE for reflectance differences (in %) all methods, 2 km flying height (nadir looking image line 2A and backward looking image line 2B for XA1), bright tarps.

The results of XPro correction of all flying heights indicated that for the evaluated challenging data set, up to 5% reflectance accuracy could be obtained with uniform targets. The accuracy was influenced by the flying altitude (1-4 km), channel (R, G, B, NIR), level of cloudiness and target properties. With the XPro there appeared a clear dependency of the reflectance error to the magnitude of reflectance - both in reflectance units and in percents. (**XI**)

An analysis of theoretical basis of XPro by Heikkinen et al. (**XXII**) showed that the correction is based on planar surfaces and that the highest quality reflectance calibration was possible only in sun

illuminated areas. The BRDF correction method is best suited for applications where visually uniform mosaics are of interest.

These results are very promising. The evaluations showed that a reflectance accuracy level of 5 % is possible with sensor laboratory calibration and without any reference measurements. With vicarious radiometric in-flight calibration of the sensor, reflectance accuracies even better than 5 % were achieved. Issue with very dark targets is that a small error in atmospheric correction leads to large relative error, so larger errors are expected with dark objects. With natural targets (grass, forest trees) the non-homogeneity of objects will cause deviations in all comparisons. The results suggested that the laboratory calibrated values might not be accurate enough especially on NIR channel, but also errors in ground truth reflectance values or in atmospheric modeling can cause similar effects. The poorer results in blue channel can be caused by larger atmospheric influences. These issues need to be studied further. The full comparative results of all data sets (including also data from cloudy conditions) and processing methods are presented in **XI** and **XXI**.

Swisstopo evaluated the XPro 4.2 and ReSe evaluated the ATCOR-4 from the productivity perspective. XPro fulfilled the productivity requirements of Swisstopo (**XV**). The evaluation of ATCOR-4 by ReSe showed that the further tuning of software is necessary to fulfil all efficiency and usability requirements of NMAs (**XXII**).

6.4 Reflectance image generation using empirical line method

An empirical line based radiometric correction was carried out with the Sjökulla image block. Dark and bright targets were used as reference, and the reflectance values measured in laboratory were used. The major objective was to calculate BRFs from the photogrammetric image block. A comparison of BRF of black gravel measured in laboratory and from DMC images is shown in Figure 11. In the reference targets, the reflectance RMSEs were 3-7%; some deterioration in accuracy might be due to the fact that reflectance values determined in laboratory were used, instead of in-situ values. The results show that the photogrammetric image block can be used indeed for providing BRFs, but the atmospheric correction is critical. Furthermore, in the case of vertical images, range of observation angles is dependent on the field of view of the sensor; observation angles are smaller than ±40º with the DMC. The empirical line based approach does not fulfil productivity requirements of NMAs, because it requires reflectance targets in object areas. However, the method is functional in small area remote sensing applications.

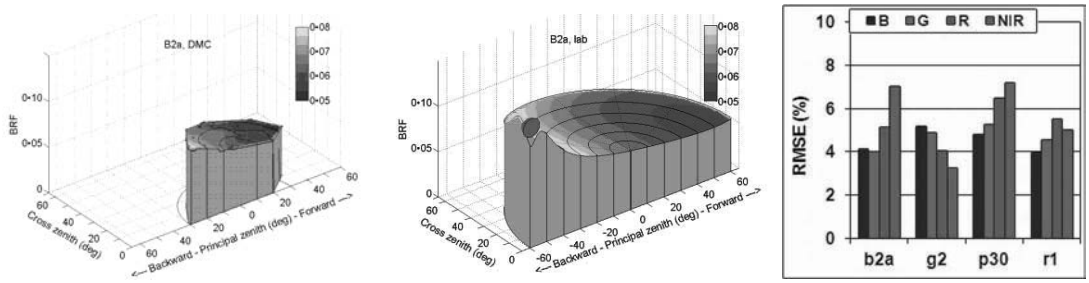

Figure 11. 3D-BRF plot of black gravel measured by the DMC (left) and at laboratory using goniospectrometer (center) and RMSEs on all evaluated images for different check targets (right). (VI)

7 Phase II – Application oriented investigations

Some application oriented investigations were carried out in the context of the project. Comprehensive investigations on tree species classification were carried out using the ADS40 image data sets collected in Hyytiälä by Heikkinen et al. **XII** and Korpela et al. **XIII**. The NDVI orthophoto layer of Catalonia is given as an example of a new possibility of the novel technology (Martinez et al., **XIV**).

7.1 Tree species classification with ADS40 data

The suitability of the ADS40 at-sensor radiance, reflectance and BRDF-corrected reflectance images created by the XPro software on single tree level species classification was studied by Heikkinen et al. (**XII**) and Korpela et al. (**XIII**). They developed a method in which the crown level illumination and occlusion conditions were determined. The method is based on modelling the crown shapes and visibility/shading conditions by using dense LiDAR data. Based on the data, the reflectance characteristics of tree species (within tree species variation, reflectance anisotropy, proximity effects, etc.) were studied in sun illuminated and shadowed conditions. The data with known illumination conditions were then used in further classification experiments by quadratic discriminant analysis by Korpela et al (**XIII)** and support vector machine classification by Heikkinen et al. (**XII)**.

Evaluations of reflectances of different versions of ADS40 images indicated that in general, reflectance variations within species in the same illumination class were high (the coefficient of variation was 13-31%) (**XIII**). Results on reflectance anisotropy showed that if BRDF correction was not applied, a clear brightening towards backward scattering direction appeared. This is an expected behavior, because in this case the sensor is observing the non shaded parts of trees, opposed to the situation in the forward scattering direction, where the shadowed parts are observed. The simple BRDF correction approach of XPro compensated efficiently the BRDF effects, but did not improve the classification results.

Classification experiments with reflectance images provided a total accuracy of about 75-79% with single ADS40 view and 78-82% with two ADS40 views (Heikkinen et al., **XII**). In some cases (the training and classification data from different flight lines) the use of reflectance images provided better classification results than the at-sensor radiance data. One limitation of the study was that the images were collected in the end of August, and this data might not be optimal for tree species separation.

7.2 NDVI data sets generation from DMC images

The good results obtained with DMC encouraged ICC to develop a NDVI orthophoto map layer of Catalonia (more than 32,000 km²) during 2011 (Figure 12) (Martinez et al., **XIV**). It consists of the Normalized Difference Vegetation Index (NDVI), which provides a measure of vegetation density and condition. It is influenced by the fractional cover of the ground by vegetation, the vegetation density and its greenness. It indicates the photosynthetic capacity of the land surface cover.

The phases of the NDVI orthophoto layer generation are the transformation of the DNs to at-sensor radiances using the laboratory radiometric calibration information of the DMC, calculation of reflec-

tance images and finally NDVI image calculation from the red and infrared reflectances. In this first implementation the at-sensor reflectance values are used; the atmospheric correction is not applied. First user of this layer will be the Agriculture Department of the Generalitat de Catalunya (regional government) just a few weeks after the flight. Next, a few months later the data will be published. Then, the vegetation layer is provided as a web map service (WMS) Geoservice and is disseminated according to ICC data policy.

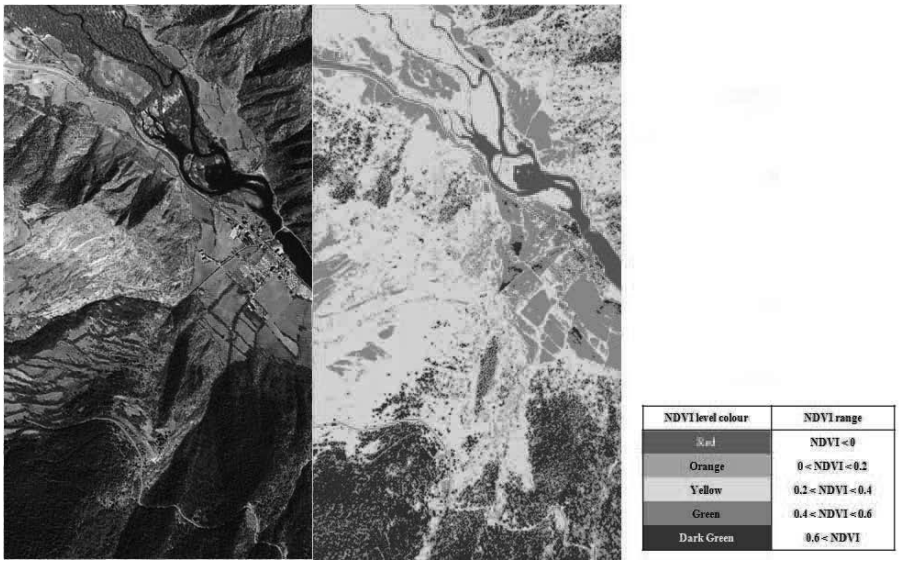

Figure 12. DMC CIR image (left) and at-sensor NDVI image (right). (Martinez et al., XIV)

8 Summary and discussion

8.1 Major conclusions of the EuroSDR project

The EuroSDR project "Radiometric aspects of digital photogrammetric airborne images" was carried out in 2008-2011. The two phases of the project were a review and empirical investigations. The project participants represented stakeholder groups from NMAs, software development and research.

The review phase consisted of a review to the theoretical background and a questionnaire on current status of the radiometric processing of photogrammetric image data. The results showed that the radiometric processing of photogrammetric sensors was inadequately managed. The high-quality sensors could give much higher performance potential, if radiometry was more rigorously processed.

Image blocks for the empirical investigation were collected by Leica Geosystems ADS40 in Finland and by Intergraph DMC in Spain and Finland. Unfortunately data from UltraCam-system was not available in the empirical investigation.

The empirical investigations were carried out on four major topics:

1. Vicarious radiometric calibration and characterization
2. Spatial resolution assessment
3. Radiometric correction of image blocks.
4. Application oriented studies.

The major emphasis in the study was the physical reconstruction of the radiometry of the imaging event, which is a mandatory step in automated, radiometrically quantitative data processing. In principle, the procedure is similar to the approaches that have been used in satellite based remote sensing and in processing of spectroradiometric image data for decades. However, the photogrammetric environment provides some new challenges for the processing. These include extremely high spatial resolution, stereoscopy, strong image block structure, huge volume of collected data and the fact that the imagery are collected in more variable atmospheric and illumination conditions, with horizontal visibilities varying typically between 15 – 50 km and very low solar elevations of 20º and even less.

The vicarious radiometric sensor calibration was the most favorable with the Banyoles campaign data because of the rigorous project set up and excellent weather conditions. The problem in the Hyytiälä campaign was the slightly unfavorable weather conditions and in the Sjökulla campaign the missing in-situ AOT measurements. Results showed that the vicarious radiometric calibration and validation was necessary. The analysis of radiometric calibration values of ADS40 indicated that the laboratory calibration was not compatible enough with the physically based atmospheric correction method ATCOR4. In the case of the hyperspectral sensor CASI, the spectral smile effect needed to be determined in flight conditions.

Spatial resolution analysis included resolution measurements using artificial targets as well as image sharpness measurement based on image data. Further evaluations included assessment of influences of exposure time, aperture and atmospheric conditions in resolution. The results showed that the resolution of DMC images was good and fulfilled theoretical expectations. Important aspects in the study were the novel Haar wavelet based approach for the estimation of the local image sharpness, which could be used to detect faults in the sensor, based on the information in images. This approach has a great value from the operational point of view. All the participants used different methods and indicators in the assessment of spatial resolution; to make results more comparable standardization of methods and indicators are needed.

There are already approaches for reflectance image calculation and radiometric equalization of photogrammetric image data that are suited for production environments. Especially, IGN's Pepita software and the XPro software fulfil the productivity requirements. At best, the accuracy of reflectance images by XPro was up to 5% without any ground reference targets. Improvements are still needed for the approaches. For many software products the processing of a whole photogrammetric block is still a limitation. Improvements are also needed in processing of shadowed regions and in treatment of object reflectance anisotropy. Finally, accurate absolute sensor calibration is needed to allow physically based radiometric processing methods.

Application oriented studies covered two aspects: tree species classification and novel NDVI data products based on national photogrammetric image data. Results showed that accurate radiometric correction is advantageous for the applications. It is important to consider the applications when developing methods for radiometric correction, and on the other hand, the applications (e.g. automatic classification methods) should take into account the level of radiometric correction of the input data. The evaluated applications are not the most urgent issues form the points of view of NMAs, but clearly indicated that the imagery have a lot of potential in new application areas. Further studies should consider the impacts of radiometric correction in applications of NMAs.

The fundamental objectives of the investigation are presented in Section 1.1. These objectives were fulfilled as follows:

1. Knowledge of radiometric aspects was improved by the means of articles, presentations in international conferences, special radiometry sessions in European Calibration and Orientation Workshops (EuroCOW) 2010 and 2012 and an EudoSDR Eduserv course „Radiometric performance of Digital Photogrammetric Cameras and Laser Scanners" organized in co-operation with Vienna University in spring 2012.

2. The existing methods and procedures for radiometric image processing were studied from quality and productivity perspectives.

3. The comparison of operative solutions using same test data set was realized comprehensively only with the ADS40 data from Hyytiälä, because general solutions for radiometric correction were available only for pushbroom type sensors. On the other hand, analysis was made from many different points of views that all are relevant for NMAs; this can be seen as very valuable approach because the technology is not yet mature.

4. The application oriented investigations showed some advantages of the rigorous radiometric calibration and correction in automated processing. Operational applications are still mostly interactive, and for these applications the rigorous radiometric processing does not provide so clear advantages. The correction approaches and interpretation methods should be further improved in order to obtain full advantage of the high-quality radiometry.

8.2 Recent developments

Since the beginning of the project, improvements were achieved in the processing of the airborne image data.

When the project started in 2008, the ADS was the only photogrammetric sensor for which absolute radiometric laboratory calibration was available (Beisl, 2006). Since 2009, a high-accuracy calibration is offered also for the frame sensor DMC (Ryan and Pagnutti, 2009). Absolute calibration methods have not been presented for other photogrammetric cameras.

In 2008, commercial software for the rigorous, physically based reflectance image generation was available only for the pushbroom scanner based images. For pushbroom scanners, physically based, rigorous atmospheric correction methods have been available for decades, because traditional airborne and spaceborne hyper- and multispectral scanners are based on this principle. Leica Geosystems has offered a high performance radiometric correction for the ADS already since 2008 (Beisl et al., 2008), and this software was evaluated in this study. The method showed a great potential, but also many improvement ideas were identified. A new ADS-sensor based version of the ATCOR-4 software is now under development by ReSe for the processing needs of the Swisstopo (Schläpfer et al., 2012). Important improvements of the software are the better usability and shadow correction optimized for high resolution imagery. These aspects are relevant for NMAs, and especially in Switzerland and in general in areas with large topographic differences.

Rigorous radiometric processing methods are becoming available for frame sensor images, too. With these sensors the radiometric block adjustment is a central part of the algorithm. During the review phase in 2008, the Pepita software of the IGN was undoubtedly the most advanced method for the correction of frame image blocks, applying the atmospheric parameters and BRDF correction (Chandelier and Martinoty, 2009). Now, similar approach has been recently implemented also to the UltraMap processing software of the UltraCamXp (UltraCam, 2012). Recently, several new approaches for BRDF correction and atmospheric compensation have been presented in scientific literature (Collings et al., 2011; López et al., 2011).

The use of airborne photogrammetric images in automation of various mapping tasks is still quite limited, and in the application related studies the level of radiometric processing is rarely considered.

International standards for airborne imaging systems are evolving, but slowly. For satellite sensors there already exists an international test field network (Chander et al., 2007). For airborne sensors, Cramer et al. (2010) recently presented a test site concept. A review of methods and test sites for assessment of spatial resolution of EO data products was presented by Pagnutti et al. (2010).

8.3 Recommendations and suggestions for the future developments and investigations

As the final conclusions we give the following recommendations and suggestions

1. The knowledge about the possibilities of the new sensors should be still improved, especially for those who produce and utilize (large-format) photogrammetric images.

2. Standardization of radiometric terminology and processing methods is needed. In particular this is to help users that purchase data from different data providers and for image fusion in general.

3. Radiometric processing methods should be improved further. Important topics for future developments include radiometric calibration of sensors, image block processing, shadow and BRDF correction, and management of image data blocks collected in different atmospheric conditions, multiple times and using different sensors.

4. Rigorous, physically based radiometric correction should be a basic procedure in photogrammetric processing chains and it is expected that it will simplify greatly subsequent data processing needs and interpretation processes of NMAs.

5. Accurate (quantitative) interpretation methods that utilize accurate image radiometry should be developed. Powerful new approaches could be based on reflectance images, laser scanning data and image matching based DSMs.

6. Possibilities for new data products should be considered. The new NDVI data product of ICC is an example of these possibilities.

7. Radiometric calibration and validation of entire data processing chain in test field was shown to be important. Permanent test fields were proven to be powerful tools for these processes. Availability of permanent targets and permanent measurement equipment will simplify greatly the in-situ measurement efforts required in campaigns; without permanent tools the calibration/validation campaigns are very laborious and there is a great risk that they will fail.

8. Not all important radiometry related topics were covered in this investigation. Uncovered topics include operational quality control methods for production processes, pansharpening, image enhancement and colorimetric calibration. Also, the applications and advantages of rigorous radiometric correction were only scratched.

9 Conclusions

We presented the results of the EuroSDR project “Radiometric aspects of digital photogrammetric images” in this report.

The new sensors and processing methods showed excellent radiometric potential. We expect that the high resolution, geometrically and radiometrically accurate, multi-spectral, stereoscopic photogrammetric imagery could provide new possibilities for remote sensing applications. The Internet-based orthophoto and environmental model servers have an important role in providing up-to-date information for large public audiences. These nationwide databases could also be one component of a more general Earth analysis process, integrated with spaceborne images, hyper-spectral images, laser point clouds and terrestrial data, and all other types of geospatial information. Investigation, development and co-operation are needed in this area in order to further standardize the processes.

Acknowledgements

Our sincere acknowledgements go to all the project participants for the fluent and innovative co-operation. Without their support this project would not have been possible.

References

Beisl, U., 2006. Absolute spectroradiometric calibration of the ADS40 Sensor. In: The International Archives of the Photogrammetry, Remote Sensing and Spatial Information Sciences, Paris, France, Vol. XXXVI, part 2.

Beisl, U., Telaar, J., and Schönermark, M. V., 2008. Atmospheric correction, reflectance calibration and BRDF correction for ADS40 image data. In: The International Archives of the Photogrammetry, Remote Sensing and Spatial Information Sciences, Beijing, China, Vol. XXXVII, part B7.

Chandelier, L., Martinoty, G., 2009. Radiometric aerial triangulation for the equalization of digital aerial images and orthoimages. Photogrammetric Engineering & Remote Sensing 2009, 75, 193-200.

Chander, G., Christopherson, J.B., Stensaas, G.L., Teillet, P.M., 2007. Online catalogue of world-wide test sites for the post-launch characterization and calibration of optical sensors. In Proceedings of IAC International Symposium, Hyderabad, India, 2007.

Collings, S., Cacetta, P., Campbell, N., Wu, X. 2011. Empirical models for radiometric calibration of digital aerial frame mosaics. - IEEE Transactions on Geoscience and Remote Sensing 49 (7): 2573-2588.

Cramer, M., Grenzdörffer, G. and Honkavaara, E., 2010. In situ digital airborne camera validation and certification -The future standard? International Archives of the Photogrammetry, Remote Sensing and Spatial Information Sciences, 38(B1), 7 pages.

Fraser, R. S., Ferrare, R. A., Kaufman, Y. J., Markham, B. L., and Mattoo, S., 1992. Algorithm for atmospheric corrections of aircraft and satellite imagery. International Journal of Remote Sensing, 13(3), pp. 541-557.

Hari, P., Kulmala, M., 2005. Station for Measuring Ecosystem-Atmosphere Relations (SMEAR II). Boreal Enviroment Research 10(5), pp. 315-322.

Holben, B.N., Eck, T.F., Slutsker, I., Tanré, D., Buis, J. P., Setzer, A., Vermote, E., Reagan, J.A., Kaufman, Y.J., Nakajima, T., Lavenu, F., Jankowiak, I., and Smirnov, A., 1998. AERONET—A federated instrument network and data archive for aerosol characterization. Remote Sensing of Environment 66(1), pp. 1–16.

Honkavaara, E., Jaakkola, J., Markelin, L., and Becker, S., 2006. Evaluation of resolving power and MTF of DMC. International Archives of Photogrammetry, Remote Sensing and Spatial Information Sciences, 36(A1), 6 pages.

Honkavaara, E., 2008. Calibrating digital photogrammetric airborne imaging systems using a test field. Doctoral thesis. Publications of the Finnish Geodetic Institute, N:o 140, Kirkkonummi, Finland, 2008.

López, D.H., García, B.F., Piqueras, J.G., Aöcázar, G.V., 2011. An approach to the radiometric aerotriangulation of photogrammetric images. ISPRS Journal of Photogrammetry and Remote Sensing 66 (2011): 883-893.

Martínez, L., Arbiol R., 2008. ICC experiences on DMC radiometric calibration. International Calibration and Orientation Workshop EuroCOW 2008. Castelldefels (Barcelona), 30 Jan-1 Feb.

Martínez, L., Palà, V., Arbiol, R., Pérez, F., 2007. Digital Metric Camera radiometric and colorimetric calibration with simultaneous CASI imagery to a CIE Standard Observer based color space. IEEE International Geoscience and Remote Sensing Symposium. Barcelona, 23-27th July.

Pagnutti, M., Blonski, S., Cramer, M., Helder, D., Holekamp, K., Honkavaara, E., Ryan, R., 2010. Targets, Methods and Sites for Assessing the In-Flight Spatial Resolution of EO Data Products. Canadian Journal of Remote Sensing, Vol. 36, No. 5, pp. 583–601, 2010.

Richter, R., and Schläpfer, D., 2002. Geo-atmospheric processing of airborne imaging spectrometry data. Part 2: atmospheric/topographic correction", Int. J. Remote Sensing 23:2631-2649.

Richter, R., Schläpfer, D., 2011. Atmospheric / Topographic Correction for Airborne Imagery (ATCOR-4 User Guide, Version 6.0.2, August 2011). - DLR report DLR-IB 565-02/11, Wessling, Germany, 194p. Available from http://www.rese.ch/download/

Ryan, R.E., Pagnutti, M, 2009. Enhanced Absolute and Relative Radiometric Calibration for Digital Aerial Cameras. In: Fritsch, D., (Ed.), Photogrammetric Week 2009, Wichmann Verlag, Heidelberg, Germany, pp. 81-90.

Schaepman-Strub, G., Schaepman M.E., Painter, T.H., Dangel, S., Martonchik, J.V, 2006. Reflectance quantities in optical remote sensing—definitions and case studies, Remote Sensing of Environment 103 (1), 27–42.

Schläpfer, D., Richter, R., Kellenberger, T., 2012. Atmospheric and topographic correction of photogrammetric airborne digital scanner data (ATCOR-ADS). International Calibration and Orientation Workshop EuroCOW 2012. Castelldefels (Barcelona), 8–10 Feb.

Schott, J.R., 2007. Remote sensing: The image chain approach. Oxford University Press, Inc. 2nd ed., 666 pages.

SMEAR, 2012. Smear research stations. http://www.atm.helsinki.fi/SMEAR/ (Accessed 27 July 2012)

Smith, G.M., Milton, E.J, 1999. The use of the empirical line method to calibrate remotely sensed data to reflectance. Remote Sensing 1999, 20, 2653-2662.

Song, J., Lu, D., and Weseley, M. L., 2003. A simplified atmospheric correction procedure for the normalized difference vegetation index. Photogrammetric Engineering & Remote Sensing, 69(5), pp. 521-528.

Suomalainen, J., Hakala, T., Peltoniemi, J., Puttonen, E., 2009. Polarised Multiangular Reflectance Measurements Using the Finnish Geodetic Institute Field Goniospectrometer. Sensors 9 (5), 3891-3907.

Talaya, J., Kornus, W., Alamús, R., Soler, E., Pla, M., Ruiz, A., 2008. Analyzing DMC performance in a production environment XXI ISPRS Congress. Beijing 3-11 July.

Vermote, E.F., Tanré, D., Deuzé, J.L., Herman M., and Morcrette, JJ., 1997. Second simulation of the satellite signal in the solar spectrum, 6S: an overview. IEEE Transactions on Geoscience and Remote Sensing, 35, 675-686, 1997.

von Schönermark M., Geiger, B., Röser, H.P., 2004. Reflection properties of vegetation and soil. Wissenschaft und Technik Verlag, Berlin. 352 pages.

UltraCam, 2012. http://www.microsoft.com/ultracam/en-us/default.aspx

Index of Figures

Index of Tables

EuroSDR Project

Commission II

"Mobile Mapping - Road Environment Mapping using Mobile Laser Scanning"

Final Report

Report by Harri Kaartinen, Juha Hyyppä, Antero Kukko, Matti Lehtomäki, Anttoni Jaakkola, George Vosselman, Sander Oude Elberink*, Martin Rutzinger**, Shi Pu***, Matti Vaaja*****

Finnish Geodetic Institute, Department of Remote Sensing and Photogrammetry, Masala, Finland

*University of Twente, Faculty of Geo-Information Science and Earth Observation – ITC, Enschede, The Netherlands

**Institute of Mountain Research: Man and Environment (IGF), Austrian Academy of Sciences
and
University of Innsbruck, Institute of Geography, Innsbruck, Austria

*** China Geoscience University, Department of Geomatics, Beijing, China

****Aalto University, Department of Real Estate, Planning and Geoinformatics, Espoo, Finland

Abstract

The objective of the “EuroSDR Mobile Mapping - Road Environment Mapping using Mobile Laser Scanning” project was to evaluate the quality of mobile laser scanning systems and methods with special focus on accuracy and feasibility. Mobile laser scanning (MLS) systems can collect high density point cloud data with high accuracy.

A permanent test field established in the project suits well for verifying and comparing the performance of different mobile laser scanning systems. The test field was measured with several commercial and research systems, such as RIEGL VMX-250, Streetmapper 360 and Optech Lynx of the TerraTec AS, FGI Roamer and FGI Sensei. A geodetic network of terrestrial laser scannings was used as the reference for the quality analysis. Each system provided the data using the system specific pre-processing standards. The system comparison focussing on planimetric and elevation errors using filtered DEM, poles and building corners as reference objects, revealed the high quality point clouds generated by all systems with good GNSS conditions. With all professional systems properly calibrated, the elevation accuracy was better than 3.5 cm up to 35 m distance. The best system had 2.5 cm planimetric accuracy even with the range of 45 m. The planimetric errors increase as a function of range, but moderately if the system was properly calibrated. The main focus on MLS development in near-future should concentrate on the improvements of trajectory solution, especially under non-ideal conditions, using both improved hardware (additional sensors) and software solutions (post-processing).

The benchmarking of algorithms did not collect a high number of inputs. The results obtained by ITC and FGI could be used to assess the present state of the art in point cloud processing of MLS. Currently, a level of 80-90 % correct detections can be obtained for object recognition (to those objects most feasible for MLS data) and the rest needs to be done in interactive editing process. Since the goal of MLS processing is to have high automation supported by minimum amount of manual work and to create accurate 3D models of roadsides and cities, there is still a significant contribution needed for future research.

Finnish Geodetic Institute, Mobile Mapping research group (www.fgi.fi/mobimap), continues the test site development for MLS, the benchmarking of MLS methods and putting MLS data to public use also in the future.

1 Introduction

Accurate and intelligent up-to-date roadside information is needed not just for road and street planning and engineering but also for increasing number of other applications, such as car and pedestrian navigation, noise modelling, road safety, and other planning purposes. Vehicle-based mobile laser scanning (MLS) is a multi-sensor system that integrates various navigation and data acquisition sensors on a rigid, moving platform (typically van or car) for road side information. The navigation sensors typically include Global Navigation Satellite System (GNSS) receivers and an Inertial Measurement Unit (IMU), while the data acquisition sensors include typically terrestrial laser scanners and digital cameras.

Today, terms Airborne Laser Scanning (ALS), Mobile Laser Scanning (MLS) and Terrestrial Laser Scanning (TLS) are applied depending whether the platform is an aircraft, moving vehicle or tripod, respectively. LS (Laser Scanning) gives the georeferenced point cloud, from which it is possible to calculate various surface, raster and object models. Additionally, the intensity and the full waveform of the laser returns can be recorded. In MLS, the data collection can be performed either in so-called stop-and-go mode or in continuous mode. The stop-and-go mode corresponds to conventional TLS measurements and therefore MLS, hereafter, refers to the continuous model, i.e. the use of continuous scanning measurements along the drive track. Data provided by MLS systems can be characterized with the following technical parameters: a) point density in the range of 100-1000 pulses per m^2 at 10 m distance, b) distance measurement accuracy of 2-5 cm, and c) operational scanning range from 1 to 100 m. The amount of data produced by such systems is huge (at the rate of 0.25-1 M pts/s), and manual processing of the data is very time-consuming, which prompts a need for automated methods that decrease the amount of manual work required to produce accurate 3D models. At present, it is possible to use software and methods developed for TLS and ALS, but due to different scanning geometry, different point density and the fast processing needed, algorithms for MLS data processing need also to be developed separately (Jaakkola et al., 2008).

Applications based on integration of ALS and TLS/MLS are currently under development. ALS/TLS integration is expected to be beneficial for forest inventories and ALS/MLS integration is expected to be useful for city 3D mapping and further applications therein (e.g. Jochem et al. 2011, Rutzinger et al. 2011a). Annually, the LS business market is growing 15 %, but the growth is at the largest with MLS. The potential of MLS is on the collection of large areas with reduced point accuracy compared to TLS. Recently, whole cities have been covered with MLS. MLS and mobile mapping (including images) is used for collecting vast 3D navigation data sets of Nokia Navteq (Navteq TrueCar), Microsoft and Google (Google Street View Car), which are currently developing automatic techniques to process the data into 3D models.

The objective of the “EuroSDR Mobile Mapping - Road Environment Mapping using Mobile Laser Scanning” project was to evaluate the quality, accuracy, and feasibility of mobile laser scanning systems and methods. This report will focus on two subjects:

1. Benchmarking of various MLS systems on the established test site in Espoonlahti in good GNSS coverage.
2. Benchmarking of two pole detection algorithms in order to describe in brief the state of the art in MLS data processing.

2 State-of-the-art in Mobile Laser Scanning

2.1 Systems

Recent studies on MLS systems and their accuracy as well as environmental modelling done with MLS can be found in Barber et al. (2008), Brenner (2009), Clarke (2004), El-Sheimy (2005), Früh and Zakhor (2004), Graham (2010), Haala et al. (2008), Hassan and El-Sheimy (2008), Jaakkola et al. (2008), Kukko et al. (2007 and 2009), Kukko and Hyyppä (2009), Lehtomäki et al. (2010), Li et al. (2004), Lin et al. (2010), Lin and Hyyppä (2011), Manandhar and Shibasaki (2002), Petrie (2010), Shen et al. (2008), Steinhauser et al. (2008), Tao and Li (2007), Weiss and Dietmayer (2007), Yu et al. (2007) and Zhao and Shibasaki (2003a,b, 2005). Currently, there is an increasing number of research MLS systems (e.g., Geomobil (ICC), GeoMaster (University of Tokyo), Lara-3D (Ecoles des Mines de Paris), ROAMER and Sensei (FGI)), and commercial and custom-made systems (for example Optech Lynx Mobile Mapper, Streetmappers of 3D Laser Mapping based on RIEGL scanners, Mitsubishi using SICK LMS 291 -scanners, RIEGL VMX-250 integrating two RIEGL VQ-250 scanners, Topcon-made systems to Google IP-S2 having three SICK LMS 291 scanners, Trimble Trident-3D based on SICK and RIEGL scanners (Petrie, 2010), Trimble MX8 and RIEGL VMX-450). Mobile laser scanning systems are developed both in the field of robotics and surveying. A more complete list of systems is depicted in Petrie (2010) and Narayana (2011).

2.2 Accuracy of MLS

The MLS accuracy is limited mainly by the GNSS signal degradation in urban and forest-covered environments. This disadvantage of GNSS can be partly corrected by appropriate data fusion approach of GNSS (GPS), IMU and odometer. The most common data fusion approach is to use Kalman filter of different flavours. The MLS accuracy has been studied in good GNSS conditions. Haala et al. (2008) demonstrated that the StreetMapper system could produce dense 3D measurements at an accuracy level of 30 mm in good GNSS conditions. Further, remaining differences between the point clouds from different scanners, due to imperfect boresight calibration of the upward looking scanner, could be corrected during post processing. Under degraded GNSS conditions, Haala et al. (2008) reported a georeferencing error up to 1 m for the horizontal position. They also reported that despite the limited quality of the absolute accuracy, 3D point measurements during bad GNSS conditions are still useful, especially if mainly their relative position is exploited. They gave an example that the standard deviation of such data is only 5 cm if points from two scanners are combined and 2.6 cm if the points are separated for each scanner. Thus, such data is feasible for the extraction of features of windows or passages, if a certain error for their absolute position is acceptable.

Since the best laser systems in MLS are capable to estimate the range with 2 mm accuracy, and direct georeferencing dominates in the error propagation, an improvement of georeferencing solution is needed. Possibilities to improve the georeferencing solution include more accurate calibration of relative orientation of the MLS system components, automatic/manual detection of objects (the position of which is known) from the road sides that could be used to improve the georeferencing, and development of new data fusion approaches for MLS.

2.3 Applications and Data Processing

Data processing methods are covered with topics “point clouds”, “range images” and “laser scanning”. Usable processing methods are listed as part of references and literature of this report. In the following, some examples of the MLS processing, quality and possibilities are given. The reader can find more details and information from the listed references and additional selection of literature.

2.3.1 MLS in Change Detection

Modern road environment faces a lot of changes all the time. Updating of e.g. road map for cars and pedestrians is done mainly manually. Multitemporal MLS provides possibilities to fully automatically monitor almost all changes in the road environment. Satellite images are used for change detection by applying image differencing and, thus, multitemporal road environment point clouds can be used to detect changes in a similar way. A change detection method should automatically find the changes in the studied area and update the corresponding map, model or database accordingly. Change detection can be done in many different ways: comparing raw point clouds, coloured point clouds, voxels, range images, surface models or modelled objects. The simplest and most universal way to do comparison between two point clouds is to measure distances between the points in different point clouds and see if a point in one point cloud has neighbours nearby in the other point cloud, otherwise the point is marked as a potential change. Adding colour data into the point clouds gives additional clues about the possible changes. If colours are used, caution is recommended, since e.g. illumination changes, reflection and registration errors may have negative influence on usability of colour information. In some cases, these problems can be reduced by calibration processes in order to produce comparable colours. Voxel-based processing could prove to be very efficient as the processing is heavily simplified when compared to point-wise processing. This is caused by grouping multiple points into a single voxel, which also inherently gives the local neighbourhood of any given voxel or point. 3D point clouds from MLS systems can be converted to 2D range images in order to apply existing image processing techniques. One advantage of using image planes and highly developed and powerful image processing techniques is that the processing speed typically increases significantly.

The possibilities of utilising MLS for mapping topographic changes have been demonstrated in Vaaja et al. (2011). The capability of MLS in erosion change mapping in river environment, using sandbars and river banks as examples, was demonstrated using ROAMER MLS system mounted on a boat and on a cart and difference elevation model technique. Fixed-point terrestrial laser scanner data was used as reference. The measurements were based on data acquisitions during the late summer in 2008 and 2009. The coefficient of determination (R^2, the square of the correlation coefficient between the observed and modelled data values) of 0.93 and a standard error of 3.4 cm were obtained as metrics for topographic change mapping based on mobile laser scanning. This, however, required a systematic elevation error calibration of the data. The possibilities of MLS for mapping biomass changes has been reported e.g. in Hyyppä et al. (2009), Jaakkola et al. (2010) and Lin et al. (2011).

MLS is extremely feasible for change detection, but the changes due to measurement geometry have to be separated from those due to real changes in the objects.

2.3.2 Integrated Use of MLS and Hyperspectral Sensing

Present trend in mobile mapping is the collection of images and possibly laser scanner point clouds. Concerning automatic extraction and classification of objects, the point cloud information has been shown to provide relatively high accuracy. By using both the images and point clouds, the object classification accuracy can be enhanced. If the automatic modelling of the environment gets increased

emphasis, object classification can be enhanced even further by integrating laser point clouds and hyperspectral data. Adding hyperspectral sensors to MLS is a straightforward process, since both the LS and hyperspectral data require direct georeferencing (GNSS/IMU). Hyperspectral images have improved classification capability over objects where as the image resolution is decreased when compared to digital camera images. Considering the registration problems between images and point clouds, it may be even possible to produce hyperspectral LS without passive imagery as shown in Kaasalainen et al. (2007).

Puttonen et al. (2011) presented the first results of using mobile laser scanning and hyperspectral sensor data in tree species classification. Tree species classification and the separation of coniferous and deciduous trees were carried out in an experimental garden in the City of Espoo, Finland. The results demonstrated that a fused data set consisting of LS-derived and hyperspectral features outperformed single-source data sets (either LS or hyperspectral) by a significant margin. The best overall coniferous and deciduous tree separation result was 95.8% when two LS-derived shape and two hyperspectral features were applied using a Support Vector Machine (SVM). The corresponding best tree species classification result including ten species in the analysis was 83.5%. The results were obtained using a low number of predictors to give a more realistic view of the potential of the data.

The concept shown in Puttonen et al. (2011) can be used in general towards improved classification of road-side environment using both LS and hyperspectral sensors. The combined data of LS and hyperspectral is expected to be even more feasible for change detection processes. The major bottleneck in hyperspectral data processing in mobile context is the illumination changes (bidirectional reflectance distribution function, BRDF) of the environment. In the mobile use, the BRDF changes are much more dramatic compared to aerial imaging, since imaging is done in all geometries (e.g. towards to sun and along the sun). Correcting and understanding illumination changes is the major drawback in using passive hyperspectral data with LS data. Therefore, it is expected that in future active multispectral or hyperspectral LS, with proper radiometric calibration scheme, is an important technique in mobile mapping. With active hyperspectral sensing, the effect of BRDF is negligible. The disadvantage of the active hyperspectral sensing is the costs of the systems and more limited possibility to have high number of channels.

2.3.3 Indoor Mobile Laser Scanning

The need for 3D maps is not only for outside environments. There is also an increasing need to get 3D models inside the buildings. Presently, inside models are created using 2D floor plans and images or using multiple scannings of TLS. When the indoor models become more complex, there is also a need for more flexible mapping systems. Indoor mobile mapping or indoor mobile laser scanning is a new coming trend in mobile mapping. According to the manufacturers, “Indoor Mobile Mapping Solution creates an excellent 2D floor plan which contains a level of detail previously unavailable. Every chair, every object in the interior will appear in the floor plan. The floor plan contains exactly what is in the space as compared with conventional floor plans which are drawn by hand.” (Trimble, 2011.) Indoor mobile laser scanning is based on high-quality laser scanner and IMU technology. Odometers and other sensor technology will help in improving the quality. The needed georeferencing solutions of indoor mobile laser scanning require improvements beyond those needed for outdoor MLS mainly due to lack of precise positioning solution. One solution to overcome this is Simultaneous localization and mapping (SLAM) –technique commonly used in robotics and autonomous vehicle navigation, see e.g., Biber et al. (2004).

2.3.4 Virtual Reality in a Smart Phone

Laser scanning has contributed significantly to the automatic 3D reconstruction in the past few years. MLS will be the main technology to provide large 3D city models for navigation in a smart phone in which low data amount and visually good looking textures of 3D models are required. As regards to building geometric reconstruction, although the use of both laser scanning and images improves the level of automation, difficulties still rise when complex models need to be reconstructed, and many developed methods are scene-based. When photorealistic textures are concerned, object occlusion is still the main problem. Due to the limited hardware resources and graphical computation power of mobile devices, 3D visualisation techniques for the specified mobile platform need to be developed. The challenge related to real-time fast 3D rendering and display of large datasets and of complex urban environments still remains. Our example in the Android Market shows the current state of the art in creating visually good appearance textures, high-quality geometry, and 3D visualization in a single demo for near-future personal geospatial infrastructures (Figure 2-1).

Figure 2-1. An example of a photorealistic 3D city model for mobile phones. (http://market.android.com/details?id=com.FGI.Tapiola3D)

3 Benchmarking of Mobile Laser Scanning Systems on a Test Field

Experiences gained in earlier research have shown that permanent test fields with accurate ground truth are valuable tools for analyzing the performance of remote sensing systems and methods in mapping tasks. To be able to compare various systems or methods, test data should be from a common test field (Kaartinen and Hyyppä, 2006 and 2008). Comparing mobile laser scanning systems is challenging, as the accuracy of the georeferenced point cloud is highly dependent on the GNSS visibility during the data acquisition, and the satellite geometry is constantly changing. Also the season can affect the satellite visibility, when tall deciduous trees are close to the trajectory. There was not much information about existing MLS test fields prior to this study. System manufacturers have carried out and published their own tests, but few publications exist where system performance is examined using a test field established and results analyzed by an independent actor. Barber et al., (2008) used RTK-GPS measurements to collect reference data on two test sites to validate the

geometric accuracy of Streetmapper MLS system. The main focus was on the elevation accuracy, only a few control points, measured on white line markings on the road, were used for planimetric accuracy analysis. University of California at Davis used total station and static TLS data to analyze the accuracy of MLS systems (Streetmapper 360, Optech Lynx and Ambercore Titan) in producing digital terrain models of pavement surfaces (Yen et al., 2010). In this test only elevation accuracy was concerned. The most in-depth analysis of MLS quality thus far is given by Haala et al. (2008).

We, therefore, concentrated on evaluating geometrical properties of laser point clouds collected by various MLS systems in an established test site with good GNSS conditions.

3.1 Material

3.1.1 Test Site

The selected test site is located in Espoonlahti, about 16 km west of Helsinki. The test site covers one block around the shopping mall Lippulaiva covering 1700 meters of road environment (Figure 3-1).

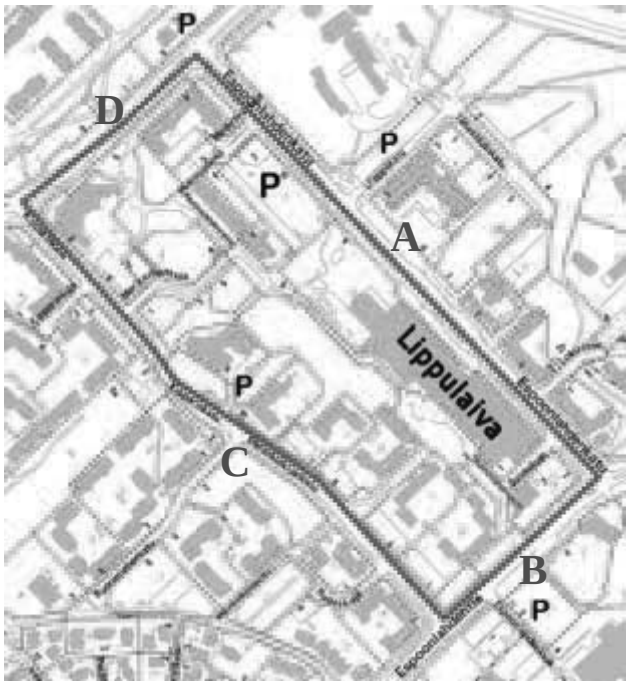

Figure 3-1. Test site for mobile laser scanning covers 1700 m of road environment. Driving route is marked with red line, and sections are marked with red letters A-D. Parking spaces are marked with P. Map data © City of Espoo.

Test field can be divided into four sections, which are separated naturally by road crossings, as can be seen in Figure 3-1. Sections A, B and D have a good GNSS visibility, although some trees and higher buildings may limit the visibility of lower satellites. As can be seen in the digital surface model in Figure 3-2, section C has large trees standing close to the road, thus making GNSS conditions much more challenging. There are many types of buildings and other constructions such as stairs and walls

in the area, as well as hundreds of pole type objects such as lamp posts, traffic signs and trees. In section A the road area, as well as most of the terrain close to the road, is very flat. On other sections there is more variation in terrain elevation, both in the road and in the surroundings. The height difference between the lowest and highest point on the road is 12 meters (Figure 3-2).

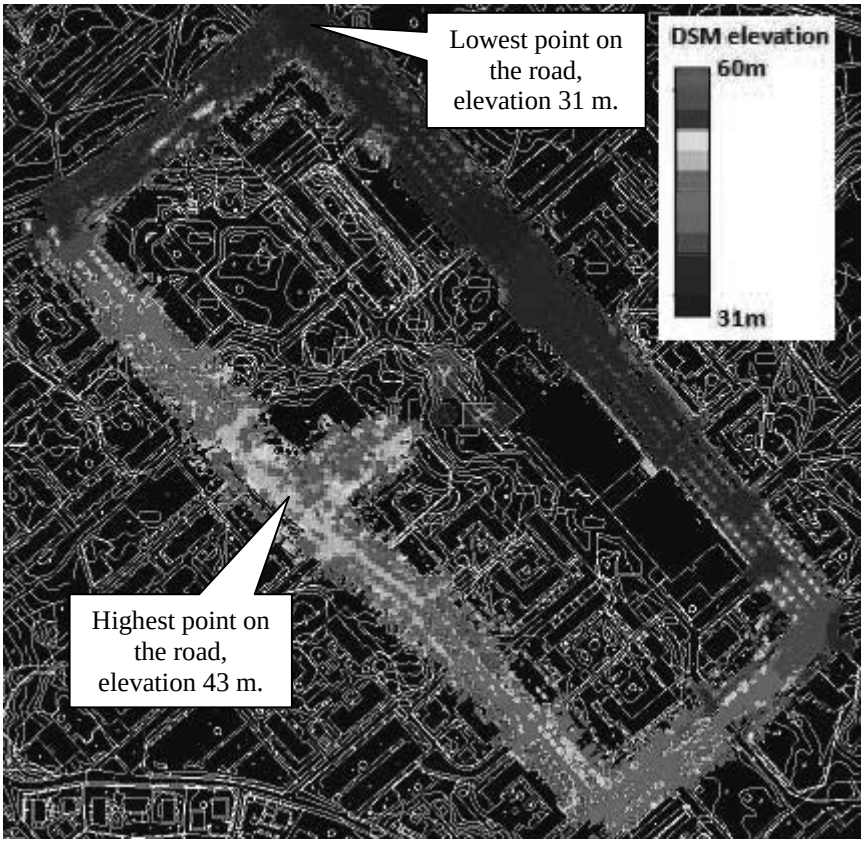

Figure 3-2. Digital surface model of Espoonlahti test field (based on MLS data). Map data © City of Espoo.

3.1.2 Reference Data

3.1.2.1 Terrestrial Laser Scanner Point Clouds

Dense terrestrial laser scanner point clouds were used to obtain reference targets for geometric accuracy analysis. Reference point clouds were collected May 7th 2009 using FGI's mobile mapping system ROAMER (Kukko, 2007 and 2012), Road Environment Mapper (Figure 3-3) in static mode. ROAMER was installed on top of a car, and the car was standing static on the road during each 360 degree scanning of the FARO Photon 80 terrestrial scanner (Figure 3-4), the average distance between the scanning stations was 30 m. The scan resolution was set to 0.0013 rad point separation. The georeferencing of altogether 58 individual scannings was computed in post-processing: scanner position and heading were obtained from the ROAMER's SPAN –navigation system, and scannings were levelled using the inbuilt inclinometer of the scanner. Virtual GPS reference station data used in GPS post-processing was downloaded from GPSNet.fi-service. SPAN-data was processed using

Waypoint Inertial Explorer –software, which gave the estimated accuracies of 11 mm in 3D-position and 0.027 degrees in heading (RMS) for the ROAMER inertial measurement unit (IMU) during the measurements. The offset between the IMU and the scanner origin as well as the offset between the SPAN and the scanner heading were determined in system calibration.

Figure 3-3. ROAMER-platform was used to collect reference terrestrial laser scannings.

Figure 3-4. An example of reference point clouds. Scanning locations can be seen as shadows on the road caused by the car.

3.1.2.2 Validation of Reference Point Clouds

ROAMER TLS/static data was validated against 150 check points measured using a total station (Trimble 5602S DR200+). In total nine ground control points (GCPs) were measured for total station setup around the Espoonlahti test site (Figure 3-5) using repeated real-time GPS-measurements (Leica SR530). Altogether eight individual measurements on each point were taken, using different reference data sources (RTK-GPS using own reference station and VRS-GPS using virtual reference station) and different satellite constellations (a few hours between the measurement sessions). On each GCP the first two sessions were measured using RTK-GPS (expected accuracy 1 cm + 1-2 ppm in plane and 1.5-2 cm + 2 ppm in height (Bilker and Kaartinen, 2001)), and then two sessions using VRS-GPS (expected accuracy 2 cm in plane and 4 cm in height (Häkli, 2004)). New GPS initialisation was acquired between each session. This procedure was carried out for a second time after a few hours. GCP-coordinates were then computed as a mean of the obtained eight coordinates. Maximum standard deviation of the eight ‘original‘ coordinates was 23 mm in plane and 30 mm in elevation (average 13 mm and 20 mm respectively).

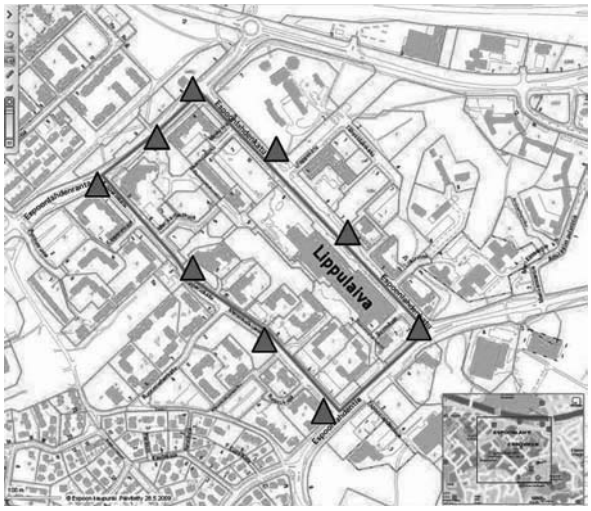

Figure 3-5. Nine ground control points were measured around the test site. Map data © City of Espoo.

On most ROAMER –scans the comparison showed that check points and point clouds match to each other within the standard deviation of the GCPs, i.e. a couple of centimetres, but on a few scans there was error in the levelling of the point cloud. On these cases there was a passing bus visible in the scanning data, so it is obvious that a large vehicle has disturbed the scanner inclinometer. These point clouds could be re-levelled by using neighbouring point clouds and check points.

3.1.2.3 Reference Targets for Accuracy Analysis

After point cloud validation, targets for accuracy analysis were measured from a 350 meter long area of section A of the test site (Figure 3-6) with the best GPS visibility. TerraScan-software by TerraSolid Ltd. was used for all point cloud operations. First ground points were classified and a regular grid with 5 cm point spacing was computed to achieve an even distribution of the ground points. This grid was thinned by selecting every 1000th point, and these thinned points were compared to the original ground points. All thinned points deviating more than 5 mm from original data were removed, and the remaining points with point density of 0.3 points per m^2 were selected as reference points for the elevation accuracy analysis. The complete ground reference data for the elevation consists of 3283 points, for which also the distance and direction to all possible driving trajectories were determined.

The ground reference data was used to separate all laser points within 10 cm below and 50 cm above the ground, and these close-to-ground points were used to measure reference targets for the planimetric accuracy evaluation. The targets include centres of poles, building corners and curb corners. Another one meter thick slice of laser points was taken at approximately five meters above the ground, and these laser points were used to measure more building corners and centres of poles. Altogether 273 planimetric reference targets were measured. Pole coordinates were measured by visually fitting a circle to the point cloud in top view, and the centre of the circle was used as the reference coordinate, example is shown in Figure 3-6.

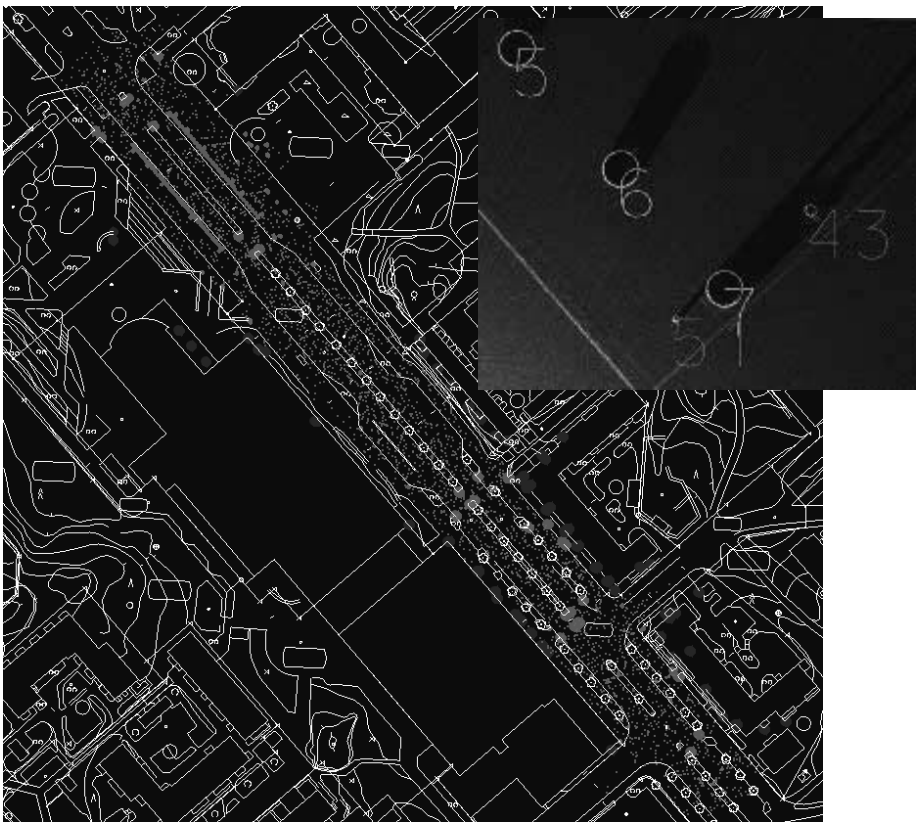

Figure 3-6. Reference targets, small orange points are elevation reference points and blue, red and green points are planimetric reference points (map data courtesy city of Espoo). Small figure in top right corner shows a detail of measured poles from close-to-ground laser points.

3.1.3 Mobile Laser Scanning Data

3.1.3.1 Mobile Mapping Systems

Mobile laser scanning data was collected from the test field using five different systems (Table 3-1). With all systems the test site was driven in both clockwise (CW) and counter-clockwise (CCW) direction at speed of about 30-40 km/h.

MLS system	Operated by	Data acquisition date
ROAMER	Finnish Geodetic Institute	June 2009
RIEGL VMX-250	RIEGL Laser Measurement Systems GmbH	March 2010
Sensei	Finnish Geodetic Institute	May 2011
Streetmapper 360	3D Laser Mapping	June 2011
Optech Lynx	TerraTec AS	June 2011

Table 3-1. Tested MLS-systems.

	Optech Lynx Mobile Mapper / TerraTec AS	Sensei	ROAMER	RIEGL VMX-250 and Streetmapper 360
Laser wavelength	N/A	905nm	785nm	Near infrared
Distance measurement principle	Time-of-flight, max 4 returns	Time-of-flight, max 3 returns	Phase-shift	Time-of-flight, no. of returns selectable
Points / sec (x1000) max	2 x 200	38	120 (2011: 976)	2 x 300
Range	200m	200m	76m (2011: 153m)	500m
Profiles / sec max	2 x 200	50	61	2 x 100
Beam divergence	N/A	1.4 x 14mrad	0.16mrad	0.3mrad
Beam size at exit	N/A	N/A	3.3mm	7mm
Distance measurement accuracy	8mm	100mm	2mm@25m	10mm@150m
Angular resolution	N/A	0.25°	0.009°	0.018°

Table 3-2. MLS specifications (FARO, 2008 and 2009; Ibeo, 2011; Optech, 2011; RIEGL, 2011; TerraTec, 2011).

Examples of acquired point clouds are show in Figure 3-7 - Figure 3-11. Laser points are visualized by the intensity value, with the exception that Sensei does not record the intensity.

Figure 3-7. Optech Lynx data.

Figure 3-8. Streetmapper data.

Figure 3-9. RIEGL VMX-250 data.

Figure 3-10. ROAMER data.

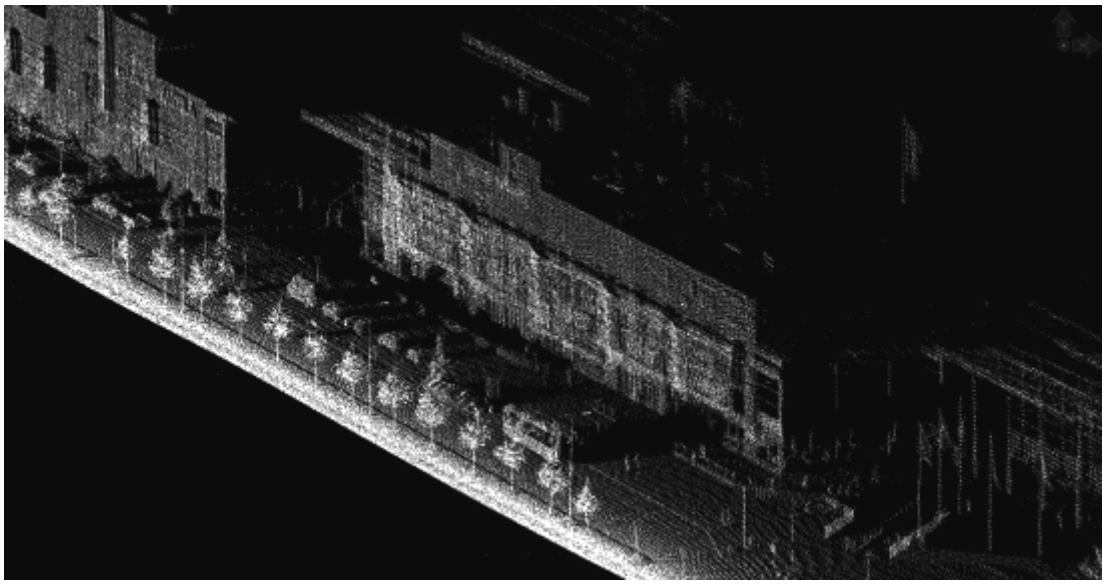

Figure 3-11. Sensei data.

3.1.3.2 ROAMER

FGI's in-house developed ROAMER-system (Kukko et al., 2007 and 2012) has been operational since the summer of 2007. Mobile mapping data from test field was acquired in June 2009. At that time ROAMER consisted of a FARO Photon 80 terrestrial laser scanner and NovAtel SPAN positioning system (NovAtel DL-4 plus GPS-receiver, NovAtel GPS-702-GG antenna and Honeywell HG1700 AG58 inertial measurement unit (IMU) with ring laser gyros). Later the laser scanner was updated and currently a FARO Photon 120 terrestrial laser scanner is used. The maximum point measurement rate of Photon 80 scanner was 120 kHz and range 76 meters (Photon 120: 976 kHz and 153 meters). Laser

profiling was carried out using 48 Hz scan frequency. ROAMER has adjustable scanning angle, in Espoonlahti the scanner was measuring profiles tilted 45 degrees below horizontal, as can be seen in Figure 3-12. ROAMER is the only system in this comparison which utilizes a laser scanner with continuous wave laser and phase-shift based distance measurement. The beam size of the scanner is also the smallest in the test.

Figure 3-12. ROAMER.

Direct georeferencing of the ROAMER point clouds was computed using Waypoint Inertial Explorer™ GPS-IMU post-processing software. GPS reference station data was acquired from Finnish virtual reference station (VRS) network GPSNet.fi. After georeferencing, dark points were removed by filtering out points with intensity value less than 8000 (range 0-20470), and isolated points were removed by filtering out points that had less than 50 points within 2 m radius around it. TerraScan by Terrasolid Ltd was used for the filtering.

Two point clouds were analyzed for the ROAMER. In the first one the georeferencing of the point cloud was computed using the calibration values between the instruments determined only in laboratory calibration. The laboratory calibration was based on measuring the physical offsets and rotations between the scanner, IMU and GPS-antenna. This laboratory calibration was fine-tuned using the measured data, for example utilizing the data acquired by driving the same location in two directions and using common targets such as building walls, road surface and poles to determine errors in calibration. The fine-tuned calibration values were applied for re-computing the data, producing the second set of point clouds for analysis.

3.1.3.3 RIEGL VMX-250

RIEGL VMX-250 (Figure 3-13) was introduced in the beginning of 2010 and the test site data was acquired in March 2010. System consists of two RIEGL VQ-250 scanners and a navigation unit with IMU, GNSS and odometer instruments. Each of the scanners measures up to 300000 points and 100 profiles per second. Maximum measurement range is 500 meters. In September 2011 RIEGL announced another mobile mapping system VMX-450 with VQ-450 scanners, capable to measure up to 550000 points and 200 profiles per second.

Figure 3-13. RIEGL VMX-250 (RIEGL, 2010).

RIEGL delivered two point clouds for analysis. The first data was received in June 2010. Later RIEGL announced that they have further developed their system calibration and wish to implement their latest expertise also to the test site data. A set of 11 control points from the test site was delivered to RIEGL to ease the calibration procedure. Second data was received in May 2011.

3.1.3.4 Sensei

The FGI Sensei is a low-cost modular measurement system consisting of a number of measurement instruments. These include a GPS/IMU positioning system, two laser scanners, a CCD camera, a spectrometer and a thermal camera.

The GPS/IMU system is a NovAtel SPAN-CPT tightly coupled GPS/INS receiver system, which integrates NovAtel's OEMV GNSS precision receiver technology with three fibre optic gyros and three MEMS accelerometers into a single unit. The SPAN-CPT delivers 3D position, velocity and attitude solutions. The measurements of the different INS subsystems are combined using Waypoint Inertial Explorer and GPS virtual reference station (VRS) data.

In Espoonlahti test site an Ibeo Lux laser scanner was used. The Ibeo Lux measures points from four different layers simultaneously and is theoretically able to measure up to 38 000 points/s if only one

return per pulse per layer is assumed. The scanner is able to record up to three returns per pulse per layer. Its distance measurement range is from 0.3 to 200 m (50 m for targets with 10% remission), ranging accuracy is 10 cm, angular resolution is 0.25° and the divergence of the laser beam is 1.4 mrad horizontally and 14 mrad vertically with respect to the scanner body, indicating that objects may appear extended in the vertical direction. When mounted on a car (Figure 3-14), this vertical elongation turns into a horizontal error as the scanner is mounted vertically. For this reason most of the reference targets for planimetric accuracy analysis could not be reliably measured, and the performance analysis was completed only for elevation accuracy. When Sensei is used on top of a car, the instruments are pointing towards the side of the car, and the laser scanner scans vertically thus covering only one side of the trajectory at a time. (Jaakkola et al., 2010.)

Figure 3-14. Sensei mounted on a car.

3.1.3.5 Streetmapper 360

Streetmapper 360 (Figure 3-15) by 3D Laser Mapping and IGI mbH was launched in October 2008 and test site data was acquired in June 2011. System consists of two RIEGL VQ-250 scanners and a IGI AEROcontrol navigation unit with a fibre optic gyro based IMU, inbuilt NovAtel OEMV-3 GPS receiver and Direct Inertial Aiding (DIA) to assist in areas of poor GPS reception. Each scanner measures up to 300000 points and 100 profiles per second. Maximum measurement range is 500 meters.

A set of 11 control points from the test site was delivered to 3D Laser Mapping for post-processing.

Figure 3-15. Streetmapper 360 mapping the roads of the Espoonlahti test field.

3.1.3.6 Optech Lynx Mobile Mapper

Optech Lynx Mobile Mapper was introduced in September 2007. The test site data was collected in June 2011 by TerraTec AS (Figure 3-16) using a system with two Optech scanners which produce 200000 points per second each with ranging up to 200 m. Navigation system is an Applanix POS LV 420 system with IMU, GPS and odometer instruments. The newest version Lynx Mobile Mapper M1 can produce up to 500000 points per second per scanner.

TerreTec's Lynx instruments are mounted on the roof of a Volkswagen Caravelle with adjustable scanning height. In Espoonlahti the lower position was used and the scanners were about 2.7 meters above the road. Collected raw GPS and POS data were processed using POSPac software. Position data, i.e. data from POSPac and raw data from laser scanners were processed using DASHMap software and the output is POS-corrected laser data. A set of 84 control points was measured using VRS-GPS and delivered to TerraTac for point cloud processing. These control points included the coordinates of road markings along the driving route. The computed point clouds were matched to control points by using TerraMatch software.

Figure 3-16. TerraTec AS mapping the Espoonlahti test field with Optech Lynx Mobile Mapper.

3.2 Methods for Accuracy Evaluation

At first the received point clouds were checked by comparing with the reference data (Chapter 3.1.2.3) to detect any gross errors either in elevation or in plane. If there were larger systematic shift than a few centimetres, this was removed to assure valid comparison, as especially a large systematic shift in plane can lead to distorted elevation accuracy results. In laser scanning surveys systematic errors can be caused by, for example, GNSS reference data, and it is a common practice to use some ground control points to eliminate the bias

Comparison between the elevation reference points and the received MLS point clouds was carried out using the Output control report tool in TerraScan-software (Terrasolid, 2005). It reads in the reference points and loads every laser point within a given search radius from the individual reference points. Then a small triangulated surface model is created from the laser points and laser elevation is computed for each of the reference point easting-northing location from the triangulated model surface. This effectively interpolates the laser elevation from three laser points which are closest to the reference point to be compared. Search radius used for the most dense point clouds (RIEGL, Streetmapper and Optech Lynx) was 20 cm, for the others a search radius of 50 cm was used. Maximum allowed slope in the triangulated model was set to 20 degrees.

Planimetric accuracy was evaluated by measuring the reference targets in the received MLS point clouds and computing the differences in easting and northing.

The most deviating values were checked against the ground truth and removed from the analysis if there was any doubt that the error is due to the target, not due to the system. These errors were mainly detected in the elevation accuracy analysis due to parked cars or changes in vegetation. After this ‘gross error filtering’, systematic errors were removed, in plane separately for easting and northing, and accuracy values were computed. Minimum, maximum and standard deviation values were computed for both elevation and planimetric accuracy. Mean and root mean squared error (abbreviated to RMSE, Equation 3-1) were determined for the description of the planimetric accuracy.

$$RMSE = \sqrt{\frac{\sum_{i=1}^{n} (d_i)^2}{n}} \qquad \text{(Equation 3-1)}$$

where d_i is the distance between the reference target and the point cloud target, and n is the number of samples.

3.3 Results

3.3.1 Elevation Accuracy

The results of the elevation accuracy analysis are depicted in Table 3-3 and Figure 3-17. For the ROAMER and the RIEGL two results are given, I before and II after fine-tuning (see Chapters 3.1.3.2 and 3.1.3.3 for details). The RIEGL data was acquired while there still was a lot of snow on the ground, so the number of reference points that could be used in RIEGL analysis is lower than with other high-density systems. Sensei covers only one side of the trajectory, which explains the lower number of used reference points.

	ROAMER I		ROAMER II		Sensei		RIEGL I		RIEGL II		Streetmapper		Optech Lynx	
	CCW	CW	CCW	CW	CCW	CW	CCW	CW	CCW	CW	CCW	CW	CCW	CW
N	2936	2946	2819	2816	1418	1450	1566	1600	1585	1585	2790	2549	2693	2527
Min	-12.9	-17.1	-6.8	-7.5	-11.1	-10.1	-5.7	-5.3	-4.6	-5.7	-5.0	-5.0	-7.1	-6.4
Max	10.4	12.6	6.0	5.0	14.3	15.0	6.1	4.1	6.5	5.2	5.4	5.1	8.1	9.1
Std	3.9	3.9	2.0	2.0	3.3	2.9	1.2	1.3	1.2	1.5	1.6	1.6	2.7	2.6

Table 3-3. Elevation accuracy values in cm for tested MLS systems. Driving directions: counter-clockwise CCW, clockwise CW.

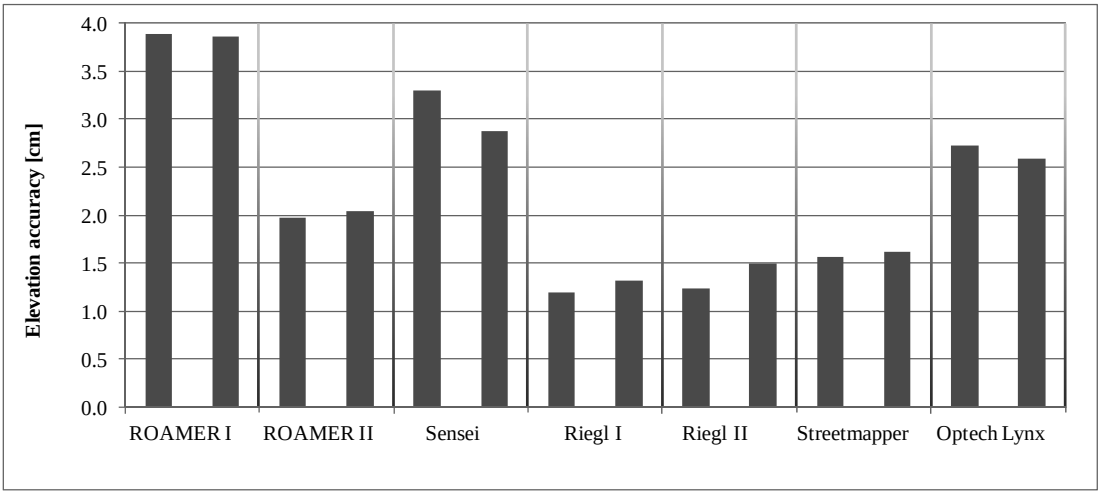

Figure 3-17. Elevation accuracy values (std) in cm for the tested MLS systems for the two driving directions. Left column stands for the CCW and right for the CW direction.

Elevation accuracy as a function of distance from the trajectory is shown in Figure 3-18. The fine-tuning has a significant effect on the ROAMER system performance.

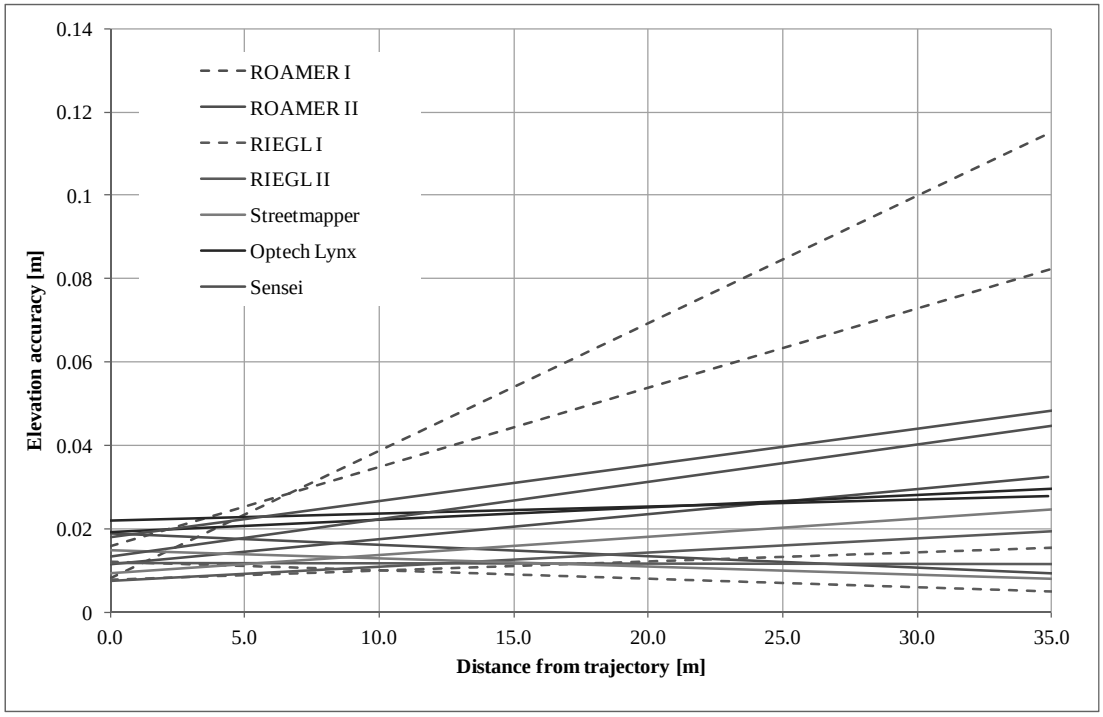

Figure 3-18. Elevation accuracy as a function of distance from trajectory, linear trend lines fitted to the observed errors in two driving directions.

According to Figure 3-18 the elevation accuracy of the best MLS systems can reach values of 1–2 cm up to a range of 35 m. In some cases the trend line suggests that the accuracy improves when the distance from the trajectory increases, but this phenomenon is most probably caused by the accuracy of the reference data having reached its limits and not being available for analysis of sub-centimeter accuracy.

3.3.2 Planimetric Accuracy

The results of the planimetric accuracy analysis are depicted in Table 3-4 and Figure 3-19. For the ROAMER and the RIEGL two results are given, I before and II after the fine-tuning (see Chapters 3.1.3.2 and 3.1.3.3 for details). The planimetric accuracy was not analyzed for the Sensei, as the reference targets could not be reliably measured from the Sensei point clouds (details in Chapter 3.1.3.4).

	ROAMER I		**ROAMER II**		**RIEGL I**		**RIEGL II**		**Streetmapper**		**Optech Lynx**	
	CCW	**CW**	**CCW**	**CW**	**CCW**	**CW**	**CCW**	**CW**	**CCW**	**CW**	**CCW**	**CW**
N	124	120	136	120	169	178	193	192	190	177	160	160
Mean	3.4	3.5	2.2	1.8	2.3	1.5	1.6	2.0	1.7	1.8	3.2	3.7
Min	0.4	0.5	0.2	0.3	0.1	0.0	0.1	0.0	0.0	0.2	0.1	0.3
Max	8.7	11.8	6.7	5.1	11.7	11.7	11.5	10.6	9.4	9.7	12.3	13.2
Std	1.8	2.2	1.1	0.9	1.7	1.3	1.4	1.5	1.5	1.3	1.8	2.3
RMSE	3.9	4.2	2.5	2.0	2.8	2.0	2.2	2.5	2.2	2.2	3.7	4.3

Table 3-4. Planimetric accuracy values in cm for the tested MLS systems. Driving directions: counter-clockwise CCW, clockwise CW.

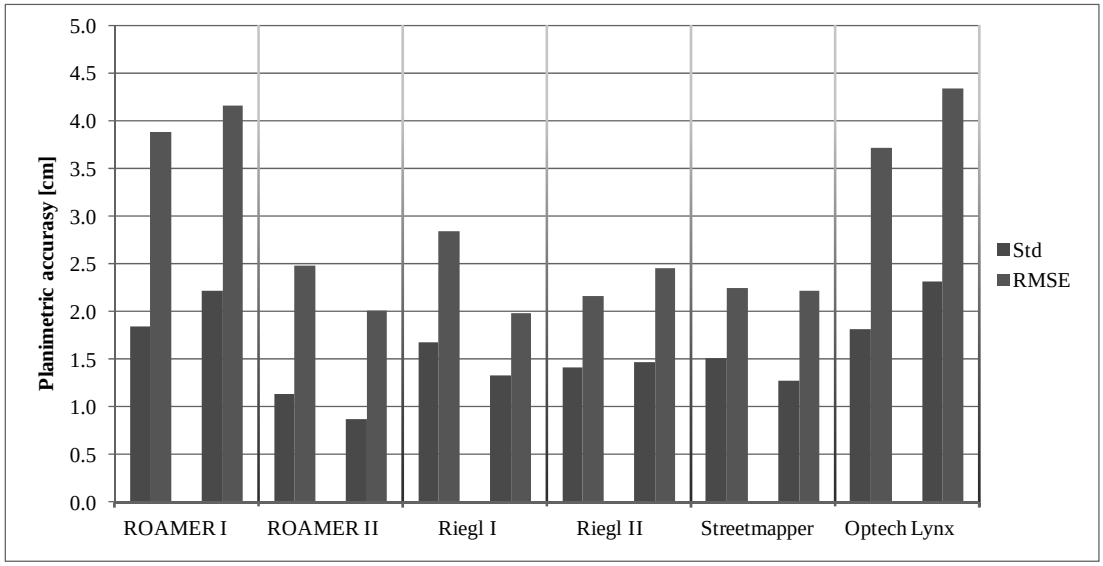

Figure 3-19. Planimetric accuracy of tested MLS systems in two driving directions. Left column stands for the CCW and right for the CW direction.

Planimetric accuracy as a function of distance from the trajectory is shown in Figure 3-20. The fine-tuning has a significant effect on the ROAMER system performance.

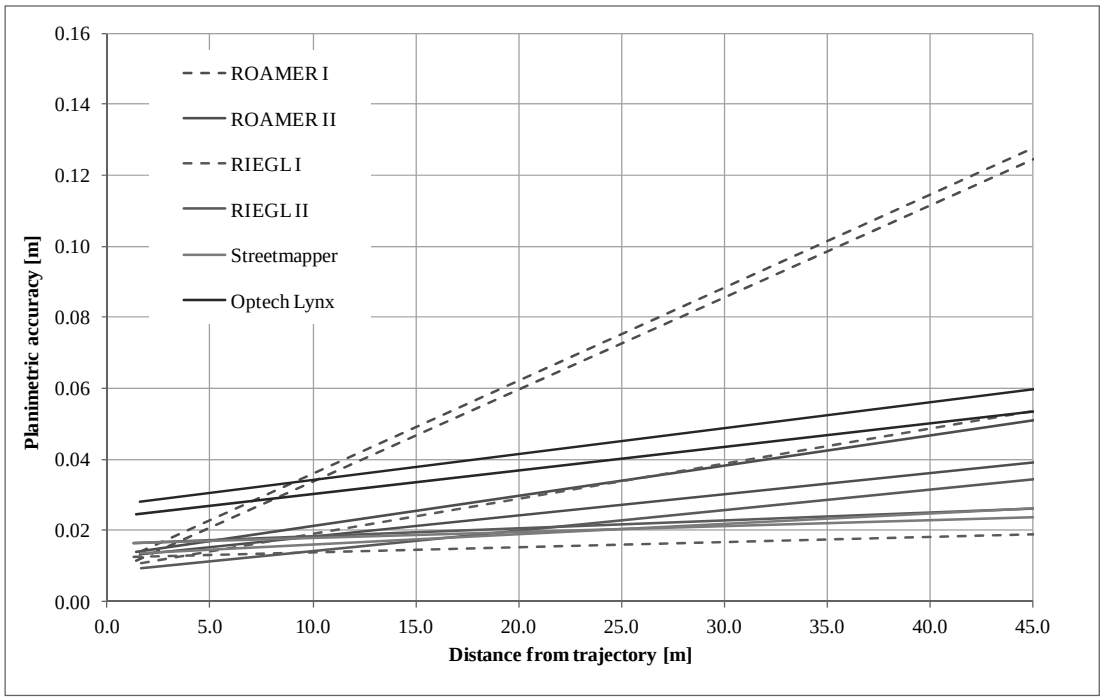

Figure 3-20. Planimetric accuracy as a function of distance from the trajectory, linear trend lines fitted to the observed errors in two driving directions.

With properly calibrated high-end MLS systems, the planimetric accuracy in good GNSS conditions is high, and in the present study it was within the limits of the used reference data accuracy, i.e., about 2 cm. Accuracy deteriorates as the distance to the trajectory increases, but very moderately, when the system calibration is in order.

The results for the ROAMER give a clear example how accuracy is affected when there are problems with calibration (ROAMER I) and how re-calibration using collected point cloud data can improve the performance (ROAMER II). Similar performance improvement can be expected when errors in trajectory, caused by satellite signal outtakes or IMU disturbances, for example, are compensated for using strip adjustments or control targets, for instance.

3.3.3 Factors Affecting the MLS Accuracy

As the results show, in good GNSS coverage the tested MLS systems can acquire accurate point cloud data. Often buildings, trees and other structures disturb the satellite visibility and the performance of other navigation instruments such as IMUs and odometers as well as post-processing algorithms define the achievable accuracy. Tools for trajectory accuracy improvement are being developed and new satellites are being launched, which should add into improved accuracy in areas where the current systems have problems.

Even though the computation of the sensor's driving path and orientation in time results in observation (GNSS, IMU) errors to be minimized, there are still errors in laser distance measurement, in scanning mirrors, in position (GNSS) and in orientation (IMU). Consequently, there are systematic offsets and random variation both in plane and height. (Pfeifer et al., 2005). These errors can be

minimized with the procedure of strip adjustment, earlier known from ALS (e.g. TerraMatch), requiring repeated measurements of the same surfaces and objects. With MLS, the possible objects and surfaces, which can be used in the correction process, include elevation model, paintings in the pavement, vertical poles and building corners.

Imperfect bore-sight calibration, additionally to the navigation errors, between the scanners on a multi-scanner systems leads to multiple reproductions of objects, as in Figure 3-21. This kind of errors in relative orientation of the instruments lead to errors in the measured point clouds, which can cause problems in the continued handling of the data, such as extraction and modelling of objects. Systematic offset errors between the sensors (ΔX, ΔY, ΔZ) can be detected using observations to common objects close to them. For example the paintings on the road are feasible for such analysis. The Δroll error can be detected using the elevation model acquired with multiple surveys. Δpitch and Δheading errors can be detected with vertical objects such as poles and building corners. These systematic errors can be corrected appropriately by even manual processing of the data. The time-dependent variation of these data (random part) needs larger number of observations for corrections which proposes the development and use of more automated techniques.

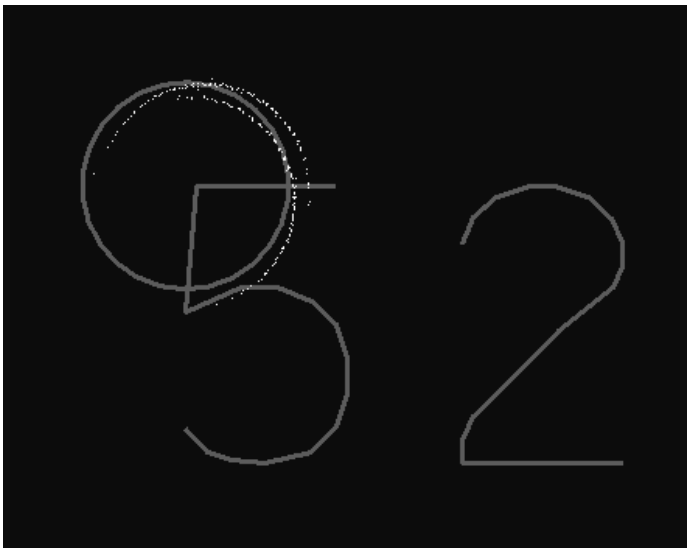

Figure 3-21. A large pole (reference target no. 52) seen double by a dual-scanner system (white points).

4 Benchmarking of Pole Detection Algorithms

The aim of the research was to study pole and tree trunk extraction methods using MLS data. Poles are important features that can also be used in the georeferencing improvement (Section 3.3.3). The method studied in this test was first described in Lehtomäki et al. (2010), and is here modified and applied to the EuroSDR data (ROAMER MLS data, Section 3.1.3.2) provided for the international partners. The results are compared with a method of the ITC (Rutzinger et al. 2011b, Pu et al. 2011, Vosselman and Klein 2010, Vosselman et al. 2004).

4.1 FGI Method for Pole Detection

Pole detection is started by segmenting the data. The aim is to find point clusters that are good candidates for poles, that is, clusters that have a narrow and elongated shape. Then, clusters are further classified as correct targets (poles and tree trunks) and false targets. In the classification, a mask is used as a model of a pole. In addition, features are extracted from the clusters to improve the classification. (Lehtomäki et al., 2010).

4.1.1 Segmentation

When tilted scanning plane is used for the scanning of the scene, typically several neighbouring profiles sweep narrow elongated objects (Figure 4-1). The segmentation method makes use of the profile or row-column information of the laser data. The laser data can be arranged in a matrix whose columns, also called profiles or scan lines, consists of an ordered set of 3D points that are measured sequentially with one full revolution of the mirror. Therefore, each 3D point has two unique indices: the index of the profile it belongs to (column index) and its placement on the profile with respect to other points on the profile (row index).

First, individual scan lines are segmented independently applying connected component labelling. Neighbouring points are compared to each other and labelled with a same label if the distance between them is shorter than a threshold. The aim is to find possible sweeps of poles and therefore too long point groups are removed. It is also advantageous to remove groups that have too few points. Next, the remaining point groups are clustered by searching overlapping groups in the horizontal plane from the neighbouring profiles. New groups are added to a cluster from next or previous profiles until no new overlapping groups are found.

The resulting clusters should be narrow and elongated and thus valid candidates for poles. Due to shadowing effect some sweeps of a target may be missing and clustering may find two or more clusters that belong to a same target. Clusters are compared to each other and merged if they are approximately coaxial and close enough to each other.

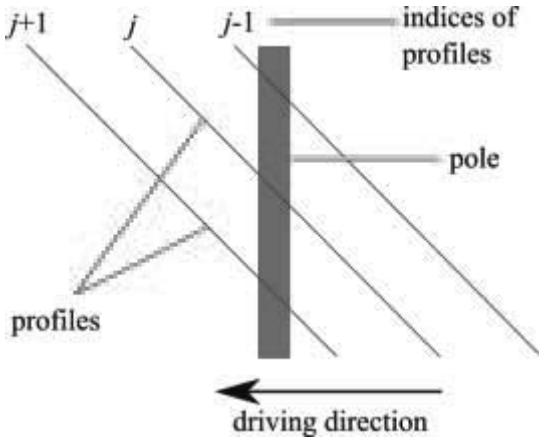

Figure 4-1. Scanning geometry of the ROAMER when backwards tilted scanning plane is used. Even narrow pole-like objects receive several hits from the neighbouring profiles. The scan line structure of the data is utilised in the segmentation process by searching short point groups that are on top of each other in the neighbouring profiles. (Modified from Kukko (2009).)

4.1.2 Extraction of Poles

A large number of candidates are found in the segmentation and only a part of them are correct targets. For example, building walls contain a lot of short point groups that form candidate clusters. Extraction of correct targets is done by calculating a set of features for each cluster and by selecting only clusters whose feature values satisfy predefined thresholds. In addition, a model of a pole is used in the extraction process. Features measure the length, shape and orientation of and the number of sweeps in the cluster. The goal is to find poles that are 1 m long or longer. Principal component analysis, that gives the directions of the largest variances and corresponding variances (eigenvalues) for the point cluster, is utilised in the feature extraction. The length of the cluster is measured along the main axis of the cluster, i.e., the line that goes through the centre point of the cluster and is parallel to the direction of the largest variance. Shape of the cluster is measured by the ratio of the two largest eigenvalues; if the ratio is large the cluster's shape is elongated and thus resembles the shape of a pole. The aim is to find approximately vertical objects and therefore clusters whose main axis is too tilted compared to vertical direction are removed. To lessen the number of false positives it is advantageous to demand that the cluster contains at least some minimum amount of sweeps on top of each other.

Poles with no vegetation or other disturbing objects around them should be elongated point clusters that are surrounded by empty space in the data. The candidates found from the walls do not generally fulfil this condition and can be removed using a mask that is placed around the cluster (Figure 4-2). The mask that is a "model" of a pole consists of two coaxial cylinders whose axes coincide with the main axis of the cluster. The inner one of the cylinders is the smallest possible cylinder with the given main axis that contains all cluster points between the lower and upper end of the mask. Larger cylinder has, for example, 20–80 cm larger radius. If the number of points inside the outer cylinder is almost equal to the number of points inside the inner cylinder, there is an almost empty space around the cluster and the data fits the pole model.

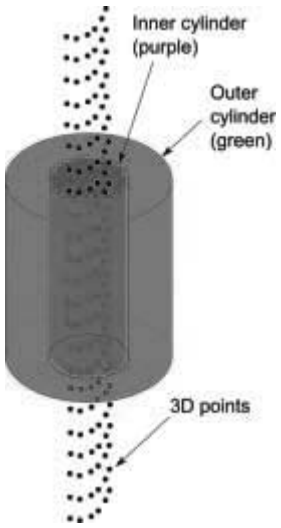

Figure 4-2. A mask consisting of two coaxial cylinders is used as a model of a pole in the algorithm. The green volume surrounding the pole that is inside the purple cylinder should be almost empty of points.

For example, the boards of the traffic signs and branches of a tree can be problematic if the mask is applied to the whole cluster. Therefore, clusters are checked by moving the mask in small steps from the bottom to the top of the cluster. The length of the mask is less than or equal to the minimum length of the target. At each step, the orientation and shape of the part of the cluster that is inside the inner cylinder is checked. If these features satisfy the thresholds and pole model fits the data the points inside the inner cylinder are classified as pole-like. Finally, all pole-like points of the cluster are merged and if the resulting merged cluster is long enough and contains enough sweeps it is classified as pole.

4.1.3 Pole Extraction Results

74.3% of the targets of the field reference were also identified in the mobile data by a human operator, rest of the targets were occluded by vegetation, cars or other structures. The algorithm detected (Table 4-1) 69.7% of the test set targets while the correctness of the detection was 86.5%. 59.1% of the trees (127 in total), 82.3% of the traffic signs (79), and 95.7% of the lamp posts (46) were detected. From the targets closer than 12.5 m to the trajectory (190 in total), the method detected 71.6% and the corresponding correctness was 95.1%. A view to the data including extracted poles can be found in Figure 4-3.

Statistical Number	**Distance < 30m**	**Distance < 12.5m**
Detection Rate (%)	69.7	71.6
Correct Detections (%)	86.5	95.1

Table 4-1. Results of the pole detection. Targets that were visible in the MLS data, closer than 30/12.5 m to the trajectory and longer than 1 m were included.

Figure 4-3. A view to the MLS data of the EuroSDR project (small bluish-green dots) including extracted poles and tree trunks (larger red dots).

Approximately half of the missed reference targets had points around the pole-like part that caused the target not to fit the model of the pole. This was caused, e.g., by vegetation around the pole or branches around the trunk. Many targets were also missed because there were too few points in single sweeps.

The corresponding point groups were discarded after scan line segmentation because the number of points did not exceed the threshold. There is a trade-off with this threshold parameter; if smaller groups are accepted, more correct targets are detected but at the same time more false positives are found. In addition, cars that are parked on the side of the road may sometimes cause the lower part of a pole or trunk to be missing in the data and this makes it more difficult for the algorithm to detect the target.

Most of the false positives were found in different building structures. Walls in which a narrow elongated part was facing the trajectory (e.g. separating walls between balconies), narrow corners in the walls (Lehtomäki et al., 2010) or narrow wall parts between windows and doors produced point clusters to the data that resembled poles. For the same reason also some billboards caused false detections.

Hofmann and Brenner (2009) reported 94% correctness in their method while 86.5% (30 m to the trajectory) and 95.1% (12.5 m) of the targets our method extracted were correct. However, comparison is not straightforward. Firstly, they did not study the detection rate of the method. By adjusting the parameters of the method, there can be a trade-off between the number of extracted references and how many percent of the detected targets are correct. Secondly, the width of the test area in the direction perpendicular to the trajectory was not reported in their study. Due to the lower point density, targets farther away from the scanner are more difficult to detect. Lastly, the properties of the test site, data density and amount of noise can have a strong effect on the detection rate and correctness. For example, single buildings with suitable wall structures (see above) can cause a large number of false detections.

The accuracy of pole diameter determination was tested using a set of 41 extracted poles. Results show that the diameter was measured with an RMSE of 0.83 cm (bias -3.1 mm).

4.2 ITC Method for Classification and Pole Detection

4.2.1 Laser Point Classification

The used methods for feature extraction of MLS point clouds follow a modular workflow, which comprises (i) pre-processing, (ii) point cloud segmentation, (iii) rough classification, and (iv) extraction of specific features. As a pre-processing step the raw point cloud is clipped along the GPS trajectory into road parts, which have a certain width and length in order to exclude far range areas with insufficient point densities for feature extraction. The point cloud is segmented to detect and label planar regions using a surface growing algorithm with 3D Hough transformation for the detection of seed surfaces (Vosselman et al. 2004, Vosselman and Klein 2010). For each segment the size, orientation and connectivity to other segments is investigated in order to roughly classify the ground, vertical walls, and raised features, which are on top of the road (such as light poles, cars, and trees). Features on top of the ground are further classified by extracting all features containing pole-like structures. After removing the ground points the remaining points are grouped by applying a connected component segmentation. Pole-like structures are detected by slicing each component horizontally and fitting an enclosed rectangle to each slice. Then the deviation of the centre point and the length difference of diagonals of neighbouring slices from a stack are compared. The detected pole-like features are separated into trees and poles including road signs and traffic lights. This is done by splitting the features into sub components (such as triangular, rectangular and round shaped subcomponents for road signs or irregular subcomponents for tree crowns). Building facades are extracted without applying pre-processing in order to include also buildings, which might be located

at a farer distance to the MLS trajectory. Also for the extraction of facades the point cloud is first segmented. Then for every segment planarity, tilt from vertical and size (height and width) are checked. (Rutzinger et al. 2011b).

4.2.2 Point Classification Results

ITC applied the above mentioned method to ROAMER 48 Hz mobile data, a combined data set from two opposite driving directions and selecting the maximum distance to the trajectory to 15 meters. The results of the corresponding analysis are presented in Table 4-2. Figure 4-4 demonstrates the quality of the classifier in extracting façade points.

Statistical Number	Distance < 15m
Detection Rate (%)	51.9
Correct Detections (%)	86.2

Table 4-2. Results of the pole detection. Targets that were visible in the MLS data, closer than 15 m to the trajectory and longer than 1 m were included.

Figure 4-4. Facade classification by ITC. White points represent original facade points, red points were classified as facade by ITC. Other colours were misclassified as facade. 87.4 % of the facade class points by ITC were true facade points.

5 Discussion and Conclusions

The EuroSDR project "Mobile Mapping - Road Environment Mapping using Mobile Laser Scanning" focused finally on two issues: benchmarking of mobile laser scanning systems in the test field established for this project and benchmarking of pole type object classification. The test field will be maintained by the Mobile mapping group of the FGI for further performance and calibration studies on the new MLS systems and data processes.

Obtained quality - In the system comparison, most of the leading manufactures, such as RIEGL, Optech and Streetmapper participated together with research systems. The system comparison revealed the high quality point clouds generated by all systems under good GNSS conditions. With all professional systems properly calibrated, the elevation accuracy was better than 3.5 cm until 35 m.

The best system had 2.5 cm planimetric accuracy even with the range of 45 cm. The planimetric errors increase as a function of range, but moderately if the system was properly calibrated. The accuracy of the systems was high. Even better accuracy may be obtained, which requires that all data is provided with higher detail than in 1 cm classes and reference data needs to be of mm level.

Test field concept - The test site for MLS established in Espoonlahti was found to be a useful concept for the verification of the MLS quality. FGI will continue to maintain the test field and it is open for all systems in the future.

Improvement in localization of the system - Since the results of all systems was adequate for high level roadside mapping, the main focus on MLS quality research should concentrate on the improvement of the trajectory solution under non-ideal (and also with ideal) conditions using both improved hardware (additional sensors) and software solutions (post-processing). In the hardware, the commercial systems already used odometers. Additional sensors improving the georeferencing/localization solution with GNSS loss should be increased. These additional sensors can be e.g. cameras, the data of which are automatically processed to solve the position changes together with IMU and odometer when GNSS signal is not appropriate. Alternative solutions include the use of signals, e.g. painted signals on the roads, as has been demonstrated (Soininen, 2012) in Helsinki tram MLS survey.

Improvements in point cloud georeferencing - The MLS data obtained for comparison was thru the standard process of the data providers. Laboratory calibration of offsets and orientations of system components can be fine-tuned by the real data. In Optech and Streetmapper both these calibrations are assumed to be done already by the data provider. With RIEGL and ROAMER, the calibration was done first with using only the laboratory-type calibration, which showed the need for further calibration in the field. The second point cloud was provided taking the aspects mentioned in Section 3.3.3, and e.g. in ROAMER a significant roll error was found with overlapping point cloud data. For the future, the improvement of georeferencing solutions via MLS strip adjustment process needs more automation. The corrections to the offsets and orientations needs to be made to the trajectory information.

The improvements in the georeferencing could also include improvements due to abrupt jumps and other errors in the data. Schwarz and El-Sheimy (2004), discussed the use of three post-processing techniques, such as de-noising, auto regression modelling and smoothing. Denoising is a noise reduction done directly to the sensor measurements. Auto regression modelling reduces noise in the data fusion step, and e.g. forward and backward Kalman filter are example of this method type and already applied in the typical GNSS/IMU integration. Also, numerical smoothing on the post-processed trajectories can be performed.

Benchmarking of algorithms for object detection - The processing of MLS data has shown to be complex. In principle, all ALS, TLS and range image-based algorithms are feasible also for MLS data processing. There are methods available, but for this comparison we got results that could be compared only from ITC and FGI. Other inputs were not obtained that had enough coverage for verification. The FGI pole detection algorithm was implemented based on the knowledge of the ROAMER measurement principle and it has been developed originally only for pole type objects. Therefore, it obtained better accuracies than the general classification concept of the ITC. The work of both groups has been continued after the EuroSDR test, and the current state can be summarized as stated in Pu et al. (2011): “While poles are recognized for up to 86%, classification into further categories requires further work and integration with imagery”. Since the goal is to have high automation rate supported by minimum amount of manual work, and to create accurate 3D models of roadsides and cities, there is still a significant contribution needed for future research. The further research methods need also to be implemented in commercial software before the exploitation can be

done in full scale. There is already software, such as from Terrasolid, that is specifically aimed also for mobile laser data processing.

In general, FGI continues the activities of benchmarking of MLS algorithms, but that is currently done mainly on bilateral basis rather than under international projects. The ROAMER data from Espoonlahti is available also in the future for benchmarking activities and we consider even making a larger public data available for future MLS research and verification.

Acknowledgments

All participants, i.e. Gerald Zach at RIEGL Laser Measurement Systems GmbH, Iain Lorraine at 3D Laser Mapping, Halvor Holvik, Morten Taraldsten Brunes, Heikki Luukkonen and Jan Biström at TerraTec AS, are gratefully acknowledged for cooperation in the project. Hannu Hyyppä from Aalto University also contributed significantly. The Academy of Finland is acknowledged for its financial support in the form of the projects “Science and Technology Towards Precision Forestry”, “Towards Improved Characterization of Map Objects”, ” Economy and technology of a global peer produced 3D geographical information system in built environment - 3DGIS”, and “Interaction of Lidar/Radar Beams with Forests Using Mini-UAV and Mobile Forest Tomography”.

References

Barber, D., Mills, J. and Smith-Voysey, S., 2008. Geometric validation of a ground-based mobile laser scanning system. ISPRS Journal of Photogrammetry & Remote Sensing, 63 (1), pp. 128–141.

Biber, P., Andreasson, H., Duckett, T. and Schilling, A., 2004. 3D modeling of indoor environments by a mobile robot with a laser scanner and panoramic camera. Proceedings of the IEEE/RSJ International Conference on Intelligent Robots and Systems IROS ’04, Sendai, Japan.

Bilker, M. and Kaartinen, H., 2001. The Quality of Real-Time Kinematic (RTK) GPS Positioning. Reports of the Finnish Geodetic Institute 2001:1, Kirkkonummi.

Brenner, C., 2009. Extraction of features from mobile laser scanning data for future driver assistance systems. In: Proc. 12th Agile Conference, AGILE, Hannover, 2–5 June, pp. 12–45.

Clarke, K.C., 2004. Mobile mapping and geographic information systems. Cartography and Geographic Information Science, 31 (3), pp. 131–136.

El-Sheimy, N., 2005. An overview of mobile mapping systems. FIG Working Week 2005 and GSDI-8—From Pharaos to Geoinformatics, FIG/GSDI, Cairo, 16–21 April. 24 p. (on CDROM).

FARO, 2008. FARO Photon 80 specifications.

FARO, 2009. FARO Photon 120 specifications.

Früh, C. and Zakhor, A., 2004. An automated method for large-scale, ground-based city model acquisition. International Journal of Computer Vision, 60 (1), pp. 5–24.

Graham, L., 2010. Mobile mapping systems overview. Photogrammetric Engineering & Remote Sensing, 76 (3), pp. 222–228.

Haala, N., Peter, M., Kremer, J. and Hunter, G., 2008. Mobile LIDAR mapping for 3D point cloud collection in urban areas—a performance test. International Archives of Photogrammetry, Remote Sensing and Spatial Information Sciences, 37 (Part B5), pp. 1119–1130.

Hassan, T. and El-Sheimy, N, 2008. Common adjustment of land-based and airborne mobile mapping system data. International Archives of Photogrammetry, Remote Sensing and Spatial Information Sciences, 37 (Part B5), pp. 835–842.

Hofmann, S. and Brenner, C., 2009. Quality assessment of automatically generated feature maps for future driver assistance systems. In: Proceedings of the 17th ACM SIGSPATIAL International Conference on Advances in Geographic Information Systems, GIS ’09, ACM, New York, NY, USA, pp. 500–503.

Hyyppä, J., Jaakkola, A., Hyyppä, H., Kaartinen, H., Kukko, A., Holopainen, M., Zhu, L., Vastaranta, M., Kaasalainen, S., Krooks, A., Litkey, P., Lyytikäinen-Saarenmaa, P., Matikainen, L., Rönnholm, P., Chen, R., Chen, Y., Kivilahti, A. and Kosonen, I., 2009. Map Updating and Change Detection Using Vehicle-Based Laser Scanning. Proceedings of 2009 Urban Remote Sensing Joint Event, 20.-22. May, Shanghai.

Häkli, P., 2004. Practical test on accuracy and usability of virtual reference station method in Finland. In: Proc. FIG Working Week 2004, FIG, Athens, 22–27 May. 16 p (on CDROM).

Ibeo, 2011. http://www.ibeo-as.com/

Jaakkola, A., Hyyppä, J., Hyyppä, H. and Kukko, A., 2008. Retrieval algorithms for road surface modelling based on mobile mapping. Sensors, 8 (9), pp. 5238–5249.

Jaakkola, A., Hyyppä, J., Kukko, A., Yu, X., Kaartinen, M., Lehtomäki, M., and Y. Lin, 2010. A low-cost multi-sensoral mobile mapping system and its feasibility for tree measurements. ISPRS Journal of Photogrammetry and Remote Sensing, Vol. 65(6), 514-522.

Jochem, A., Höfle, B. and Rutzinger, M., 2011. Extraction of vertical walls from mobile laser scanning data for solar potential assessment. Remote Sensing. Vol. 3, pp. 650-667.

Kaasalainen, S., Lindroos, T. and Hyyppä, J., 2007. Toward hyperspectral lidar - Measurement of spectral backscatter intensity with a supercontinuum laser source. IEEE Geoscience and Remote Sensing Letters, 4(2), pp. 211- 215.

Kaartinen, H,. and Hyyppä, J., 2006. EuroSDR-Project Commission 3 "Evaluation of Building Extraction", Final Report, In: EuroSDR - European Spatial Data Research, Official Publication No 50, pp. 9-77.

Kaartinen, H. and Hyyppä, J., 2008. EuroSDR/ISPRS Project Commission II, Tree Extraction, Final Report. EuroSDR. European Spatial Data Research, Official Publication No 53, 56 p.

Kukko, A., Andrei, C.-O., Salminen, V.-M., Kaartinen, H., Chen, Y., Ronnholm, P., Hyyppä, H., Hyyppä, J., Chen, R., Haggrén, H., Kosonen, I. and Čapek, K., 2007. Road environment mapping system of the Finnish Geodetic Institute - FGI ROAMER. International Archives of Photogrammetry, Remote Sensing and Spatial Information Sciences, 36(3/W52), pp. 241–247.

Kukko, A., Jaakkola, A., Lehtomäki, M., Kaartinen, H. and Chen, Y., 2009. Mobile mapping system and computing methods for modelling of road environment. 2009 Joint Urban Remote Sensing Event , art. no. 5137703.

Kukko, A. and Hyyppä, J., 2009. Small-footprint laser scanning simulator for system validation, error assessment and algorithm development. Photogrammetric Engineering & Remote Sensing, 75 (10), pp. 1177–1189.

Kukko, A., 2009. Road Environment Mapper—3D Data Capturing with Mobile Mapping. Licentiate's Thesis. Helsinki University of Technology, Espoo, Finland.

Kukko, A., Kaartinen, H., Hyyppä, J. and Chen, Y., 2012. Multiplatform Mobile Laser Scanning: Usability and Performance. Sensors, 12 (9), pp. 11712-11733.

Lehtomäki, M., Jaakkola, A., Hyyppä, J., Kukko, A. and Kaartinen, H., 2010. Detection of vertical pole-like objects in a road environment using vehicle-based laser scanning data. Remote Sensing, 2 (3), pp. 641–664.

Li, B.J., Li, Q.Q., Shi, W.Z. and Wu, F.F., 2004. Feature Extraction And Modeling Of Urban Building From Vehicle-Borne Laser Scanning Data. Proceedings of the XXth ISPRS Congress, July

2004, Istanbul, Turkey, International Archives of Photogrammetry, Remote Sensing and Spatial Information Sciences, Vol. 35(B5), 6 p.

Lin, Y., Jaakkola, A., Hyyppä, J. and Kaartinen, H., 2010. From TLS to VLS: Biomass Estimation at Individual Tree Level. Remote Sensing, 2(8), pp. 1864-1879. http://www.mdpi.com/2072-4292/2/8/1864/

Lin, Y. and Hyyppä, J., 2011. k-segments-based Geometric Modeling of VLS Scan Lines. IEEE Geoscience and Remote Sensing Letter, 8(1), pp. 93-97.

Lin, Y., Hyyppä, J. and Jaakkola, A., 2011. Combining mobile and static terrestrial laser scanners to investigate individual crown attributes during foliation. Canadian Journal of Remote Sensing, 37(4), pp. 359-375.

Manandhar, D. and Shibasaki, R., 2002. Auto-extraction of urban features from vehicle-borne laser data. International Archives of Photogrammetry, Remote Sensing and Spatial Information Sciences, 34 (4), 6 p. (on CDROM).

Narayana, K., 2011. Solutions for the localization of Mobile Mapping Systems in structured environments. Doctoral thesis, MINES ParisTech, 267 p.

Optech, 2011. Lynx Mobile Mapper Spec Sheet. http://www.optech.ca/pdf/Lynx_SpecSheet_110909_web.pdf

Petrie, G., 2010. An introduction to the technology, mobile mapping systems. Geoinformatics, 13 (1), pp. 32–43.

Pfeifer, N., Oude Elberink, S. and Filin, S., 2005. Automatic tie elements detection for laser scanner strip adjustment. Proceedings of the ISPRS Workshop "Laser scanning 2005", September 12-14, 2005, Enschede, The Netherlands, pp. 174-179, CD-ROM.

Pu, S., Rutzinger, M., Vosselman, G. and Oude Elberink, S., 2011. Recognizing basic structures from mobile laser scanning data for road inventory studies. ISPRS Journal of Photogrammetry and Remote Sensing 66 (Commercial Supplement Issue on Advances in lidar data processing and applications), pp. 28-39.

Puttonen, E., Jaakkola A., Litkey, P. and Hyyppä, J., 2011. Tree Classification with Fused Mobile Laser Scanning and Hyperspectral Data. Sensors, 11(5), pp. 5158-5182. http://www.mdpi.com/1424-8220/11/5/5158/pdf

RIEGL, 2010. http://www.riegl.com/nc/products/mobile-scanning/gallery/

RIEGL, 2011. Datasheet RIEGL VQ-250, http://riegl.com/uploads/tx_pxpriegldownloads/10_DataSheet_VQ250_13-04-2010.pdf

Rutzinger, M., Pratihast, A., K., Oude Elberink, S. and Vosselman, G., 2011a. Tree modelling from mobile laser scanning datasets. The Photogrammetric Record. Vol. 26(134), pp. 1-12.

Rutzinger, M., Höfle, B., Oude Elberink, S. and Vosselman, G., 2011b. Feasibility of facade footprint extraction from mobile laser scanning data. Photogrammetrie, Fernerkundung, Geoinformation. Vol. 3(3), pp. 97-107.

Shen, Y., Sheng, Y., Zhang, K., Tang, Z. and Yan, S., 2008. Feature extraction from vehicle-borne laser scanning data. In: Proc. International Conference on Earth Observation Data Processing and Analysis. SPIE, Wuhan, 28–30 December. 10 p. (on CDROM).

Schwarz K. P. and El-Sheimy, N., 2004. Mobile Mapping Systems – State of The Art and Future Trends. Proceedings of the XXth International ISPRS Congress, July 2004, Istanbul, Turkey, International Archives of Photogrammetry, Remote Sensing and Spatial Information Sciences, XXXV(B5), pp. 759-768.

Soininen, A., 2012. Presentation in Terrasolid European User's Event 2012 in Levi, Finland, http://www.terrasolid.fi/system/files/helsinki_tram_survey.ppt

Steinhauser, D., Ruepp, O. and Burschka, D., 2008. Motion segmentation and scene classification from 3D LIDAR data. In: Proc. IEEE Intelligent Vehicles Symposium. IEEE, Eindhoven, pp. 398–403.

Tao, C.V. and Li, J. (Eds.), 2007. Advances in Mobile Mapping Technology. In: ISPRS Book Series, Vol. 4. Taylor & Francis, 176 p.

Terrasolid, 2005. TerraScan User’s Guide 03.10.2005.

TerraTec, 2011. Report 16.09.2011, Mobile Mapping, Geodetic Institute .

Trimble, 2011. Trimble Indoor Mobile Mapping Solution; Enabling high productivity for indoor mapping. 6 p.

Vaaja, M., Hyyppä, J., Kukko, A., Kaartinen, H., Hyyppä, H. and Alho, P., 2011. Mapping Topography Changes and Elevation Accuracies Using a Mobile Laser Scanner. Remote Sensing, 3(3), pp. 587-600.

Vosselman, G., Gorte, B.G.H., Sithole, G. and Rabbani, T., 2004. Recognising structure in laser scanner point clouds. International Archives of Photogrammetry, Remote Sensing and Spatial Information Sciences, vol. 46, part 8/W2, Freiburg, Germany, October 4-6, pp. 33-38.

Vosselman, G. and Klein, R., 2010. Visualisation and structuring of point clouds. In: Airborne and Terrestrial Laser Scanning, Vosselman, G. and Maas, H.-G. (Eds.), Whittles Publising, ISBN 978-1904445-87-6, pp. 43-79.

Weiss, T. and Dietmayer, K., 2007. Automatic detection of traffic infrastructure objects for the rapid generation of detailed digital maps using laser scanners. In: Proc. IEEE Intelligent Vehicles Symposium. IEEE, Istanbul, pp. 1271–1277.

Yen, K.S., Akin, K., Lofton, A., Ravani, B. and Lasky, T.A., 2010. Using Mobile Laser Scanning to Produce Digital Terrain Models of Pavement Surfaces. Final report of the Advanced Highway Maintenance and Construction Technology Research Center research project, University of California at Davies. http://ahmct.ucdavis.edu/pdf/UCD-ARR-10-11-30-01.pdf

Yu, S.-J., Sukumar, S.R., Koschan, A.F., Page, D.L. and Abidi, M.A., 2007. 3D reconstruction of road surfaces using an integrated multi-sensory approach. Optics and Lasers in Engineering, 45 (7), pp. 808–818.

Zhao, H. and Shibasaki, R., 2003a. Reconstructing a textured CAD model of an urban environment using vehicle-borne laser range scanners and line cameras. Machine Vision and Applications, 14 (1), pp. 35–41.

Zhao, H. and Shibasaki, R., 2003b. A vehicle-borne urban 3-D acquisition system using single-row laser range scanners. IEEE Transactions on Systems, Man and Cybernetics, 33 (4), pp. 658–666.

Zhao, H. and Shibasaki, R., 2005. Updating a digital geographic database using vehicle-borne laser scanners and line cameras. Photogrammetric Engineering & Remote Sensing, 71 (4), pp. 415–424.

Literature

Alamús, R., Baron, A., Bosch, E., Casacuberta, J., Miranda, J., Pla, M., Sànchez, S., Serra, A. and Talaya, J., 2004. On the accuracy and performance of the Geomòbil system. International Archives of Photogrammetry, Remote Sensing and Spatial Information Sciences, 35 (Part 5), pp. 262–267.

Alho, P., Kukko, A., Hyyppä, H., Kaartinen, H., Hyyppä, J. and Jaakkola, A., 2009. Application of boat-based laser scanning for river survey. Earth Surface Processes and Landforms, 34 (13), pp. 1831-1838.

Alshawa, M., Grussenmeyer, P. and Smigiel, E.,2009. A low cost tls based land mobile mapping system assisted by photogrammetry | [Um sistema de mapeamento terrestre de baixo custo baseado em um tls assistido por fotogrametria]. Boletim de Ciencias Geodesicas 15 (5), pp. 743-761.

Andersen, J.A, Andersen, N. and Ravn, O., 2008. Vision Assisted Laser Scanner Navigation for Autonomous Robots. Springer Tracts in Advanced Robotics, Vol. 39.

Becker, S. and Haala, N., 2009. Quality dependent reconstruction of building façades. Lecture Notes in Computer Science (including subseries Lecture Notes in Artificial Intelligence and Lecture Notes in Bioinformatics) 5786 LNCS, pp. 174-184.

Bileschi, S., 2009. Fully automatic calibration of LIDAR and video streams from a vehicle. IEEE 12th International Conference on Computer Vision Workshops, ICCV Workshops 2009 , art. no. 5457439, pp. 1457-1464.

Brostow, G.J., Shotton, J., Fauqueur, J. and Cipolla, R., 2008. Segmentation and recognition using structure from motion point clouds. Lecture Notes in Computer Science (including subseries Lecture Notes in Artificial Intelligence and Lecture Notes in Bioinformatics) 5302 LNCS (PART 1), pp. 44-57.

Bucksch, A. and Lindenbergh, R., 2008. CAMPINO - A skeletonization method for point cloud processing. ISPRS Journal of Photogrammetry and Remote Sensing 63 (1), pp. 115-127.

Caroti, G. and Piemonte, A., 2010. Measurement of cross-slope of roads: Evaluations, algorithms and accuracy analysis. Survey Review 42 (315), pp. 92-104.

Chen, Y.-Z., Zhao, H.-J. and Shibasaki, R., 2007. A mobile system combining laser scanners and cameras for urban spatial objects extraction. Proceedings of the Sixth International Conference on Machine Learning and Cybernetics, ICMLC 2007 3, art. no. 4370426, pp. 1729-1733.

Chiang, K.-W., Lin, Y.-C., Huang, Y.-W. and Chang, H.-W., 2009. An ANN-RTS smoother scheme for accurate INS/GPS integrated attitude determination. GPS Solutions 13 (3), pp. 199-208.

Chon, J., 2009. The GEO-localization of a mobile mapping system. Journal of the Korean Society of Surveying Geodesy Photogrammetry and Cartography 27 (5), pp. 555-563.

Deschaud, J.-E., Brun, X. and Goulette, F., 2009. Colorisation et texturation temps reel d'environnements urbains par systeme mobile avec scanner laser et camera fish-eye. Revue Francaise de Photogrammetrie et de Teledetection (192), pp. 29-37.

Dorninger, P. and Pfeifer, N., 2008. A comprehensive automated 3D approach for building extraction, reconstruction, and regularization from airborne laser scanning point clouds. Sensors 8 (11), pp. 7323-7343.

Dunbar, M. and Neuman, M., 2008. Mobile mapping and data collection. GEO: connexion 7 (4), pp. 40-42.

Escalera, S., Pujol, O. and Radeva, P., 2009. Traffic sign recognition system with β –correction. Machine Vision and Applications 21(2), pp. 99-111.

Feng, J., Zhong, R., Yang, Y. and Zhao, W., 2009. Quality evaluation of spatial point-cloud data collected by vehicle-borne laser scanner. 2008 International Workshop on Education Technology and Training and 2008 International Workshop on Geoscience and Remote Sensing, ETT and GRS 2008 2, art. no. 5070370, pp. 320-323.

Gao, C. and Spletzer, J.R., 2010. On-line calibration of multiple LIDARs on a mobile vehicle platform. Proceedings - IEEE International Conference on Robotics and Automation , art. no. 5509880, pp. 279-284.

Gharavi, H. and Shaoshuai, G., 2007. 3-D Motion Estimation Using Range Data. Intelligent Transportation Systems, IEEE Transactions, Vol. 8(1), pp. 133 – 143.

Grejner-Brzezinska, D., Toth, C. and Yi, Y., 2005. On improving navigation accuracy of GPS/INS systems. Photogrammetric Engineering & Remote Sensing, 71(4), pp. 377-389.

Grejner-Brzezinska, D., Toth, C., Markiel, J., Moafipoor, S. and Czarnecka, K., 2009. Personal navigation: Extending mobile mapping technologies into indoor environments | [Navegação pessoal: Tecnologias de mapeamento móvel na ampliação da navegação em ambientes internos]. ..... Boletim de Ciencias Geodesicas 15 (5), pp. 790-806.

Gräfe, G., 2007. High precision kinematic surveying with laser scanners. Journal of Applied Geodesy. 1 (4), pp.185–199.

Hiremagalur, J., Yen, K.S., Lasky, T.A. and Ravani, B., 2009. Testing and performance evaluation of fixed terrestrial three-dimensional laser scanning systems for highway applications. Transportation Research Record 2098, pp. 29–40.

Hodge, R., Brasington, J. and Richards, K., 2009. In situ characterization of grain-scale fluvial morphology using terrestrial laser scanning. Earth Surface Processes and Landforms 34 (7), pp. 954–968.

Hongchao, M. and Wang, Z., 2011. Distributed data organization and parallel data retrieval methods for huge laser scanner point clouds. Computers and Geosciences 37 (2), pp. 193-201.

Höfle, B. and Rutzinger, M., 2011. Topographic airborne LiDAR in geomorphology: A technological perspective. Zeitschrift für Geomorphologie, Supplementary Issues, 55(2), pp. 1-29.

Jochem, A., Höfle, B., Rutzinger, M. and Pfeifer, N., 2009. Automatic roof plane detection and analysis in airborne LiDAR point clouds for solar potential assessment. Sensors 9, pp. 5241–5262.

Kaasalainen, S., Kaartinen, H., Kukko, A., Anttila, K. and Krooks, A., 2010. Brief communication: "Application of mobile laser scanning in snow cover profiling. Cryosphere Discussions 4 (4), pp. 2513-2522.

Karamanou, A., Papazissi, K., Paradissis, D. and Psarianos, P., 2009. Precise estimation of road horizontal and vertical geometric features using mobile mapping techniques | [Estimativa precisa de feições geométricas horizontais e verticais em rodovias usando técnicas de mapeamento móvel]. Boletim de Ciencias Geodesicas 15 (5), pp. 762-775.

Karimi, H.A., Khattak, A.J. and Hummer, J.E., 2000. Evaluation of mobile mapping systems for roadway data collection. Journal of Computing in Civil Engineering 14(3), pp. 168-173.

Kirchhof, M., Jutzi, B. and Stilla, U., 2008. Iterative processing of laser scanning data by full waveform analysis. ISPRS Journal of Photogrammetry and Remote Sensing 63 (1), pp. 99-114.

Kukko, A., Kaartinen, H., Kaasalainen, S., Anttila, K. and Vaaja, M., 2010. Experiences of mobile mapping in environmental monitoring. 2010 Ubiquitous Positioning Indoor Navigation and Location Based Service, UPINLBS 2010 , art. no. 5653572.

Laefer, D.F., Truong-Hong, L. and Fitzgerald, M., 2011. Processing of terrestrial laser scanning point cloud data for computational modelling of building facades. Recent Patents on Computer Science 4 (1), pp. 16-29.

Lasky, T., Swanston, T. and Ravani, B., 2006. StructView: A Vehicle-Based Laser Scanning System for Roadway Structure Profile Assessment. Intelligent Transportation Systems Conference, 2006. ITSC '06. IEEE, pp. 331-336.

Lee, S.Y., Choi, K.H., Joo, I.H., Cho, S.I. and Park, J.H., 2006. Design and implementation of 4S-Van: A mobile mapping system. ETRI Journal, 28(3), pp. 265-274.

Liang, Z., 2009. Extraction of road sides from high point density airborne laser scanning data. Degree of Master of Science. International Institute for Geoinformation Science and Earth Observation, Enchede, Netherlands, Master of Science thesis in Geo-information Science and Earth Observation.

Liu, M. and Bao, F., 2009. To improveing precision of mobile mapping system with reference points. Journal of Geomatics 34 (3), pp. 35-36.

Liu, D., Dai, B., Li, Z. and He, H., 2008. Method for calibration of single line laser radar and camera. Huazhong Keji Daxue Xuebao (Ziran Kexue Ban)/Journal of Huazhong University of Science and Technology (Natural Science Edition) 36 (SUPPL. 1), pp. 68-71.

Livny, Y., Yan, F., Olson, M., Chen, B., Zhang, H. and El-Sana, J., 2010. Automatic Reconstruction of Tree Skeletal Structures from Point Clouds. ACM Transactions on Graphics 29 (6), art. no. 1866177.

Maas, H.-G., Bienert, A., Scheller, S. and Keane, E., 2008. Automatic forest inventory parameter determination from terrestrial laser scanner data. International Journal of Remote Sensing 29 (5), pp. 1579-1593.

Mallet, C. and Bretar, F., 2009. Full-waveform topographic lidar: State-of-the-art. ISPRS Journal of Photogrammetry and Remote Sensing 64 (1), pp. 1-16.

Mumtaz, S., 2010. Extracting Physical and Environmental Information of Irish Roads Using Airborne and Mobile Sensors. Doctoral Thesis. Dublin, Dublin Institute of Technology, 269 p.

Nagai, M., Tianen, C., Shibasaki, R., Kumagai, H. and Ahmed, A., 2009. UAV-borne 3-D mapping system by multisensor integration. IEEE Transactions on Geoscience and Remote Sensing 47 (3), pp. 701–708.

Nebiker, S., Bleisch, S. and Christen, M., 2010. Rich point clouds in virtual globes - A new paradigm in city modeling? Computers, Environment and Urban Systems 34 (6), pp. 508-517.

Oh, D., 2010. Radiometric correction of mobile laser scanning intensity data. International Institute for Geoinformation Science and Earth Observation, Enchede, Netherlands, Master of Science thesis in Geo-information Science and Earth Observation, 77 p.

Ou, J., 2009. 3D line-segment extraction and object recognition based on ground mobile mapping sequential stereo imagery data. Acta Geodaetica et Cartographica Sinica 38 (5), p. 470.

Oude Elberink, S. and Vosselman, G., 2009. Building reconstruction by target based graph matching on incomplete laser data: Analysis and limitations. Sensors 9, pp. 6101–6118.

Oude Elberink, S. and Vosselman, G., 2011. Quality analysis on 3D building models reconstructed from airborne laser scanning data. ISPRS Journal of Photogrammetry and Remote Sensing 66 (2), pp. 157-165.

Pu, S. and Vosselman, G., 2009. Knowledge based reconstruction of building models from terrestrial laser scanning data. ISPRS Journal of Photogrammetry and Remote Sensing 64 (6), pp. 575–584.

Ridene, T. and Goulette, F., 2009. Coregistration of DSM and 3D point clouds acquired by a mobile mapping system | [Corregistro do DSM e nuvem de pontos 3D adquiridos através de um sistema de mapeamento móvel]. Boletim de Ciencias Geodesicas 15 (5), pp. 824-838.

Rottensteiner, F., 2009. Status and Further Prospects of Object Extraction from Image and LiDAR Data". Proc. Joint IEEEGRSS/ ISPRS Workshop on Remote Sensing and Data Fusion over Urban Areas (Urban 2009), on CD-ROM, Shanghai, China, 20-22 May 2009.

Rottensteiner, F., 2010. Automation of object extraction from LiDAR in urban areas. International Geoscience and Remote Sensing Symposium (IGARSS), art. no. 5652949, pp. 1343-1346.

Ruofei, Z., Yongwei, K., Weibing, F. and Jianxi, H., 2008. Accuracy analysis of geo-referencing by vehicle-borne position and orientation system in laser scanning. International Geoscience and Remote Sensing Symposium (IGARSS) 2 (1), art. no. 4779199, pp. II1132-II1135.

Rutzinger, M., Höfle, B. and Pfeifer, N., 2008. Object detection in airborne laser scanning data - an integrative approach on object-based image and point cloud analysis. In Object-Based Image

Analysis: Spatial Concepts for Knowledge-Driven Remote Sensing Applications; Blaschke, T., Lang, S., Hay, G., Eds.; Springer-Verlag: Berlin/Heidelberg, Germany, 2008, pp. 645–662.

Rutzinger, M., Oude Elberink, S., Pu, S. and Vosselman, G., 2009. Automatic extraction of vertical walls from mobile and airborne laser scanning data. International Archives of Photogrammetry, Remote Sensing and Spatial Information Sciences, vol. 37, part 3/W8, Paris, France, 1-2 September, pp. 7-11.

Schmitt, A. and Vögtle, T., 2009. An advanced approach for automatic extraction of planar surfaces and their topology from point clouds. Photogrammetrie, Fernerkundung und Geoinformation 1, pp. 43–52.

Shen, Y., Li, L. and Ruan, Y.T., 2009. Mobile mapping technology by vehicle-borne lidar. Hongwai yu Jiguang Gongcheng/Infrared and Laser Engineering 38 (3), pp. 437-440+451.

Shen, Y. and Sheng, Y. 2010. Segmentation of building façades from vehicle-borne laser scanning data based on mathematical morphology. Proceedings of SPIE - The International Society for Optical Engineering 7841 (1), art. no. 784107.

Shi, Y., Shibasaki, R. and Shi, Z.C., 2008. The Towards automatic road mapping by fusing vehicle-borne multi-sensor data. The International Archives of the Photogrammetry, Remote Sensing and Spatial Information Sciences. Vol. XXXVII. Part B5. Beijing 2008, pp. 867-872.

Sithole, G. and Vosselman, G., 2004. Experimental comparison of filter algorithms for bare-Earth extraction from airborne laser scanning point clouds. ISPRS Journal of Photogrammetry and Remote Sensing, 59 (1-2), pp. 85-101.

Song, H. and Feng, H.-Y., 2009. A progressive point cloud simplification algorithm with preserved sharp edge data. The International Journal of Advanced Manufacturing Technology 45(5-6), pp. 583-592.

Sturzenegger, M. and Stead, D., 2009. Close-range terrestrial digital photogrammetry and terrestrial laser scanning for discontinuity characterization on rock cuts. Engineering Geology 106 (3–4), pp. 163–182.

Talaya, J., Bosch, E., Alamús, R., Serra, A. and Baron, A., 2004. GEOVAN: The mobile mapping system from the ICC Proceedings del 4th International Symposium on Mobile Mapping Technology (MMT'2004). Kumming, 2004, 6p.

Tao, C.V., Chapman, M.A. and Chaplin, B.A., 2001. Automated processing of mobile mapping image sequences. ISPRS Journal of Photogrammetry and Remote Sensing 55(5-6): pp. 330-346.

Toth, C., Grejner-Brzezinska, D.A., Oh, J.H. and Markiel, J.N., 2009. Terrain-based navigation: A tool to improve navigation and feature extraction performance of mobile mapping systems | [Navegação terrestre: Um instrumento para melhorar a navegação e o desempenho na extração de feições do sistema de mapeamento móvel]. Boletim de Ciencias Geodesicas 15 (5), pp. 807-823.

Vosselman, G., 2009. Advanced Point Cloud Processing. Proceedings of Photogrammetric Week (PhoWo09), pp. 135-147.

Vosselman, G. and Zhou, L., 2009. Detection of Curbstones in Airborne Laser Scanning Data. International Archives of the Photogrammetry, Remote Sensing and Spatial Information Sciences XXXVIII – 3/W8, Paris, France, 2009, pp. 111-117.

Vosselman, G. and Maas, H.-G., 2010. Airborne and Terrestrial Laser Scanning. Whittles Publishing, Caithes, GB, 336 p.

Wand, M., Berner, A., Bokeloh, M., Jenke, P., Fleck, A., Hoffmann, M., Maier, B., Staneker, D., Schilling, A. and Seidel, H.-P., 2008. Processing and interactive editing of huge point clouds from 3D scanners. Computers & Graphics 32 (2), pp. 204-220.

Wang, J. and Jin, F.-X., 2010. Precision estimation of mobile laser scanning system. Survey Review 42 (317), pp. 270-278.

Yang, B., Wei, Z., Li, Q. and Mao, Q., 2010. A classification-oriented method of feature image generation for vehicle-borne laser scanning point clouds. Acta Geodaetica et Cartographica Sinica 39 (5), pp. 540-545.

Yang, H.-J., Zhang, W.-Z. and Liu, X.-L., 2011. Rapid method for point clouds registration based on reference points. Applied Mechanics and Materials 48-49, pp. 873-876.

Yao, W. and Stilla, U., 2010. Mutual enhancement of weak laser pulses for point cloud enrichment based on full-waveform analysis. IEEE Transactions on Geoscience and Remote Sensing 48 (9), art. no. 5462965, pp. 3571-3579.

Yao, W. and Stilla, U., 2011. Comparison of Two Methods for Vehicle Extraction From Airborne LiDAR Data Toward Motion Analysis. IEEE Geoscience and Remote Sensing Letters, 8(4), pp. 607-611.

Yiu, K. and King, B., 2009. Stereonet Data from Terrestrial Laser Scanner Point Clouds. Survey Review, 41(314), pp. 324-338.

Yoo, H.-J., Goulette, F., Senpauroca, J. and Lepère, G., 2009. Simulation based comparative analysis for the design of laser terrestrial mobile mapping systems | [Simulação baseada numa análise comparativa para o projeto de um sistema movel de mapeamento terrestre a laser.] Boletim de Ciencias Geodesicas 15 (5), pp. 839-854.

Yu, X., Hyyppä, J., Vastaranta, M., Holopainen, M., and Viitala, R., 2011. Predicting individual tree attributes from airborne laser point clouds based on the random forests technique. ISPRS Journal of Photogrammetry and Remote Sensing 66 (1), pp. 28-37.

Zhao, H., Chen, Y. and Shibasaki, R., 2007. An efficient extrinsic calibration of a multiple laser scanners and cameras' sensor system on a mobile platform. IEEE Intelligent Vehicles Symposium, Proceedings, art. no. 4290151, pp. 422-427.

Zhao, H., Chiba, M., Shibasaki, R., Shao, X., Cui, J. and Zha, H., 2008. SLAM in a dynamic large outdoor environment using a laser scanner. Proceedings - IEEE International Conference on Robotics and Automation, art. no. 4543407, pp. 1455-1462.

Zhou, L., 2009. Extraction of road sides from high point density airborne laser scanning data. M.Sc. thesis, International Institute of Geo-Information Sciences and Earth Observation (ITC), Enschede, the Netherlands, 55 p.

Zhou, Y., Zhang, W.-B., Du, F.-R. and Yao, X.-J., 2010. Algorithm for reduction of scattered point cloud data based on curvature. Beijing Ligong Daxue Xuebao/Transaction of Beijing Institute of Technology 30 (7), pp. 785-789.

Zhu, C., Zhang, X., Hu, B. and Jaeger, M., 2008. Reconstruction of Tree Crown Shape from Scanned Data.Technologies for E-Learning and Digital Entertainment, Lecture Notes in Computer Science, 5093/2008, pp. 745-756.

Index of Figures

Index of Tables

LIST OF OEEPE/EuroSDR OFFICIAL PUBLICATIONS

State – March 2013

1 *Trombetti, C.:* „Activité de la Commission A de l'OEEPE de 1960 à 1964" – *Cunietti, M.:* „Activité de la Commission B de l'OEEPE pendant la période septembre 1960 – janvier 1964" – *Förstner, R.:* „Rapport sur les travaux et les résultats de la Commission C de l'OEEPE (1960–1964)" – *Neumaier, K.:* „Rapport de la Commission E pour Lisbonne" – *Weele, A. J. v. d.:* „Report of Commission F." – Frankfurt a. M. 1964, 50 pages with 7 tables and 9 annexes.

2 *Neumaier, K.:* „Essais d'interprétation de »Bedford« et de »Waterbury«. Rapport commun établi par les Centres de la Commission E de l'OEEPE ayant participé aux tests" – „The Interpretation Tests of »Bedford« and »Waterbury«. Common Report Established by all Participating Centres of Commission E of OEEPE" – „Essais de restitution »Bloc Suisse«. Rapport commun établi par les Centres de la Commission E de l'OEEPE ayant participé aux tests" – „Test »Schweizer Block«. Joint Report of all Centres of Commission E of OEEPE." – Frankfurt a. M. 1966, 60 pages with 44 annexes.

3 *Cunietti, M.:* „Emploi des blocs de bandes pour la cartographie à grande échelle – Résultats des recherches expérimentales organisées par la Commission B de l'O.E.E.P.E. au cours de la période 1959–1966" – „Use of Strips Connected to Blocks for Large Scale Mapping – Results of Experimental Research Organized by Commission B of the O.E.E.P.E. from 1959 through 1966." – Frankfurt a. M. 1968, 157 pages with 50 figures and 24 tables.

4 *Förstner, R.:* „Sur la précision de mesures photogrammétriques de coordonnées en terrain montagneux. Rapport sur les résultats de l'essai de Reichenbach de la Commission C de l'OEEPE" – „The Accuracy of Photogrammetric Co-ordinate Measurements in Mountainous Terrain. Report on the Results of the Reichenbach Test Commission C of the OEEPE." – Frankfurt a. M. 1968, Part I: 145 pages with 9 figures; Part II: 23 pages with 65 tables.

5 *Trombetti, C.:* „Les recherches expérimentales exécutées sur de longues bandes par la Commission A de l'OEEPE." – Frankfurt a. M. 1972, 41 pages with 1 figure, 2 tables, 96 annexes and 19 plates.

6 *Neumaier, K.:* „Essai d'interprétation. Rapports des Centres de la Commission E de l'OEEPE." – Frankfurt a. M. 1972, 38 pages with 12 tables and 5 annexes.

7 *Wiser, P.:* „Etude expérimentale de l'aérotriangulation semi-analytique. Rapport sur l'essai »Gramastetten«." – Frankfurt a. M. 1972, 36 pages with 6 figures and 8 tables.

8 „Proceedings of the OEEPE Symposium on Experimental Research on Accuracy of Aerial Triangulation (Results of Oberschwaben Tests)" *Ackermann, F.:* „On Statistical Investigation into the Accuracy of Aerial Triangulation. The Test Project Oberschwaben" – „Recherches statistiques sur la précision de l'aérotriangulation. Le champ d'essai Oberschwaben"– *Belzner, H.:* „The Planning. Establishing and Flying of the Test Field Oberschwaben" – *Stark, E.:* Testblock Oberschwaben, Programme I. Results of Strip Adjustments" – *Ackermann, F.:* „Testblock Oberschwaben, Program I. Results of Block-Adjustment by Independent Models" – *Ebner, H.:* Comparison of Different Methods of Block Adjustment" – *Wiser, P.:* „Propositions pour le traitement des erreurs non-accidentelles"– *Camps, F.:* „Résultats obtenus dans le cadre du project Oberschwaben 2A" – *Cunietti, M.; Vanossi, A.:* „Etude statistique expérimentale des erreurs d'enchaînement des photogrammes"– *Kupfer, G.:* „Image Geometry as Obtained from Rheidt Test Area Photography" – *Förstner, R.:* „The Signal-Field of Baustetten. A Short Report" – *Visser, J.; Leberl, F.; Kure, J.:* „OEEPE Oberschwaben Reseau Investigations" – *Bauer, H.:* „Compensation of Systematic Errors by Analytical Block Adjustment with Common Image Deformation Parameters." – Frankfurt a. M. 1973, 350 pages with 119 figures, 68 tables and 1 annex.

9 *Beck, W.:* „The Production of Topographic Maps at 1 : 10,000 by Photogrammetric Methods. – With statistical evaluations, reproductions, style sheet and sample fragments by

Landesvermessungsamt Baden-Württemberg Stuttgart.“ – Frankfurt a. M. 1976, 89 pages with 10 figures, 20 tables and 20 annexes.

10 „Résultats complémentaires de l’essai d’«Oberriet» of the Commission C de l’OEEPE – Further Results of the Photogrammetric Tests of «Oberriet» of the Commission C of the OEEPE“
Hárry, H.: „Mesure de points de terrain non signalisés dans le champ d’essai d’«Oberriet» – Measurements of Non-Signalized Points in the Test Field «Oberriet» (Abstract)“ – *Stickler, A.; Waldhäusl, P.:* „Restitution graphique des points et des lignes non signalisés et leur comparaison avec des résultats de mesures sur le terrain dans le champ d’essai d’«Oberriet» – Graphical Plotting of Non-Signalized Points and Lines, and Comparison with Terrestrial Surveys in the Test Field «Oberriet»“ – *Förstner, R.:* „Résultats complémentaires des transformations de coordonnées de l’essai d’«Oberriet» de la Commission C de l’OEEPE – Further Results from Co-ordinate Transformations of the Test «Oberriet» of Commission C of the OEEPE“ – *Schürer, K.:* „Comparaison des distances d’«Oberriet» – Comparison of Distances of «Oberriet» (Abstract).“ – Frankfurt a. M. 1975, 158 pages with 22 figures and 26 tables.

11 „25 années de l’OEEPE“
Verlaine, R.: „25 années d’activité de l’OEEPE“ – „25 Years of OEEPE (Summary)“ – *Baarda, W.:* „Mathematical Models.“ – Frankfurt a. M. 1979, 104 pages with 22 figures.

12 *Spiess, E.:* „Revision of 1 : 25,000 Topographic Maps by Photogrammetric Methods.“ – Frankfurt a. M. 1985, 228 pages with 102 figures and 30 tables.

13 *Timmerman, J.; Roos, P. A.; Schürer, K.; Förstner, R.:* On the Accuracy of Photogrammetric Measurements of Buildings – Report on the Results of the Test “Dordrecht”, Carried out by Commission C of the OEEPE. – Frankfurt a. M. 1982, 144 pages with 14 figures and 36 tables.

14 *Thompson C. N.:* Test of Digitising Methods. – Frankfurt a. M. 1984, 120 pages with 38 figures and 18 tables.

15 *Jaakkola, M.; Brindöpke, W.; Kölbl, O.; Noukka, P.:* Optimal Emulsions for Large-Scale Mapping – Test of “Steinwedel” – Commission C of the OEEPE 1981–84. – Frankfurt a. M. 1985, 102 pages with 53 figures.

16 *Waldhäusl, P.:* Results of the Vienna Test of OEEPE Commission C. – *Kölbl, O.:* Photogrammetric Versus Terrestrial Town Survey. – Frankfurt a. M. 1986, 57 pages with 16 figures, 10 tables and 7 annexes.

17 *Commission E of the OEEPE:* Influences of Reproduction Techniques on the Identification of Topographic Details on Orthophotomaps. – Frankfurt a. M. 1986, 138 pages with 51 figures, 25 tables and 6 appendices.

18 *Förstner, W.:* Final Report on the Joint Test on Gross Error Detection of OEEPE and ISP WG III/1. – Frankfurt a. M. 1986, 97 pages with 27 tables and 20 figures.

19 *Dowman, I. J.; Ducher, G.:* Spacelab Metric Camera Experiment – Test of Image Accuracy. – Frankfurt a. M. 1987, 112 pages with 13 figures, 25 tables and 7 appendices.

20 *Eichhorn, G.:* Summary of Replies to Questionnaire on Land Information Systems – Commission V – Land Information Systems. – Frankfurt a. M. 1988, 129 pages with 49 tables and 1 annex.

21 *Kölbl, O.:* Proceedings of the Workshop on Cadastral Renovation – Ecole polytechnique fédérale, Lausanne, 9–11 September, 1987. – Frankfurt a. M. 1988, 337 pages with figures, tables and appendices.

22 *Rollin, J.; Dowman, I. J.:* Map Compilation and Revision in Developing Areas – Test of Large Format Camera Imagery. – Frankfurt a. M. 1988, 35 pages with 3 figures, 9 tables and 3 appendices.

23 *Drummond, J.* (ed.): Automatic Digitizing – A Report Submitted by a Working Group of Commission D (Photogrammetry and Cartography). – Frankfurt a. M. 1990, 224 pages with 85 figures, 6 tables and 6 appendices.

24 *Ahokas, E.; Jaakkola, J.; Sotkas, P.:* Interpretability of SPOT data for General Mapping. – Frankfurt a. M. 1990, 120 pages with 11 figures, 7 tables and 10 appendices.

25 *Ducher, G.*: Test on Orthophoto and Stereo-Orthophoto Accuracy. – Frankfurt a. M. 1991, 227 pages with 16 figures and 44 tables.

26 *Dowman, I. J.* (ed.): Test of Triangulation of SPOT Data – Frankfurt a. M. 1991, 206 pages with 67 figures, 52 tables and 3 appendices.

27 *Newby, P. R. T.; Thompson, C. N.* (ed.): Proceedings of the ISPRS and OEEPE Joint Workshop on Updating Digital Data by Photogrammetric Methods. – Frankfurt a. M. 1992, 278 pages with 79 figures, 10 tables and 2 appendices.

28 *Koen, L. A.; Kölbl, O.* (ed.): Proceedings of the OEEPE-Workshop on Data Quality in Land Information Systems, Apeldoorn, Netherlands, 4–6 September 1991. – Frankfurt a. M. 1992, 243 pages with 62 figures, 14 tables and 2 appendices.

29 *Burman, H.; Torlegård, K.:* Empirical Results of GPS – Supported Block Triangulation. – Frankfurt a. M. 1994, 86 pages with 5 figures, 3 tables and 8 appendices.

30 *Gray, S.* (ed.): Updating of Complex Topographic Databases. – Frankfurt a. M. 1995, 133 pages with 2 figures and 12 appendices.

31 *Jaakkola, J.; Sarjakoski, T.*: Experimental Test on Digital Aerial Triangulation. – Frankfurt a. M. 1996, 155 pages with 24 figures, 7 tables and 2 appendices.

32 *Dowman, I. J.*: The OEEPE GEOSAR Test of Geocoding ERS-1 SAR Data. – Frankfurt a. M. 1996, 126 pages with 5 figures, 2 tables and 2 appendices.

33 *Kölbl, O.*: Proceedings of the OEEPE-Workshop on Application of Digital Photogrammetric Workstations. – Frankfurt a. M. 1996, 453 pages with numerous figures and tables.

34 *Blau, E.; Boochs, F.; Schulz, B.-S.*: Digital Landscape Model for Europe (DLME). – Frankfurt a. M. 1997, 72 pages with 21 figures, 9 tables, 4 diagrams and 15 appendices.

35 *Fuchs, C.; Gülch, E.; Förstner, W.*: OEEPE Survey on 3D-City Models.
Heipke, C.; Eder, K.: Performance of Tie-Point Extraction in Automatic Aerial Triangulation. – Frankfurt a. M. 1998, 185 pages with 42 figures, 27 tables and 15 appendices.

36 *Kirby, R. P.*: Revision Measurement of Large Scale Topographic Data.
Höhle, J.: Automatic Orientation of Aerial Images on Database Information.
Dequal, S.; Koen, L. A.; Rinaudo, F.: Comparison of National Guidelines for Technical and Cadastral Mapping in Europe ("Ferrara Test") – Frankfurt a. M. 1999, 273 pages with 26 figures, 42 tables, 7 special contributions and 9 appendices.

37 *Koelbl, O.* (ed.): Proceedings of the OEEPE – Workshop on Automation in Digital Photogrammetric Production. – Frankfurt a. M. 1999, 475 pages with numerous figures and tables.

38 *Gower, R.*: Workshop on National Mapping Agencies and the Internet. *Flotron, A.; Koelbl, O.*: Precision Terrain Model for Civil Engineering. – Frankfurt a. M. 2000, 140 pages with numerous figures, tables and a CD.

39 *Ruas, A.*: Automatic Generalisation Project: Learning Process from Interactive Generalisation. – Frankfurt a. M. 2001, 98 pages with 43 figures, 46 tables and 1 appendix.

40 *Torlegård, K.; Jonas, N.*: OEEPE workshop on Airborne Laserscanning and Interferometric SAR for Detailed Digital Elevation Models. – Frankfurt a. M. 2001, CD: 299 pages with 132 figures, 26 tables, 5 presentations and 2 videos.

41 *Radwan, M.; Onchaga, R.; Morales, J.*: A Structural Approach to the Management and Optimization of Geoinformation Processes. – Frankfurt a. M. 2001, 174 pages with 74 figures, 63 tables and 1 CD.

42 *Heipke, C.; Sester, M.; Willrich, F.* (eds.): Joint OEEPE/ISPRS Workshop – From 2D to 3D – Establishment and maintenance of national core geospatial databases. *Woodsford, P.* (ed.): OEEPE Commission 5 Workshop: Use of XML/GML. – Frankfurt a. M. 2002, CD.

43 *Heipke, C.; Jacobsen, K.; Wegmann, H.*: Integrated Sensor Orientation – Test Report and Workshop Proceedings. – Frankfurt a. M. 2002, 302 pages with 215 figures, 139 tables and 2 appendices.

44 *Holland, D.; Guilford, B.; Murray, K.*: Topographic Mapping from High Resolution Space Sensors. – Frankfurt a. M. 2002, 155 pages with numerous figures, tables and 7 appendices.

45 *Murray, K.* (ed.): OEEPE Workshop on Next Generation Spatial Database – 2005. *Altan, M. O.; Tastan, H.* (eds.): OEEPE/ISPRS Joint Workshop on Spatial Data Quality Management. 2003, CD.

46 *Heipke, C.; Kuittinen, R.; Nagel, G.* (eds.): From OEEPE to EuroSDR: 50 years of European Spatial Data Research and beyond – Seminar of Honour. 2003, 103 pages and CD.

47 *Woodsford, P.; Kraak, M.; Murray, K.; Chapman, D.* (eds.): Visualisation and Rendering – Proceedings EuroSDR Commission 5 Workshop. 2003, CD.

48 *Woodsford, P.* (ed.): Ontologies & Schema Translation – 2004. *Bray, C.* (ed.): Positional Accuracy Improvement – 2004. *Woodsford, P.* (ed.): E-delivery – 2005. Workshops. 2005, CD.

49 *Bray, C.; Rönsdorf, C.* (eds.): Achieving Geometric Interoperability of Spatial Data, Workshop – 2005. *Kolbe, T. H.; Gröger, G.* (eds.): International Workshop on Next Generation 3D City Models – 2005. *Woodsford, P.* (ed.): Workshop on Feature/Object Data Models. 2006, CD.

50 *Kaartinen, H.; Hyyppä J.*: Evaluation of Building Extraction. *Steinnocher, K.; Kressler, F.*: Change Detection. *Bellmann, A.; Hellwich, O.*: Sensor and Data Fusion Contest: Information for Mapping from Airborne SAR and Optical Imagery (Phase I). *Mayer, H.; Baltsavias, E.; Bacher, U.*: Automated Extraction, Refinement, and Update of Road Databases from Imagery and Other Data. 2006, 280 pages.

51 *Höhle, J.; Potuckova J.*: The EuroSDR Test "Checking and Improving of Digital Terrain Models". *Skaloud, J.*: Reliability of Direct Georeferencing, Phase 1: An Overview of the Current Approaches and Possibilities. *Legat, K.; Skaloud, J.; Schmidt, R.*: Reliability of Direct Georeferencing, Phase 2: A Case Study on Practical Problems and Solutions. 2006, 184 pages.

52 *Murray, K.* (ed.): Proceedings of the International Workshop on Land and Marine Information Integration. 2007, CD.

53 *Kaartinen, H.; Hyyppä, J.*: Tree Extraction. 2008, 56 pages.

54 *Patrucco, R.; Murray, K.* (eds.): Production Partnership Management Workshop – 2007. Ismael *Colomina, I.; Hernández, E.* (eds.): International Calibration and Orientation Workshop, EuroCOW 2008. *Heipke, C.; Sester, M.* (eds.): Geosensor Networks Workshop. *Kolbe, T. H.* (ed.): Final Report on the EuroSDR CityGML Project. 2008, CD.

55 *Cramer, M.*: Digital Camera Calibration. 2009, 257 pages.

56 *Champion, N.*: Detection of Unregistered Buildings for Updating 2D Databases. *Everaerts, J.*: NEWPLATFORMS – Unconventional Platforms (Unmanned Aircraft Systems) for Remote Sensing. 2009, 98 pages.

57 *Streilein, A.; Kellenberger, T.* (eds.): Crowd Sourcing for Updating National Databases. *Colomina, I.; Jan Skaloud, J.; Cramer, M.* (eds.): International Calibration and Orientation Workshop EuroCOW 2010. *Nebiker, S.; Bleisch, S.; Gülch, E.*: Final Report on EuroSDR Project Virtual Globes. 2010, CD.

58 *Stoter, J.*: State-of-the-Art of Automated Generalisation in Commercial Software. *Grenzdörffer, G.*: Medium Format Cameras. 2010, 266 pages and CD.

59 *Rönnholm, P.*: Registration Quality – Towards Integration of Laser Scanning and Photogrammetry. *Vanden Berghe, I.; Crompvoets, J.; de Vries, W.; Stoter, J.*: Atlas of INSPIRE Implementation Methods. 2011, 292 pages and CD.

60 *Höhle, J.; Potuckova M.*: Assessment of the Qualityof Digital Terrain Models. 2011, 85 pages.

61 *Fritsch, D.; Pfeifer, N.; Franzen, M.*: High Density Image Matching for DSM Computation Workshop. 2012, CD.

The publications can be ordered using the electronic order form of the EuroSDR website
www.eurosdr.net